AN EXPERIMENTAL INVESTIGATION INTO NANOFLUIDS (CuO-H_2O &CuO-ETHYLENE GLYCOL) BASED PARABOLIC SOLAR COLLECTOR

A Dissertation submitted in partial fulfillment of the requirements for the award of degree of

MASTER OF ENGINEERING
IN
THERMAL ENGINEERING

Submitted by

SHAILJA KANDWAL
(ROLL NO. 801383024)

Under the Guidance of

MR. KUNDAN LAL
Assistant Professor, MED
Thapar University, Patiala

DEPARTMENT OF MECHANICAL ENGINEERING
THAPAR UNIVERSITY
PATIALA – 147004, INDIA

JULY 2015

CERTIFICATION

I, Shailja Kandwal, declare that this thesis report entitled "***An Experimental Investigation into nanofluids (CuO-H_2O & CuO- Ethylene Glycol) based parabolic solar collector***", submitted towards fulfillment of the requirements for the award of Master's Degree in Thermal Engineering, in Mechanical Engineering Department of Thapar University, Patiala, is entirely my own work. This document has not been submitted for any degree in any other institution.

Date: 13/7/15

Place: TU, Patiala

Shailja Kandwal

801383024

Thapar University, Patiala

This is to certify that above statement made by the candidate is correct and true to the best of my knowledge.

Supervisor:

Mr. Kundan Lal

(Assistant Professor)

Mechanical Engineering Department

Thapar University, Patiala

Countersigned by

Dr. S.K. Mohapatra

Sr. Professor and Head

Mechanical Engineering Department

Thapar University, Patiala

Dr. S.S. Bhatia

Dean

Academic Affairs

Thapar University, Patiala

ACKNOWLEDGEMENT

With deep sense of gratitude I express my sincere thanks to my esteemed and worthy supervisor, **Mr. KundanLal,** Assistant Professor, Department of Mechanical Engineering, Thapar University, Patiala for his valuable guidance in carrying out work under his effective supervision, encouragement, enlightenment and cooperation. Most of the novel ideas and solutions found in this dissertation are the result of our numerous stimulating discussions. His feedback and editorial comments were also invaluable for writing of this dissertation.

I shall be failing in my duties if I do not express my deep sense of gratitude towards **Dr. S.K Mohapatra,** SeniorProfessor and Head of the Department of Mechanical Engineering, Thapar University, Patiala who has been a constant source of inspiration for me throughout this work, and for the providing us with adequate infrastructure in carrying the work.

I am greatly indebted to all my friends who constantly encouraged me and also would like to thank the entire faculty and staff members of Mechanical Engineering Department for their unyielding encouragement. I am also thankful to the authors whose work have been consulted and quoted in this work.

At last but not the least my gratitude towards my parents, who always supported me in doing the things my way and whose everlasting desires, selfless sacrifice, encouragement, affectionate blessings and help made it possible for me to complete my degree. I would also like to render my gratitude to the Almighty God who bestowed self-confidence, ability and strength in time to complete this task and for not letting me down at the time of crisis and showing me the silver lining in the dark clouds.

Place: TU, Patiala **ShailjaKandwal**

Date: Roll No. 801383024

ABSTRACT

The concept of renewable energy gained importance after the degradation as well as the shortage of fossil fuels. Out of many renewable resources, solar energy has better prospect. Solar energy is available in bounty offering the benefits of being non- polluting, limitless and sustainability. It can be best used by converting it into other forms of energy as heat and electricity. The present study has been carried out to examine the performance of parabolic solar collector using CuO-water based nanofluids, CuO-ethylene glycol based nanofluids, water and ethylene glycol. A comparison has been made among all the four fluids at different concentrations (0.01%, 0.05% and 0.1%) and mass flow rates (160l/hr, 130l/hr and 100l/hr). Data has been collected from9:30 am to 2:30 pm in the months of April, May and June. CuO-water based nanofluids are found to have the maximum overall efficiency of 6.6% followed by CuO-ethylene glycol based nanofluids (5.73%), water (5.17%) and ethylene glycol (3.93%). These results are validated by the computational fluid dynamics (CFD) software using ANSYS 14.5. Solar load model has been used to calculate the solar heat flux. The input parameters used in the model are latitude and longitude of the location (Patiala), time and date of a particular day and orientation of the experimental setup. The experimental results are found to be in good agreement with the CFD results; within accuracy levels of ±5%.

TABLE OF CONTENTS

LIST OF FIGURES

LIST OF TABLES

NOMENCLATURE

H	Efficiency
F_r	Heat removal factor
η_o	Overall efficiency
U	Overall loss coefficient (W/K*m2)
Ti	Inlet fluid temperature (°C)
Ta	Ambient temperature (°C)
I	Solar intensity (W/m2)
C	Concentration ration ratio
$\dot{m}$	Mass flow rate (Kg/s)
Cp	Specific heat
T_{out}	Outlet temperature (°C)
T_{in}	Inlet temperature (°C)
A	Cover area of the collector (m2)
G_T	Solar flux incident on collector (W/m2)
Nm	Nanometre
Conc.	Concentration
vol.	volumetric

ABBREVIATIONS:

CSP	Concentrated Solar Power
MW	Megawatt
HTF	Heat Transfer Fluid
PTC	Parabolic Trough Collector

SEGS	Solar Electric Generating System
LFR	Linear Fresnel Collector
CFD	Computational Fluid Dynamics
CVD	Chemical Vapor Deposition
TES	Thermal Energy Storage
NCPSC	Nanofluid Based Concentrating Parabolic Solar Collector
XRD	X-Ray Diffraction

CHAPTER 1

INTRODUCTION

1.1 Solar Energy

Since 1980s, renewable energy has gained momentum and contributed much to the energy supply reserves and the environment. Due to the spiral energy demands around the world and diminution of the fossil fuels in long run, sustainability of energy resources is concerning researchers and scientists throughout the world. Therefore, there has been a huge attempt to unsheathe the potential of renewable energies and thus, reducing the collective dependency on fossil fuels. The sun is probably the most significant and abundant source of renewable energy at present. The earth obtains enough energy in one minute from the sun which is more than sufficient to meet the energy demands for an entire year. (David et al. 2003). Though there are several other traditional energy sources too which can be used in lieu of solar energy such as wind energy, hydro energy, tidal energy, geothermal energy etc. Selection of energy source must be based on the basis of environmental, economic and safety concerns. And solar energy accomplish the desired deliverables due to its better environmental and safety details.

The greatest edge solar energy has over other natural resources is that it is the cleanest and accessible energy source with minimal environmental impact. It also assists in the reduction of greenhouse gases pollution. Earth receives a total of 63 MW/m^2 of solar irradiation (Tian and Zhao, 2011). Out of the total amount of energy irradiated from the sun, Earth-Sun geometry diminish the solar rays to around 1 KW/m^2 on the earth's surface which is enough to provide for annual global energy consumption 10,000 times over (Nerella,2014).

Several attempts have been made by researchers and engineers to harness the solar energy for power generation. Employing solar energy in a variety of applications such as, electricity generation, steam generation, heating, cooling etc. results in an enhanced energy security, improving energy stability and increasing energy sustainability (Mahian, 2013).

There are two conventional model of devices deployed for efficiently collecting and converting solar energy into something useful-photovoltaics and concentrated solar power (CSP). The former one works on the principle of photoelectric effect and use photovoltaic cells to generate

electricity while the latter is concerned with generation of thermal energy by different methods based mainly on concentrating collectors.

In a solar collector, solar rays irradiated on the receiver tube are transmitted to the heat transfer fluid (HTF) such as water, air or oil. This heat could be used either in electricity generation, process heating or can be stored for the later use in a thermal storage tank (Tian and Zhao, 2013).

1.2 Solar Collectors

A Solar energy collector is a heat-exchanging device that utilizes solar radiation energy to generate thermal energy. The basic function of a solar collector is to absorb the incident solar radiation, converts it into heat, and transfers this heat to the working fluid circulating throughout the whole system. This heat can either be used directly in industrial applications or can be stored.

Solar collectors can be classified broadly in two types:(Kalogirou, 2004)

1.2.1 Non-concentrating collectors:

This type of collector has the same area for intercepting the radiations as well as for absorption. It captures direct as well as diffuse solar radiations. They are restricted only to low temperature (<120°C) applications such as heating of swimming pools, space heating, water pre heating for domestic or industrial use. Three main types of non-concentrating collectors are:

i. **Flat plate collectors:**

   When solar radiation passes through a transparent cover and impinges on the absorber surface, a large portion of this energy is absorbed by the plate and then transferred to the transport medium in the tubes to be carried away for storage. They are usually stationary in position and require no tracking of the sun.

ii. **Hybrid PVT collectors:**

   Hybrid photovoltaic/thermal (PVT) collectors simultaneously convert solar energy into electricity and heat.

iii. **Enhanced hybrid PVT collectors-Bifacial PVT:**

These can be classified into those that use water as the heat removal medium, and those that use air.

1.2.2 Concentrating solar collectors

These types of solar collector make use of an optical device to concentrate a large amount of solar rays to a smaller intercepting area reducing the heat losses. This increases the radiation heat flux which in turn increases the temperature achieved, resulting in higher thermodynamic efficiency. Concentration can be accomplished by the use of mirrors or lens, through the reflection or refraction of solar radiation.

The collectors which fall in this category are:

I. Parabolic trough collector (PTC):

The collector used in this experimental study is the parabolic trough collector and its performance is studied using nanofluids and validated with computational fluid dynamics (CFD). Across all the concentrated solar power innovations, parabolic trough collector (PTC) is the most mature and well-known technology available for solar harnessing (Hachicha, 2013). This solar collector utilize mirrored parabolic trough to direct the sun's energy to a receiver tube placed on the focal point of a parabolic trough reflector. It takes up the total incident radiation, convert it into heat, and transfer the heat to a heat transfer fluid (usually air, water or oil) flowing inside the linear receiver (Kalogirou, 2009). PTCs can operate in the temperature range of 50 to 400°C. They can be oriented in either north-south direction, tracking the sun from east to west or oriented in an east-west direction, tracking from north to south. Solar Electric Generating Systems (SEGS) is the biggest commercial parabolic trough power plant in the world which has an installed capacity of 354 MW located in the Mojave Desert of Southern California. The second largest PTC plant has a capacity of 280 MW is situated in Arizona.

New developments in the PTC design such as modification in reflector and receiver design have been made to lower the heat losses and boost the efficiency. It paves a way for an efficient and relatively inexpensive power production process. The PTC can also

be coupled with conventional and unconventional resources for an optimized performance.

II. Parabolic dish collectors:

This type of collectors can achieve temperature till 1500°C. They employ parabolic dish shaped mirrors to focus solar energy onto a receiver located at the common focal point of the mirrors. Heat transfer fluid contained in the receiver is then heated up to the desirable working temperature in order to generate electricity in a small engine attached to the receiver or is sent to the storage system. They track the sun on two axes.

III. Heliostat field collectors:

The Heliostat Field Collector, also called the Central Receiver Collector, consists of a large array of flat mirrors/heliostats to reflect incident solar radiations onto the central receiving unit (solar tower). The orientation of every individual heliostat is controlled by an automatic control system powered by altazimuth tracking technology.

IV. Linear fresnel reflectors(LFR) :

LFR consists of long flat mirrors mounted on one or two-axis tracking devices. A receiver is mounted on the focus to collect the heat.

1.3 Advantages of Concentrating Collectors

1) Higher thermodynamic efficiency can be attained as heat transfer fluid can reach to higher temperature in a concentrating surface as compared to flat plate collector.
2) Simple in design and reflecting surfaces require less material, thus reducing the cost per unit area of the solar collecting surface.
3) Selective surface treatment and vacuum insulation are done to reduce the heat losses, thus increasing the collector efficiency.
4) Due to the relatively small area of the receiver, heat losses are less, thus increasing the thermal efficiency.
5) Since higher temperature can be attained with concentrating solar collector, the amount of heat which can be stored per unit volume is larger; therefore the cost of heat storage is less as compared to non-concentrated collectors.

6) Higher temperatures ease the use of power generation equipment to produce both electricity and heat.

1.4 Disadvantages of Concentrating Collectors

1) Out of the diffuse and beam solar radiation components, concentrating collectors can intercept only the beam component because diffuse component is difficult to be reflected and thus, disappear.
2) Flux on the absorber surface is non-uniform while the flux in flat plate collectors is uniform.
3) Costly orienting systems are required to track the sun.
4) High initial cost.
5) To maintain the quality of reflecting surface against weather, dirt, oxidation etc., additional maintenance cost is required.

1.5 Nanofluids

Traditional heat transfer fluids (HTFS) such as water, ethylene glycol, and oil have significantly been used in many industrial processes such as electric generation, heating &cooling processes, chemical processes etc. Inherently, they possess low thermal conductivity in contrast to metals and metal oxides. During the past few decades, a great deal of research has been put into the enhancement of heat transfer and the use of Nanofluids has been advocated. (Mahian, 2013).Choi (1995),firstlyintroduced the term "nanofluid". Nanofluids are best described as a suspension of ultra-fine solid particles (nanoparticles) in common fluids (base fluid). These ultrafine particles are of dimensions approximately 0.1-1000 nm in size. According to the studies conducted, solid metallic particles suspended in fluid have higher thermal conductivity, better stability and good heat transfer rates. However, millimeter and micrometer sized particles bring about abrasion, clogging of the channel and greater pumping power (Jin and Wang, 2007). Due to its small size (10^{-9} m), nanofluids do not encounter any drop in pressure and other flow aspects, under low concentrations.

Advent of nanofluids appealed the attention of researchers as a new generation heat transfer fluids because of its great thermal performance and its benefits: (Pathipakka, 2010)

1. Improved heat transfer and increase in thermal conductivity.

2. Superior stability and minimal settling of particles.
3. Better lubrication.
4. Diminished pumping power.
5. Micro channel cooling.
6. Miniaturization of systems.
7. Less corrosion and clogging in micro channels.

Nanofluids are probably the best choice to modernize the way of meeting the heating or cooling demands in future. Usage of nanofluids for increasing the efficiency of heat transfer will lead to less capital and operational costs which results in more cost savings, waste-reduction and positive impact on environment. Nanotechnology is an emerging novice technology and more research and studies are required to understand the mechanism of heat transfer in nanofluids and apply the benefits in thermal applications.

The materials used for making nanoparticles are as follows:

1) Metals (Copper, Aluminium, Silver etc.)
2) Metal Oxides (Copper oxide, Silicon oxide, Aluminium oxide etc)
3) Semiconductors (Titanium oxide, Silicon Carbide)
4) Carbon nanotubes
5) Nitride Ceramics (Aluminium nitride, Silicon nitride)

Nanoparticles can be manufactured by two methods:

1) Physical method : Inert gas condensation and Mechanical grinding
2) Chemical method: Chemical precipitation, Micro emulsion, Thermal spray, Spray pyrolysis

While, nanoparticles are suspended in base fluid in two ways:

1) One step method
2) Two step method

Two step method is most commonly used method due to its commercial production while One step method is not carried out in large scale.

1.6Computational Fluid Dynamics (CFD)

A mathematical model is described using mathematical concepts and language and the process to develop a mathematical model is called mathematical modeling. It checks whether a specific model depicts a system accurately or not or whether it fits experimental measurements or empirical data. Mathematical modeling of a problem leads to a set of integral, differential and integro-differential equations. An approximate numerical solution is desired for most of the problems of practical interest. The discipline and practice by which the numerical solution can be estimated is called computational mechanics and for thermo-fluid problems, it's called computational fluid dynamics.

CFD helps predict the fluid flow by means of:

1) Mathematical modeling: mathematical equations are developed using governing equation based on the fundamental conservation laws of physics namely, mass, momentum and energy conservation.
2) Numerical methods: It involves discretization i.e. conversion of governing equations into a set of discrete algebraic equations and solution techniques.
3) Software tools: solvers, pre- and post-processing utilities.

The usage of Computational Fluid Dynamics (CFD) simulation tool gives an insight into the complex fluid flows and provides a thorough understanding of the flow of fluid as well as heat transfer behaviour. CFD simulations are processed by the CFD package from the Computational fluid dynamics research corporation. In the fluent software, boundary conditions are used in simulation procedure to deliver the results.

When experimental, theoretical or analytical results match well with simulated results, it is said to be validated. That process which defines the extent to which a model accurately represent the experimental study is called validation. If a model is not validated, it needs to be reassessed and modified to be a reliable model.

1.6.1Applications of CFD:

1) Heat transfer processes in the industry such as boilers, heat exchangers, combustion equipment, pumps, blowers etc.
2) Aerodynamic shape of aircraft and missiles.
3) Heat transfer applications for electronics packaging industry.
4) Ventilation in buildings.
5) Process heat transfer in power generation systems.
6) Chemical vapor deposition (CVD) for integrated circuit manufacturing.

1.6.2 Advantages of CFD:

1) Using CFD helps to simulate real conditions. It can theoretically simulate any physical condition which cannot be easily tested e.g. hypersonic flow.
2) Ideal conditions can be simulated as well. A particular phenomenon can be isolated for study such as a heat transfer process can be idealized with adiabatic, constant heat flux or constant temperature boundaries.
3) CFD simulations can be performed in a short period of time as compared to the physical tests which can take longer time.
4) CFD simulations are relatively inexpensive and costs can further be reduced if computers used for simulation are of high specifications.
5) During experimentation, only limited amount of parameters can be tested and at a limited number of locations in the system while in CFD, there is no such restrictions. A large number of locations and a set of parameters can be examined.

CHAPTER 2

LITERATURE REVIEW

This chapter contains an extensive literature review of several research papers on flat plate collector and parabolic solar collector, usage of nanofluids in collector and numerical models for the validation of the experimental results.

Previous research work includes:

Barlev et al. (2011) stated an innovation in concentrated solar power (CSP).It was observed that parabolic trough was the most mature concentrated solar power technology. It can be easily coupled to direct steam generation (DSG) where research is being carried out to replace water as heat transfer fluid (HTF) by the ionic liquids. The use of a stirling engine in parabolic dish collector helps to reduce the losses and costs associated with heat transport and can be made more effective by combined cycles. Improvements have been made in reflector and collector design and materials, heat absorption and transport, power production and thermal storage.CSP can be incorporated with various other applications besides generating electricity such as hydrogen production, desalination, zinc production, carbon-dioxide recycling, solar cooling etc.

Basavanna et al. (2013) showed CFD simulation on the flat plate collector with triangular absorber tubes to increase the surface area of contact between the absorber plate and tube, resulting in more heat absorption and hence, enhanced performance of the collector. Working fluid taken is water. There was a good agreement between the experimental and simulated results; deviation of merely 5%.

Chaudhari and Walke (2014) reviewed the applications of nanofluid in solar energy. The experimental and numerical studies for solar collectors have been reviewed. It was reported that the overall efficiency of system increased by using nanofluids. Collector efficiency was affected by the variations in particle size and volume fractions. Addition of surfactant and a suitable selection of the PH value of nanofluid improve the efficiency of the collector.Effect of nanofluids on the efficiency enhancement of solar collectors with economic and environmental considerations was studied.

Hachicha et al. (2013) has carried out numerical simulation of the parabolic trough collector. A detailed thermal radiative heat transfer analysis has been proposed to simulate the solar heat flux distribution around the absorber tube. The results of the thermal model were compared with the experimental results of radiated and un-irradiated receivers. At low temperatures, results matched but disagreements occur at higher temperatures. All in all, it was proved that the model can estimate the heat losses and temperature in the receiver.

Ingle et al. (2013) presented the numerical simulation of the solar flat plate collector with air flow by CFD tool using FLUENT software for the better understanding of the flow and temperature distribution of air inside the collector. The CFD model was validated with the experimental result. The simulation was carried out throughout the day i.e 9 am to 5pm. It was found that experimental and simulated outlet temperature differ by almost 5°C at different times.

John et al. (2013) investigated the variation in thermal conductivity and viscosity of ethylene glycol based titania and copper oxide nanofluids with respect to particle volume concentration and temperature. Volume fraction of 0.1% and 0.5% was taken. The increase in thermal conductivity values were slightly greater than the prediction of Hamilton Crosser model and the effective viscosity of nanofluids were much higher than the values predicted by Einstein-Batchelor model. The stability of nanofluids increased with increase in viscosity of the base fluid and decreased with increasing particle volume concentration.

Khullar and Tyagi(2012) used four different base fluids namely water, ethylene glycol, propylene glycol and therminol VP-1 with aluminium nanoparticle. A mathematical model was prepared using matlab code to compare their solar energy capturing capability. Water was found having the highest capturing ability and with increasing volume fraction, difference narrowed down.

Khullar and Tyagi (2010)used nanofluid as a heat transfer fluid in linear parabolic solar collector. While analyzing the collector theoretically, the radiation source, receiver, nanofluid, and concentrator had been modeled numerically. Finite difference technique had been applied to solve the set of equations. After the theoretical and numerical formulation of the model, the results were obtained using a code developed in matlab programming. Results indicated that nanofluid based collector had a higher efficiency than a conventional collector under similar

operating conditions. Finally various system performance indicators such as thermal and optical efficiencies and mean outlet temperatures were evaluated. Optimization of the model was done by varying the operating parameters (concentration ratio, volume fraction, and receiver length and flow velocity) and analyzing its effects on the performance indicators. It was observed that addition of the trace amounts of aluminium nanoparticles into the base fluid (water) improves its absorption characteristics and increases the thermal and optical efficiencies as well as mean outlet temperature.

Khullar and Tyagi (2012) compared the solar energy capturing capability of different nanofluids in parabolic solar collector. For this purpose aluminum nanoparticles dispersed in base fluids namely water, ethylene glycol, propylene glycol and therminol VP-1 have been assessesed theoretically. A mathematical model of interaction between the radiation and nanofluids was developed. Lambert beer's law was used to compute the attenuation as solar rays reaches the nanofluids. Optical and thermal efficiencies had been found out. Water was shown to have the highest solar energy capturing capacity among the four base fluids and the difference narrowed down with increase in volume fraction of nanoparticles.

Kuravi et al. (2013) gave the review of different thermal energy storage (TES) concepts available in the literature and the factors to be considered at different hierarchical levels for concentrating solar power (CSP) plants. When TES is coupled with CSP, the thermal energy can be stored for later use to drive a heat engine. For a practical CSP plant design with storage, plant level strategy and design considerations come first, followed by selection of the storage materials and design of components incorporating the storage materials, and, design of the system consisting of storage tanks, heat exchangers, piping and pumps respectively, that meet the requirements of the power plant .Though all three basic types of storage media (sensible, latent, thermochemical) have the potential to make solar power plants viable, more research is still needed to improve the thermal performance and economics of these systems.

Mahian et al. (2013) investigated the nanofluids applications in solar thermal engineering systems. He reviewed the effects of nanofluids on the performance of solar collectors from efficiency, economic and environmental considerations viewpoints:

- Tyagi et al. showed the effect of particle volume fraction (0.1% to 5%) and size on collector efficiency and found that by adding nanoparticles to the working fluid, efficiency increases for low values of volume fraction of nanoparticles and with particles size. The efficiency can be obtained by:

$$\eta = \dot{m}c_p(T_{out} - T_{in})/AG_T \quad (1)$$

- Otanicar et al .showed the effects of different nanofluids (CNT, graphite and silver) on the performance of a direct absorption solar collector and observed that efficiency increases until a volume fraction of 0.5% and efficiency decreases with the increase in size of nanoparticles.
- Taylor et al. compared a nanofluid based thermal system with a conventional one and concluded that use of a nanofluid improve the efficiency by 10%.
- Heetal et al. investigated the light-heat conversion characteristics of water-TiO_2 and water-CNT and found latter mixture better with the weight concentration of 0.5%.
- Li et al. studied the effect of three different nanofluids (Al_2O_3/water, ZnO/water and MgO/water) on the performance of a tubular solar collector. ZnO/water nanofluid with 0.2% was chosen the best.
- Taylor et al. investigated the optical property characterization of graphite, gold, silver, copper and aluminium nanoparticles in water and VP1 as the base fluids in direct absorption solar collectors and revealed that with very low nanoparticle volume fractions, over 95% of incoming light can be absorbed.
- Khullar et al. theoretically studied a nanofluid based parabolic collector (NCPSC) and compared the results obtained with the experimental results of concentrating parabolic collector using aluminium nanoparticles in therminol VP-1. He found that thermal efficiency of NCPSC is about 5-10% higher than conventional one.

Manikandan et al. (2012)investigated the viability of the solar parabolic trough collector (PTC) for thermal storage. A thermal analysis was done to evaluate the performance of a PTC by considering the mass flow rate, efficiency, useful energy, and the concentration ratio of the collector ant the heat removal factor. The efficiency of the PTC was also obtained for different heat transfer fluids (HTF_s) by:

$$\eta = F_R\left\{\eta_o - \left(\frac{U(T_i - T_a)}{I} * C\right)\right\} \quad (2)$$

Results obtained were:

- Thermal efficiency increased with the increase in mass flow rate of the nanofluids and concentration ratio increase for a given value of the solar intensity.
- With the increase in the inlet temperature of the heat transfer fluid, the efficiency of the PTC decreased. Also, the system performance was considered for different fluids. Efficiency increased when water is used as a HTF than the castor oil. This is due to water having more specific heat than castor oil that reflects in the PTC efficiency variation.
- With the increase in solar isolation and concentration ratio, the useful heat gained by the HTF also increased.

These theoretical results are well considered as input parameters for further development of the experimental work.

Matthew (2007) showed a numerical study of the parabolic solar collector focusing on receiver. It consists of a metallic tube with therminol-VP1^{TM} fluid flowing through it. The comprehensive analysis was performed using the CFD tool. Radiation effects have been modeled using solar load model.

Nerella et al. (2014) stated the enhancement of heat transfer by nanofluids in solar collector. Mechanisms are Brownian motion of nanoparticles, clustering of nanoparticles and liquid layering around nanoparticles. The thermal conductivity increment was found to depend on the particle concentration, method of preparation and base fluid.

Phelan et al. (2012) introduced the idea of harnessing solar energy through usage of nanofluid based concentrating parabolic solar collector (NCPSC). It has been mathematically modeled and the governing equations have been numerically solved using finite difference technique. The results of the model were compared with the experimental results of conventional concentrating parabolic solar collectors under similar conditions. It was observed that NCPSC has about 5-10% higher efficiency than the conventional one.

Saidur et al. (2010) outlined the latest advances in the study of heat transfer using nanofluids. Nanofluids are a new class of fluids which consist of nano-sized particles (1–100 nm) suspended in base fluids. For the augmentation in heat transfer, thermal conductivity is the most important parameter as the increase in conductivity of nanofluids is linearly related with particle volume fraction and non-linearly with temperature. In literature, the number of rheological studies conducted are limited while many experimental studies has been found on thermal conductivity of nanofluids. It was observed that with the increase in temperature, viscosity of nanofluids decreased.

Selmi et al. (2008) simulated the flat plate collector performance with CFD and performed the validation with the experimental results. Two experiments were performed: with water flow and no water flow. It was found that due to the convection heat transfer, temperature of the water flow experiment is less than one without flow. Good agreement was observed between the simulated and experimental results for outlet water temperatures.

Taylor et al. (2011) tried to show the feasibility of using a directly absorbing nanofluid to improve the efficiency of a high temperature solar collector. Heat transfer oil was taken as a base fluid and graphite particles as nanopowders due to their highly absorptive nature. High temperature collector (solar power tower and parabolic dish) was chosen. A conceptual design of this type of nanofluid receiver was presented. Using this design, it was found that a nanofluid collector may operate more efficiently than a conventional surface solar collector under optimum conditions i.e.upto 10% higher for solar concentration ratios in the range of 100-1000 and graphite nanofluids with lower volume fractions(0.001% or less) are suitable for 10-100 MW plants. Experiments were also conducted on a laboratory-scale nanofluid dish receiver. Therminol VP-1 heat transfer oil and graphite nanoparticles were used with concentration ratio of nearly 400 and direct normal irradiances of 800-950 W/m^2.

Tian and Zhao (2012) reviewed solar collectors and thermal energy storage in solar thermal applications. Solar collectors and thermal energy storage systems are the two crucial components of solar applications. Various forms of solar collectors were studied i.e. non-concentrating collectors (low temperature applications) and concentrating collectors (high temperature applications) and three types of storage systems such as latent heat method, sensible heat method and thermochemical storage. Comparison was made among the materials to be used in the for

high-temperature thermal energy storage systems. For high-temperature thermal storage applications, molten salts were suggested as an ideal materials.

Waghole et al. (2013) studied the effect of nanoparticle concentration on the performance of absorber and found that convective heat transfer coefficient increases with increase in concentration. At various heat loads, this experiment was carried out. Nusselt number ratio of absorber is more at low heat load.

Wu et al. (2014)used fluent software to simulate a parabolic trough receiver model to analyze the detailed temperature distribution. This model was validated with the indoor experimental results. It was concluded that temperature difference changes inversely with the heat transfer fluid velocity. Stagnation temperature of the receiver increases linearly with time.

Xie et al. (2002) stated the thermal conductivity behavior of the alumina suspension. Base fluids taken were deionized water, ethylene glycol and pump oil. With increase in volume fraction, thermal conductivity ratio increases. The suspensions in which the same nanoparticles were used, there was a decrement in the enhanced thermal conductivity ratio, with the increase in thermal conductivity of the base fluid while for the suspensions that used the same base fluid, the enhancements in the thermal conductivities were found to hinge on the surface area. On performing a comparison between the experimental and theoretical conductivity values, former one was found to be higher.

Yu-hua et al. (2007) analyzed and calculated temperature dependence of the thermal conductivity. Higher temperature would lead to the decrease in surface energy and decrease the agglomeration of nanoparticles which would result in less size and hence more thermal conductivity. Viscosity also reduced due to which Brownian motion get rigorous.

Yaseen.T.A (2012) conducted an experimental and theoretical study inboth, winters and summers, for determining the thermal efficiency of a parabolic trough collector. Fortran 90 program was used for the theoretical study. The results signified that the experimental value of thermal efficiency of collector was less than the theoretical one. No significant change was observed in thermal efficiency, above 40kg/h mass flow rate.

CHAPTER 3

GAP STUDY AND OBJECTIVES

3.1 Gap Study

Khullar et al. (2010), Application of nanofluids as the working fluid in concentrating parabolic solar collectors

- Numerical and theoretical investigations are employed for the application of nanofluids as the working fluid in parabolic solar collectors.
- Finite difference method has been used to solve the equations numerically.
- No experimental work has been done using nanofluids on the concentrating type parabolic solar collectors.

Otanicar et al. (2010), Nanofluid based direct absorption solar collector

- Experimental, theoretical & numerical investigations have been carried out to study the performance of a nanofluid based micro scale direct absorption solar collector (DASC).

Taylor et al. (2011), Applicability of nanofluids in high flux solar collectors

- Comparison was performed between the nanofluid-based parabolic dish type concentrating collector and the conventional one using experimental and theoretical investigations.
- Limited mathematical modeling was done on this type of collector.

Chaji et al. (2013), Experimental study on thermal efficiency of flat plate solar collector using TiO_2/water nanofluid

- To check the thermal efficiency of nanofluid based flat plate solar collector, experimental investigation has been performed.
- Limited mathematical modeling was employed.
- Experimental results were not compared with conventional flat plate solar collector.

Khullar et al. (2012), Solar energy harvesting using nanofluids-based concentrating based solar collector

- Theoretical examination has been employed for studying the concentrating type parabolic solar collectors.

- Nanofluid based concentrating parabolic solar collectors has been mathematically modelled using finite difference method technique.
- No experimental work has been done on the concentrating type solar collectors.

A comprehensive literature study has been carried out which seems to suggest that not much research has been done on the performance of nanofluids in the parabolic solar collector. Nanofluids possess better thermal properties which makes it suitable as a working fluid in the collector to improve its performance. Conventional base fluids (water and ethylene glycol/water) have less absorption capacity as compared to nanofluids. This work also states the difference between using conventional base fluids and nanofluids in the solar collector, in terms of efficiency. Also, there have been little efforts to model and validate the experimental data using CFD models. Extensive study has already been done on the flat plate collector. Hence, experimental as well as numerical study of parabolic collector needs to be focused on.
This work studies the solar absorbing ability of nanofluids inside the parabolic collector as well as CFD simulation of nanofluids as working fluid in parabolic collector.

3.2 Objectives

The following specific objectives are undertaken in this study:

1) To study the variations in efficiency of parabolic solar collector by using nanofluids.
2) To study the variations in efficiency of parabolic solar collector by using water and ethylene glycol.
3) To study the variations in efficiency of parabolic solar collector by using different volume fractions of nanoparticles (0.01%, 0.05% and 0.1%) and different volume flow rates of nanofluids and base fluids (160 l/hr, 130 l/hr and 100 l/hr).
4) Comparison of performance of parabolic solar collector with nanofluids and without nanofluids.
5) Computational Fluid Dynamics (CFD) modeling and simulation of water flow inside parabolic collector.
6) Validation of the CFD models by comparing the present simulated results with the experimental data.

CHAPTER 4

METHODOLOGY

4.1 Structural Characterization

For the better understanding and to control the application and synthesis of nanoparticles, nanoparticles characterization is required. X-ray diffraction is generally used in phase recognition of a crystalline matter. It provide information on unit cell dimensions. It's a common technique to study the crystal structures and atomic spacing. XRD is centered on constructive interference of monochromatic X-rays and a crystalline sample.

XRD of CuO Nanoparticles

Specifications:

Company name:	Nanoshel
Nanopowder:	Copper oxide
pH value:	7
Purity:	99.95%
APS:	25-55 nm
BET specific surface area:	>13 m^2/g
Color:	Black
True Density:	6.4 g/cm^3
Content of CuO:	>99%

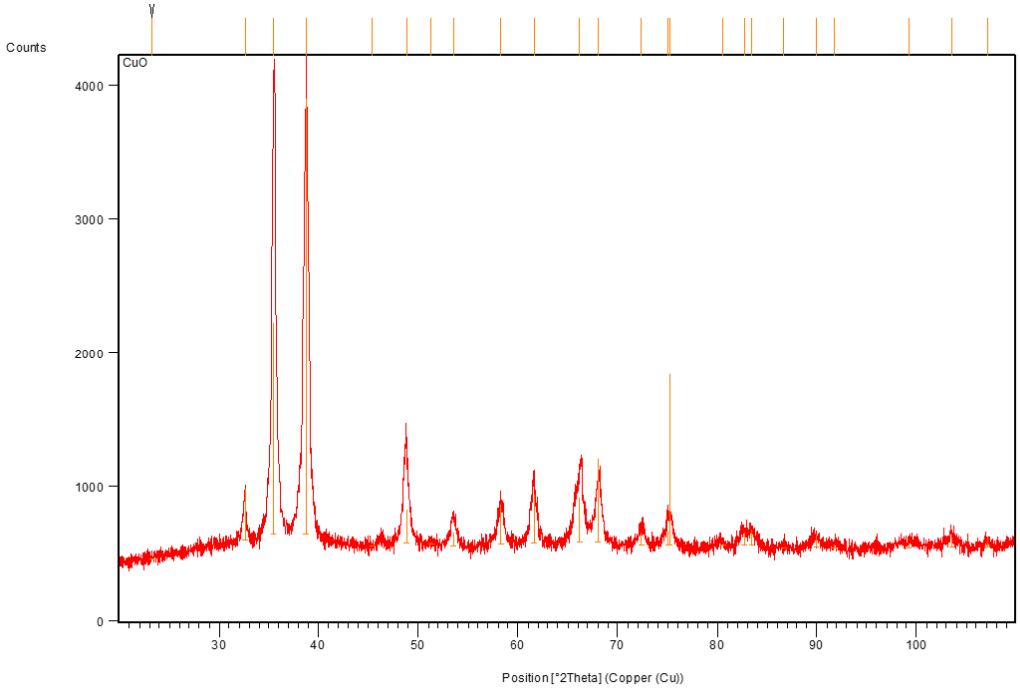

Figure 4.1: XRD ofSAI LAB CuO sample

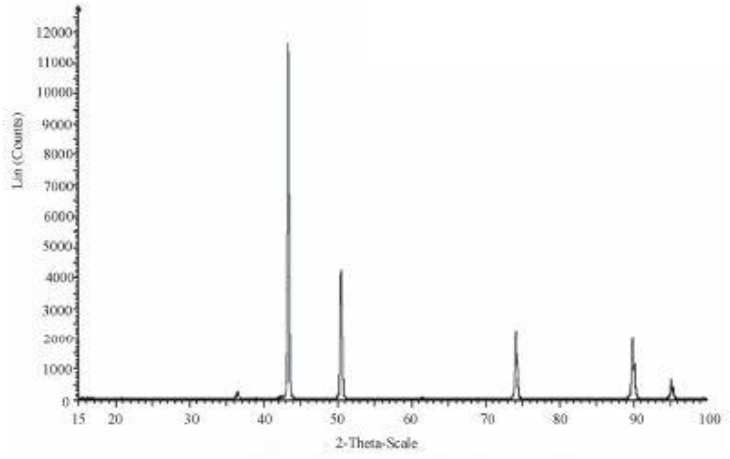

Figure 4.2: XRD of purchased CuO sample

4.2 Nanofluid Preparation

A. Weighing:

In this experiment, CuO nanoparticle is dispersed in two types of base fluids: water and ethylene glycol/water. CuO-water based nanofluids and CuO-ethylene glycol/water based nanofluids are prepared in three different concentrations (0.01%, 0.05% and.0.1%). Amount of nanoparticles taken in the nanofluids was measured by the following expression:

$$\%(\text{percent})\text{by mass} = \frac{\text{mass of solute}}{\text{mass of solution}} * 100 \quad (3)$$

Where,

$$\text{mass of solution} = \text{density}(\text{ of nanoparticle}) * \text{volume}(\text{of base fluid}) \quad (4)$$

Total volume of base fluid (water and ethylene glycol/water) = 4 litre

Density of water = 1000 kg/m^3

Density of ethylene glycol/water = 1048 kg/m^3

Density of CuO nanoparticles = 6.31 g/cm^3

Table 4.1: Following table illustrates the mass of CuO nanoparticles in water and ethylene glycol/water base fluids to make the nanofluids at three concentrations

Concentration	Mass of CuO nanoparticles in CuO-water based nanofluids in gm	Mass of CuO nanoparticles in CuO-ethylene glycol/water based nanofluids in gm
0.01	2.524	2.524
0.05	12.62	12.62
0.1	25.24	25.24

Required quantity of nanoparticles is weighed in the weighing machine (Fig 4.3).

Figure 4.3: Weighing Machine

In the next step, CuO nanoparticles are added in small amount to the base fluid in the magnetic stirrer with hot plate system. Stirring is done continuously for about 30 minutes to disperse the nanoparticles in base fluid as shown in Fig 4.4.

Figure 4.4: Magnetic Stirrer with Hot Plate

Last step is the sonication process, which is done to further stabilize the nanoparticles. The solution is put on the ultra sonicator for about two and half hours as shown in Fig 4.5.

Figure 4.5: Ultra bath sonicator

4.3Thermophysical Properties Measurement:

4.3.1 Thermal conductivity

- Thermal conductivity of nanofluids can be estimated by the relation provided by Maxwell is as follows:

$$\frac{k_{eff}}{k_m} = 1 + \frac{3 \times (\alpha - 1) \times v}{(\alpha + 2) - (\alpha - 1) \times v} \quad (5)$$

Where,

k_{eff}= Thermal Conductivity of solid / liquid (CuO)

k_m = Thermal Conductivity of base fluid (DIW)

k_2 = Thermal Conductivity of nanoparticle, v = Particle volume fractions

$\alpha = k_2/k_m$

- The other model used to calculate thermal conductivity is proposed by Hamilton Crosser is as follows:

$$\frac{k_{eff}}{k_m} = \frac{\alpha + (n-1) - (n-1)(1-\alpha) \times v}{\alpha + (n-1) + (1-\alpha) \times v} \quad (6)$$

Where,

k_{eff} = Thermal Conductivity of solid / liquid (CuO)

k_m = Thermal Conductivity of base fluid (DIW)

k_2 = Thermal Conductivity of nanoparticle, v = Particle volume fractions

n = For spherical particles (data)

$\alpha = k_2/k_m$

- Thermal conductivity of the nanofluid is determined by the following equation (Javadi et al. 2013):

$$K_{eff} = K_f\left[K_p + 2K_f + 2\varphi_p\left(K_p - K_f\right)\right]/\left[K_p + 2K_f - \varphi_p\left(K_p - K_f\right)\right] \quad (7)$$

Where,

K_{eff} = thermal conductivity of nanofluid

K_p = thermal conductivity of nanoparticle

K_f = thermal conductivity of base fluid

Φ_p = concentration of nanoparticle

Above models are used to find out the thermal conductivity and give comparable results. The model suggested in Javadi et al. 2013 gives better and accurate results for the thermal conductivity.

4.3.2 Viscosity

- Viscosity of nanofluids can be calculated by the relation given by Einstein is as follows:

$$\mu_{nf} = \mu_f \times (1 + 2.5\emptyset + 6.5\emptyset^2) \quad (8)$$

Where,

μ_{nf} = Viscosity of nanofluid (CuO)

μ_f= Viscosity of base fluid,

Ø = Particle of Volume fraction

- Lundgen has also given a model to calculate the viscosity which is as follows:

$$\mu_{nf} = \mu_f \times (1 + 2.5\emptyset + 6.5\emptyset^2 + 0.01\emptyset^3) \quad (9)$$

Where,

μ_{nf} = Viscosity of nanofluid (CuO)

μ_f = Viscosity of base fluid,

Ø = Particle of Volume fraction

- Viscosity of nanofluid is determined by applying the following equation (Javadi et al. 2013):

$$\mu_{eff} = {\mu_f}/{(1 - \varphi_p)^{2.5}} \quad (10)$$

Where,

μ_{eff}= viscosity of the nanofluid

μ_f = viscosity of the base fluid

φ_p = concentration of nanoparticle

Above models are used to find out the viscosity and give comparable results. The model suggested in Javadi et al. 2013 gives better and accurate results for the viscosity.

4.3.3 Density

Density of nanofluid is determined by applying the following equation (Javadi et al. 2013):

$$\rho_{eff} = (1 - \varphi_p)\rho_f + \varphi_p\rho_p \quad (11)$$

Where,

ρ_{eff} = density of nanofluid

ρ_p = density of nanoparticle

ρ_f= density of base fluid

φ_p = concentration of nanoparticle

4.3.4 Specific heat

Specific heat of nanofluid is determined by applying the following equation (Javadi et al. 2013):

$$c_{eff} = \{(1 - \varphi_p)\rho_f c_f\}/\rho_{eff} \quad (12)$$

Where,

C_{eff} = specific heat of nanofluid

ρ_{eff} = density of nanofluid

ρ_p= density of nanoparticle

ρ_f = density of base fluid

φ_p = concentration of nanoparticle

c_f = specific heat of base fluid

c_p = specific heat of nanoparticle

4.4 Experimental Setup

Figure 4.6: Experimental setup

Table 4.2: Collector specifications

Parameters	Specification
Collector length	1.20 m
Collector breadth	0.915 m
Aperture area	1.0188 m^2
End plate thickness	2 mm
Rim angle	90°

Receiver inside diameter	0.027 m
Receiver outside diameter	0.028 m
Receiver length	1000 mm
Glass envelope inside diameter	0.064 mm
Glass envelope outside diameter	0.066 mm
Insulation on pipes	Aluminium foil, Superlon
Concentration ratio	11.30
Tank material	Plastic
Tank insulation material	Glass wool
Circulating pump	18 W
Nanoparticle	CuO
Base fluid	Distilled water, Ethylene glycol/water
Nanofluid flow rate	160l/hr, 130l/hr, 100l/hr

4.5 Different Constituents of the Parabolic Solar System:

A parabolic system consists of the following parts explained in detail:

1) **Reflector**

It is made up of the mirrors arranged parabolicaly in curved shape. A total of 26 glass mirror strips are used which has a thickness of 5mm and length of each strip is 90 cm. These glass

strips have high 96%. A sheet of stainless steel is employed to give the parabolic structure. Stainless steel is suitable to give mechanical strength to the parabolic structure.

2) Receiver Tube

The receiver tube consists of a copper tube painted black on outside to absorb maximum radiations having inner diameter 27mm, outside diameter 28mm and 120cm length inside which the working fluid flows. It is concentrically covered by the glass tube of inside diameter 64mm, outside diameter 66mm and length 90 cm which is attached to the copper tube by the glass to metal seals on both ends.

3) Storage Tank

It's made up of plastic and has the capacity of 6 litre. The fluid stored inside it is circulated throughout the whole system by using a pump of 18 W capacity. This pump is placed inside the storage tank. Fluid from the tank flows to the inlet and passes through the receiver tube. After gaining heat in the tube, it flows out from the inlet. The inlet of the tank is connected to the inlet of the receiver tube and outlet of the storage tank is connected to the outlet of the ball valve. Glass wool insulation is used on the tank to protect it from heat loss.

4) Support Structure

It is used to support the whole parabolic system and provide resistance against wind loads, stress loads etc. It minimizes the alignment errors. Cast iron is the material used to construct it. It's painted in green colour to prevent it from corroding. The manual tracking system is also attached to the support structure.

5) Insulation

In the parabolic system, pipes and storage tank are insulated. Pipe is firstly covered with aluminum foils to reduce the heat loss during the heat flow in piping system and then soflon insulation is used over that.

The insulation used on the storage tank is glass wool. It can be easily obtained from the refrigeration and air-conditioning spare parts shop. It is used to avoid heat loss due to its low conductivity. Thermocol sheets are also used for wrapping the glass wool insulation.

6) Tracking Mechanism

It is a manual tracking mechanism consists of rectangular support structure of cast iron, bicycle hub, handle, stopper and clutch wire. One end of clutch wire is placed on bicycle hub and the other end is connected to the back side of the reflector. A handle is attached to the hub to rotate it manually. A Stopper is used to fix the reflector at required angle. It is oriented in north-south direction and track the sun from east to west direction.

7) Ball Valve

Ball valve is used to regulate the flow of working fluid in the inlet pipe and the variation of volume flow rate of nanofluid. Its one side is connected to the outlet of the receiver tube and the other end is connected to the outlet of the storage tank. It is opened according to the required mass flow rate. In this experiment, three mass flow rates are used: 160l/hr, 130l/hr and 100l/hr.

4.6 Working Principle of Parabolic Solar System

Schematic diagram explaining the working of parabolic trough collector is shown in fig.4.7

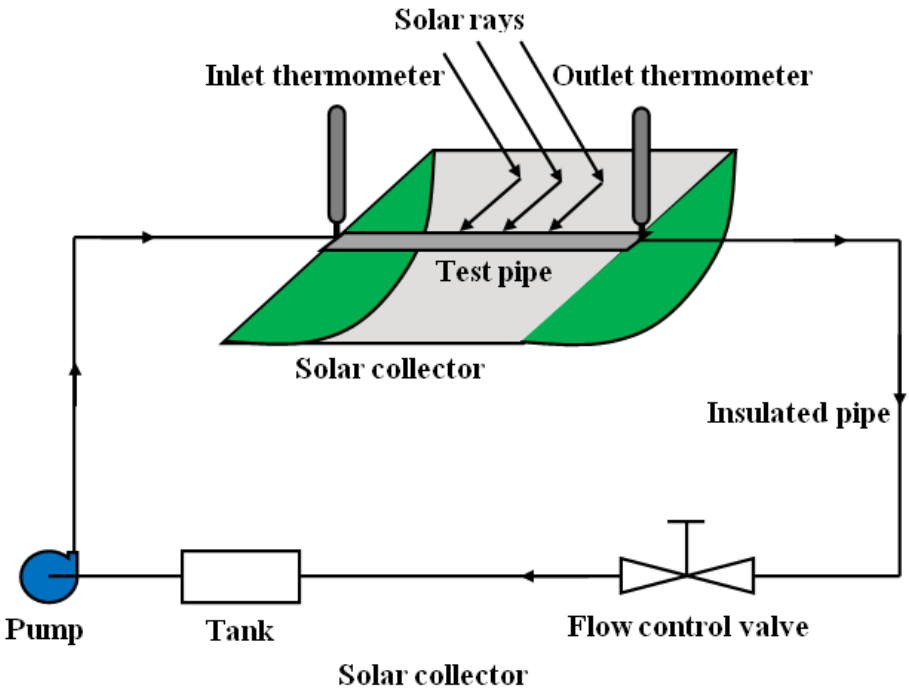

Figure 4.7: Schematic diagram

It consists of a reflector in a parabolically curved shape to reflect direct solar radiation and concentrating them onto the focal line of the parabola. A receiver tube is placed on this focal axis, which absorbs the concentrated solar radiation flux. It is either made up of stainless steel, iron or copper or plated with a selective coating on the outside surface. The selective coating has a high absorptance for incoming radiations but low emittance for the infrared radiations in the solar energy spectrum to decrease the thermal radiation losses. Inside the receiver tube, heat transfer fluid (HTF) flows, takes up the concentrated radiation which falls on the tube and transforms the solar radiation into thermal energy. Receiver tube is enclosed by a glass cover to minimize the thermal losses to the surroundings. The annulus space between the concentric glass cover and the tube is evacuated to maintain the vacuum which is generally a material of low thermal conductivity and high viscosity as heat transfer takes place through radiation in this zone. CuO/water nanofluid and CuO/ethylene glycol nanofluid were used as the working fluid in three different concentrations with the mass flow rate ranging from 160 l/hr to 100 l/hr. The test consists of pumping nanofluid mixture, from the storage tank, through the collector inlet to the receiver tube, where it get heated and then flows back to the storage tank. A pump circulates the working fluid in the system. Two thermocouples are mounted on the inlet and oulet to measure the temperature rise. With the help of solar power meter and anemometer, solar radiation intensity and wind speed were continually measured during the experiment. The PTC was oriented in north-south direction to track the sun. The experiments were performed at different mass flow rates and varying concentrations of nanofluids. Readings of inlet and outlet temperature were measured from 9:30 am to 2:30 pm in a day.

4.7 Simulation Procedure

4.7.1 Mathematical model

Assumptions

In order to carry out the simulation of nanofluids, single phase model was employed (Delavari, 2014). In recent years, Akbarinia et al. (2007) advocated that at a low volume concentration of nanoparticles in a base fluid, it can be presumed that the nanofluid will act as a single phase fluid. In the single phase approach, nanofluid would be considered as a homogeneous fluid which is very much dependent on its effective thermophysical properties which further depends

upon the volume concentration and temperature (Delavari(2014),Pathipakka(2010). It was also assumed that nanoparticles and base fluid are in thermal equilibrium with zero relative velocity (Goktepe(2014), Pathipakka(2010)). In this study, the HTF flow in a receiver tube is a three dimensional transient state turbulent flow under varying heat flux.

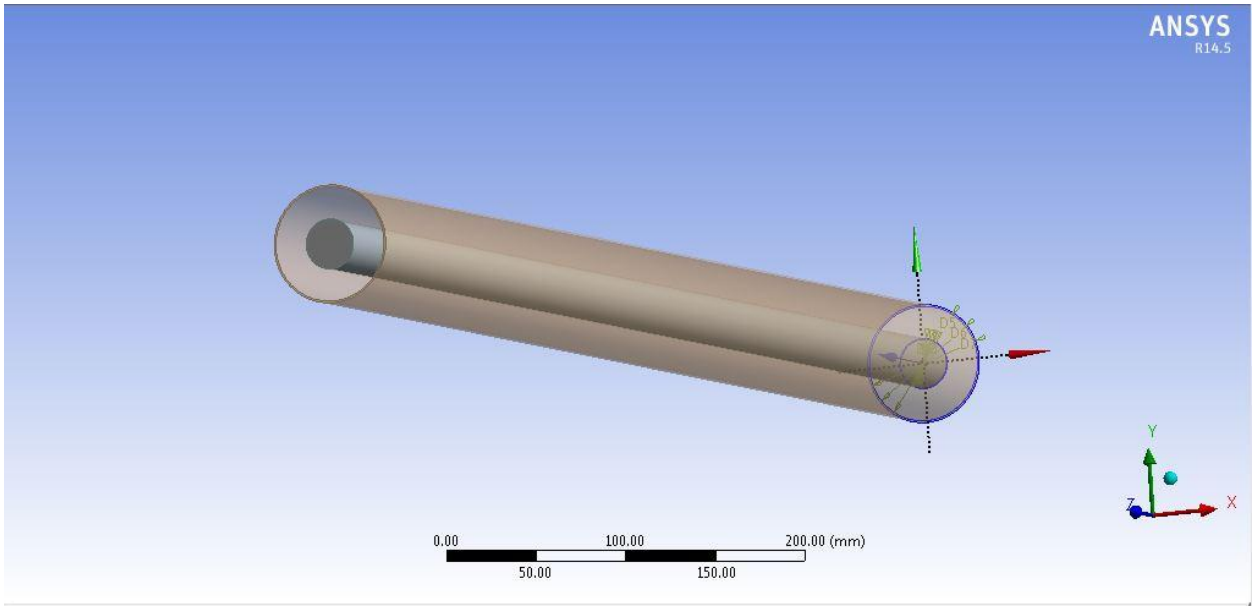

Figure 4.8: Geometry Model

4.7.2 Governing equations

The governing equations of fluid flow and heat transfer are assumed to be of steady state and are described as the Navier-stokes equations.

A. Continuity equations

The principle of conservation of mass is given by:

$$\frac{\partial \rho}{\partial t} + \frac{\partial}{\partial x_i}(\rho u_j) = 0 \tag{13}$$

B. Conservation of momentum

$$\frac{\partial}{\partial t}(\rho u_i) + \frac{\partial}{\partial x_i}(\rho u_i u_j) = \frac{\partial}{\partial x_j}\left[-\rho\delta_{ij} + \mu\left(\frac{\partial u_i}{\partial x_j} + \frac{\partial u_j}{\partial x_i}\right)\right] + \rho g_i \tag{14}$$

C. Conservation of energy

$$\frac{\partial}{\partial t}(\rho C_p T) + \frac{\partial}{\partial x_i}(\rho u_i C_p T) - \frac{\partial}{\partial x_j}\left(\lambda \frac{\partial T}{\partial x_j}\right) = s_T \tag{15}$$

The flow of heat transfer fluid inside the pipe is turbulent. Hence, two turbulence models named turbulence kinetic energy (k-ω) and specific dissipation rate (k-ε) are used for evaluating the turbulent viscosity which appears as an additional term in the transport equations (Menter,1994).

Turbulence kinetic energy

$$\frac{\delta}{\delta t}(\rho k) + \frac{\delta}{\delta x_i}(\rho k u_i) = \frac{\delta}{\delta x_j}\left(\Gamma_k \frac{\delta k}{\delta x_j}\right) + G_k - Y_k + S_k \tag{16}$$

Specific dissipation rate

$$\frac{\delta}{\delta t}(\rho \omega) + \frac{\delta}{\delta x_i}(\rho \omega u_i) = \frac{\delta}{\delta x_j}\left(\Gamma_\omega \frac{\delta \omega}{\delta x_j}\right) + G_\omega - Y_\omega + S_\omega + D_\omega \tag{17}$$

The right hand side of the equations represents diffusion, generation, dissipation and source terms. The second equation has an additional term for cross diffusion effects.

4.7.3 Meshing

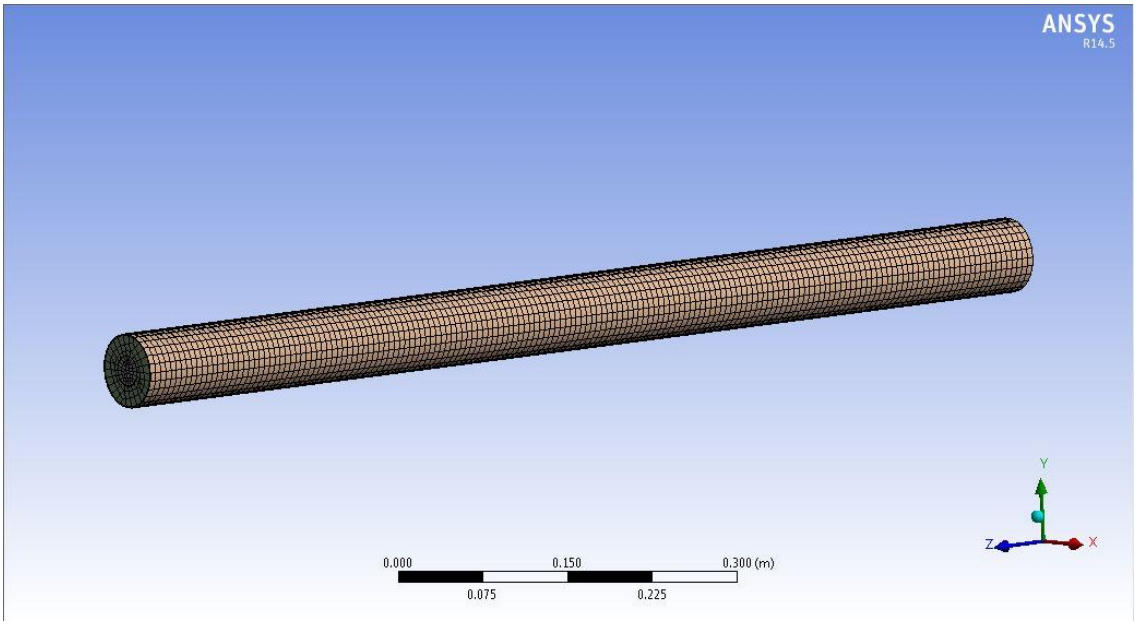

Figure 4.9: Meshing

A commercial mesh generator, ANSYS Meshing 14.5, was used to generate the grids. Fig.11 shows the refined mesh and grid setup of the model. Mesh sizewas 0.0003 mm. Hexahedral and tetrahedral mesh was used.

4.7.4 Solar load model

ANSYS Fluent 14.5 provides a unique ability to calculate the solar heat flux for a certain time and position, based on the given inputs: the latitude, longitude and time zone of the geographical location, grid orientation, Date and time and sunshine factor. This model easily calculates the solar radiation effects, entering in computational domain. From the total solar radiations incident on the domain, solar ray tracing algorithm evaluates heat fluxes and takes into account both the direct as well as diffuse solar radiations. It can be used to model steady and unsteady flows in the 3d solver only. The values calculated are the direct normal solar irradiation at earth's surface, diffuse solar irradiation both for vertical and horizontal surface, sun direction vector and ground reflected solar irradiation for vertical surface.

4.7.5 Surface-surface radiation model (S-2-S Model)

The S-2-S model allows the simulation of thermal radiation exchange between diffuse surfaces forming a closed set. It depends on the orientation of the surfaces and the distance between them. It is assumed that the surfaces are grey and diffuse and the medium that is present between the surfaces is non-participating i.e. it doesn't emit, absorb or scatter any radiation.

4.7.6 Boundary conditions (B.C)

(1) For the fluid domain:

Inlet: At the inlet, flow was assumed to be as uniform mass flow. Inlet temperatures vary according to the time. Due to the concentration of heat at the receiver, heat transfer fluid entering under ambient conditions is subjected to a thermally developing flow. Recirculation inlet is used so that previous outlet becomes the new inlet and the process gets repeated for the desired time. Surrounding temperature and heat transfer coefficient is also provided to consider the heat losses by convection from fluid to the atmosphere.

Outlet: The outlet is set at an ambient pressure. To prevent the reverse flow at outlet, backflow temperature is provided. Mass flow inlet condition is used to input the flow rate and inlet temperature.

Wall: Stationary and no-slip condition. Constant heat flux is provided on the surface of wall for the desired time.

(2) On the walls of receiver, no-slip conditions are assumed while turbulent kinetic energy and dissipation of turbulent kinetic energy are termed zero.

(3) The outer surface of the glass envelope was defined with a mixed boundary with convection and radiation. The convection was assumed to be natural convection with an estimated heat transfer coefficient of 1-2 W/ (m^2 K).

(4) The outer surfaces of the bellows were defined as adiabatic walls because they are usually wrapped with insulation materials and a metal sheet to reduce heat loss. The two ends of the absorber tube were defined as adiabatic.

(5) Heat flux was calculated using solar load model. At any particular day, heat flux can be computed for any time. Input parameters were the latitude and longitude of the given location as well as the orientation of the solar collector.

4.7.7 Numerical method

All the simulations were executed on ANSYS Fluent 14.5. Finite volume method was employed for solving the governing equations. The governing differential equations was discretized to the algebraic equations while second order upwind scheme was used to discretize the convection terms, diffusion terms and other terms. The SIMPLE (Semi Implicit Method for Pressure Linked Equations) algorithm was employed for pressure-velocity coupling discretization. For the energy and momentum equations, first order upwind scheme was used.

The simulation was run for every 30 minutes by giving the time step size and number of time steps. The solution was converged in 4000 iterations and more.

4.8Measuring Instruments

Following instruments are used for the experimental study:

1. Solar Power Meter

This device is used to measure the solar heat flux falling on the collector. A sensor is attached to it which measures the solar intensity (W/m^2) and displays it on the screen. It is calibrated with the actual pyranometer. Following relation is used to measure the actual solar intensity:

$$Y= 0.745 X+ 1.839 \quad (18)$$

Where,

Y= actual solar intensity

X= intensity measured from the solar power meter

2. Thermometer

Thermometer is used to measure the temperature of working fluid at the inlet and outlet. Two thermometers are used in this experiment. There is a red mercury line on it which shows the temperature and the range is 10°C-110°C.

3. Anemometer

Anemometer is used to measure the wind speed. It has a small fan and a sensor. The fan rotates on putting it in the direction of wind flow; the sensor senses it and display the value on the screen.

4.9 Formulae Used

To study the performance of nanofluid using parabolic solar collector, following formulae are used (Sukhatme S.P., 1984):

1) Useful heat gain

Useful heat gain under steady state condition can be obtained by the equation:

$$q_u = \dot{m}_{eff} c_{eff} (T_0 - T_i) \quad (19)$$

Where,

q_u= useful heat gain in watt

c_{eff}= specific heat of nanofluid in J/kg K

$\dot{m}_{eff}$ = mass flow rate of nanofluid in kg/s

T_0 = outlet temperature of nanofluid in K

T_i = inlet temperature of nanofluid in K

2) Thermal efficiency (per half an hour)

Thermal efficiency under steady state condition can be obtained by the equation:

$$\eta_{th} = m_{eff} c_{eff} (T_0 - T_i) / A_{aper} G_T t \quad (20)$$

Where,

η_{th}=thermal efficiency

A_{aper} = aperture area in m^2

G_T = incident solar flux in W/m^2

m_{eff} = mass of nanofluid in storage tank in kg

3) Overall thermal efficiency (average)

Thermal efficiency under steady state condition can be obtained by the equation:

$$\eta = m_{eff} c_{eff} (T_{max} - T_{min}) / A_{aper} G_{av} t \quad (21)$$

Where,

η= overall thermal efficiency

A_{aper} = aperture area in m^2

G_{av}= average incident solar flux in W/m^2

m_{eff} = mass of nanofluid in storage tank in kg

4) Instantaneous efficiency

$$\eta_i = q_u / G_T R_b WL \tag{22}$$

5) Optical efficiency

$$\eta_o = \rho \Upsilon(\alpha\tau)(W - d_{co})/W + (\tau\alpha)\frac{d_{co}}{W} \tag{23}$$

6) Absorbed flux

$$S = G_T R_b \rho \Upsilon(\alpha\tau) \tag{24}$$

Where,

R_b = bond resistance

$\boldsymbol{\Upsilon}$ = Intercept factor

α = Absorptivity of absorber tube

τ = Glass cover transmitivity

ρ = Specular reflectivity of the concentrated surface

7) Convective heat transfer coefficient

$$h_f = N_u \times k/D_i \tag{25}$$

Where,

N_u = Nusselt number = $0.023 \times {R_e}^{0.8} \times {P_r}^{0.4}$

R_e = Reynold number = VD_i/ν

V = Average velocity = $4\dot{m}/\pi {D_i}^2 \rho$

P_r = Prandtl number = $c_p \nu \rho / k$

8) Concentration ratio

$$C_R = \text{Aperture area/Absorber area} = (W - d_{co})L/\pi L D_o = \frac{(W - d_{co})}{\pi D_o} \qquad (26)$$

Where,

C_R = concentration ratio

W= width of the reflector

d_{co}= diameter of glass cover tube

D_o = diameter of receiver tube

L= length of receiver tube

CHAPTER 5

RESULTS AND DISCUSSION

5.1 Performance Of Parabolic Solar Collector Using Cuo-H_2o Based Nanofluids

5.1.1 Variation in solar intensity and temperature with time

I. For CuO- H_2O based nanofluid (0.01% conc.)

Figures 5.1, 5.2 and 5.3 show the variation in solar intensity and temperature with time at 0.01% concentration of nanoparticles for 100, 130 and 160 l/hr, respectively. Readings has been taken from 9:30 am to 2:30 pm in the month of May. In this case, initially, solar intensity rises from 9:30 am to 12:30 pm and after that, it goes on decreasing. Due to the recirculating system, inlet and outlet temperature continuously increases with time from 9:30 am to 2:30 pm. But in the beginning, upsurges in temperature were found to be higher and with the increase in time, it gets lessened. These results are also validated with the CFD simulations.

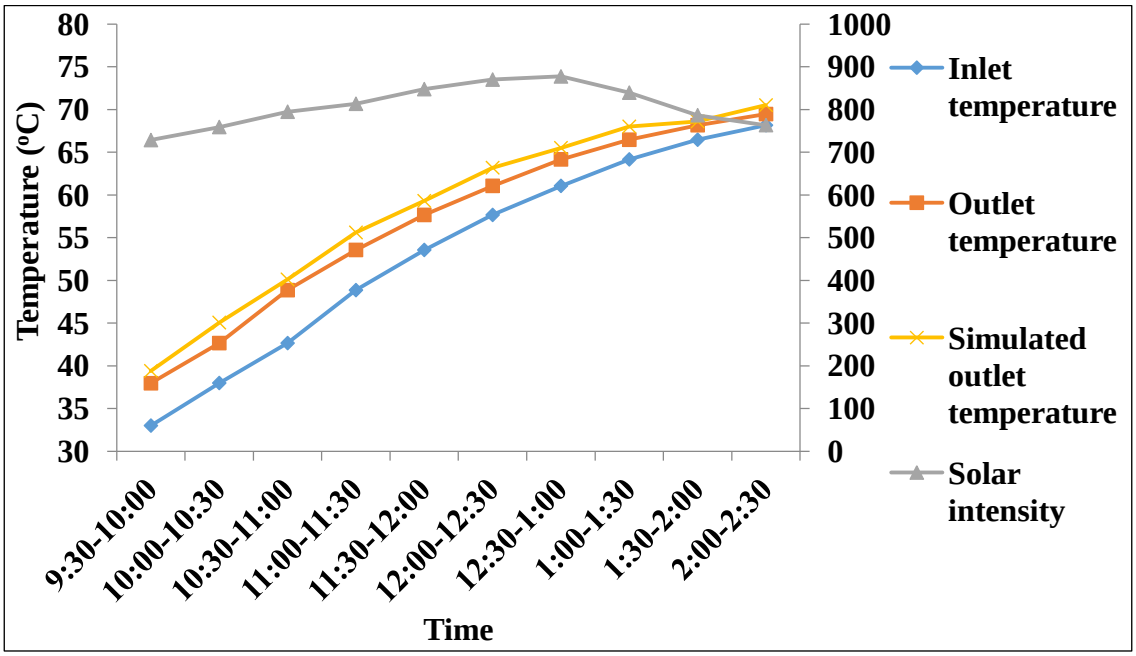

Figure 5.1: Variation in solar intensity and temperature with time for CuO-H_2O based nanofluid (0.01% conc.) at vol. flow rate of 100 l/hr

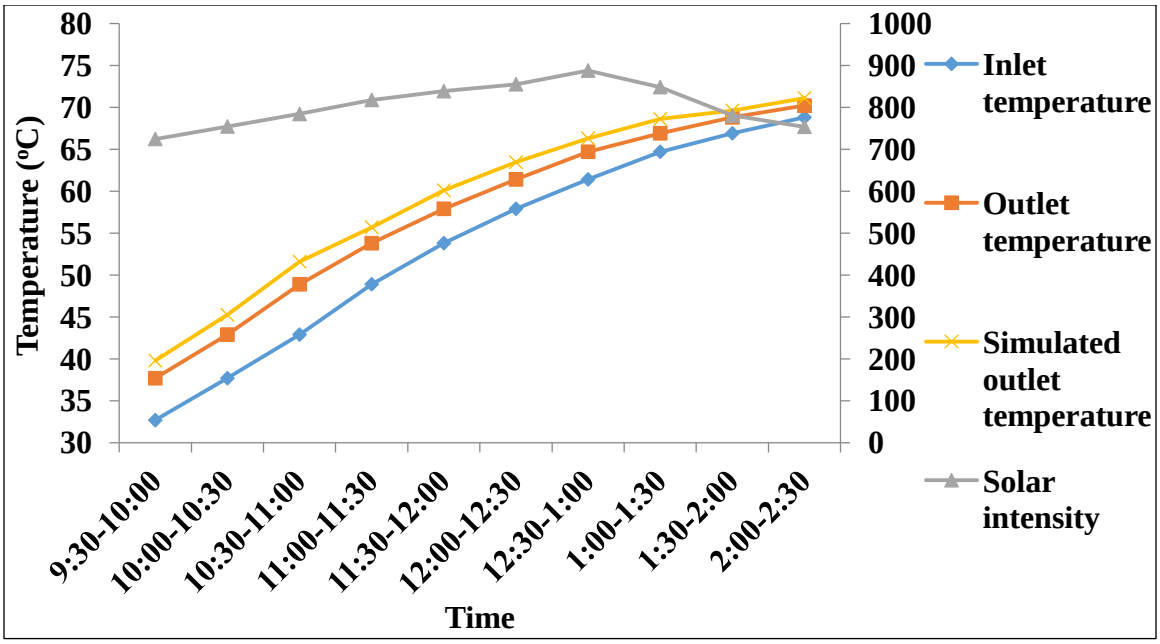

Figure 5.2: Variation in solar intensity and temperature with time for CuO-H_2O based nanofluid (0.01% conc.) at vol. flow rate of 130 l/hr

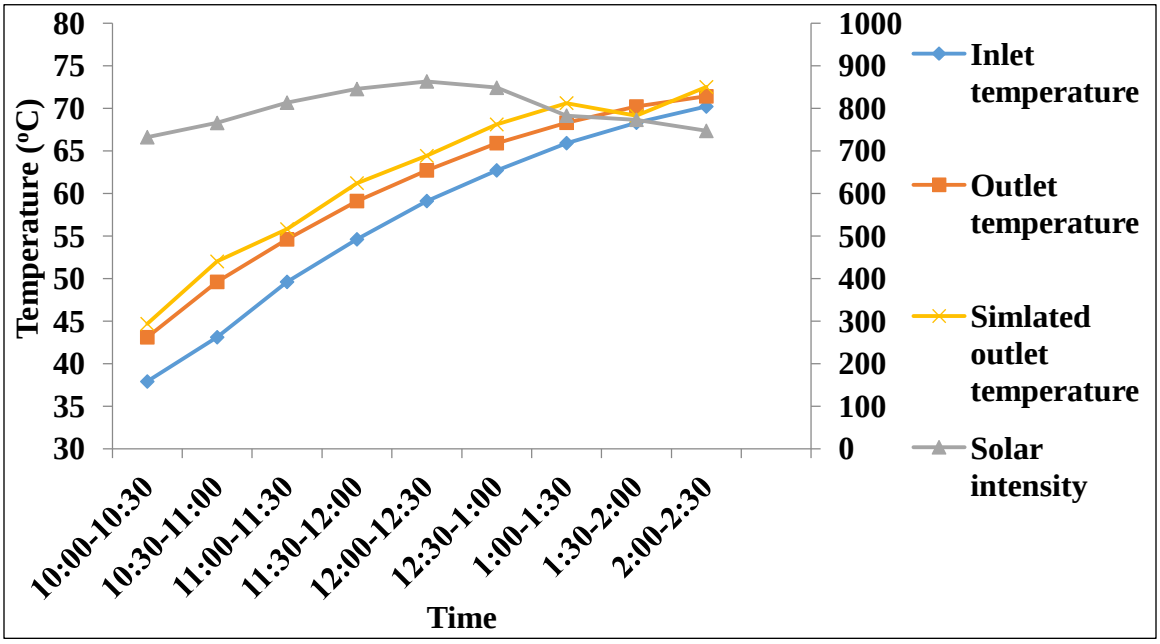

Figure 5.3: Variation in solar intensity and temperature with time for CuO-H_2O based nanofluid (0.01% conc.) at vol. flow rate of 160 l/hr

Results showed that simulated outlet temperature are little higher than the experimentally outlet temperature. This is mainly because of the higher losses due to convection to the atmosphere in the actual conditions. The maximum solar intensity observed in figure 5.1, 5.2 and 5.3 was found to be 877.214, 887.644 and 863.059 W/m^2, respectively.

II. For CuO- H_2O based nanofluid (0.05% conc.)

The figures 5.4, 5.5 and 5.6 show the variation in solar intensity and temperature with time at 0.05% concentration of nanoparticles for 100, 130 and 160 l/hr, respectively. Readings has been taken from 9:30 am to 2:30 pm in the month of May. In this case also, solar intensity shows the similar trend as at the 0.01% volume concentration i.e. rises from 9:30 am to 12:30 pm and after that, it goes on decreasing. These graphs also show that with the increase in concentration, maximum temperature also increases. These results are also validated with the CFD simulations.

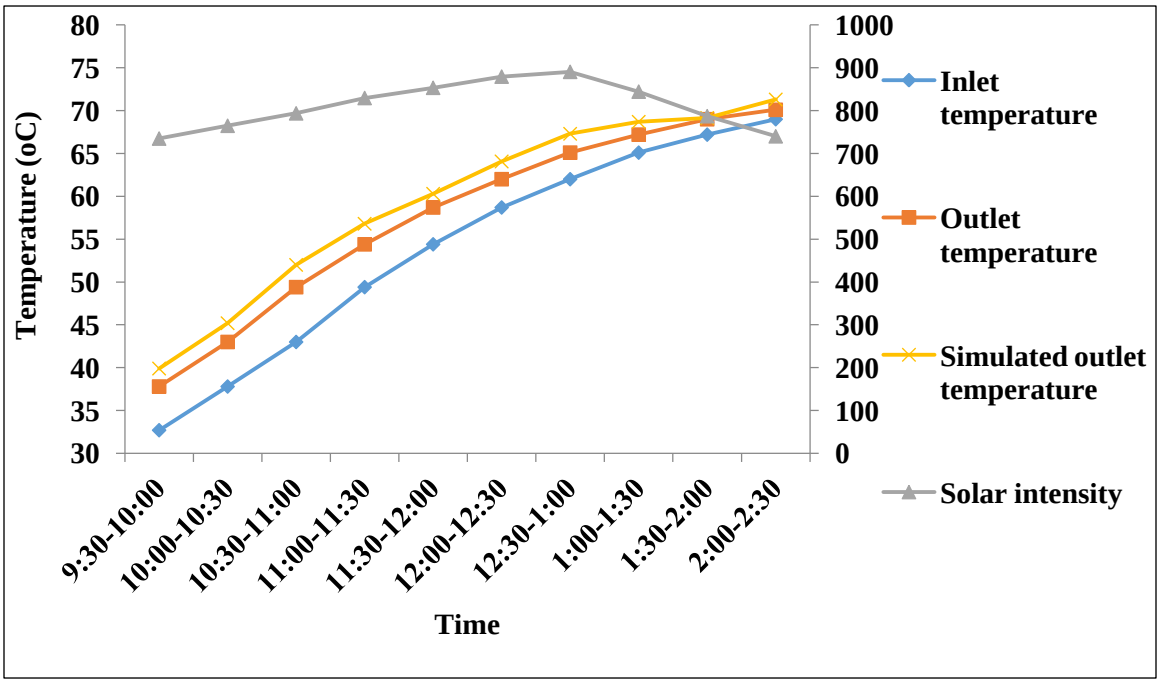

Figure 5.4: Variation in solar intensity and temperature with time for CuO-H_2O based nanofluid (0.05% conc.) at vol. flow rate of 100 l/hr

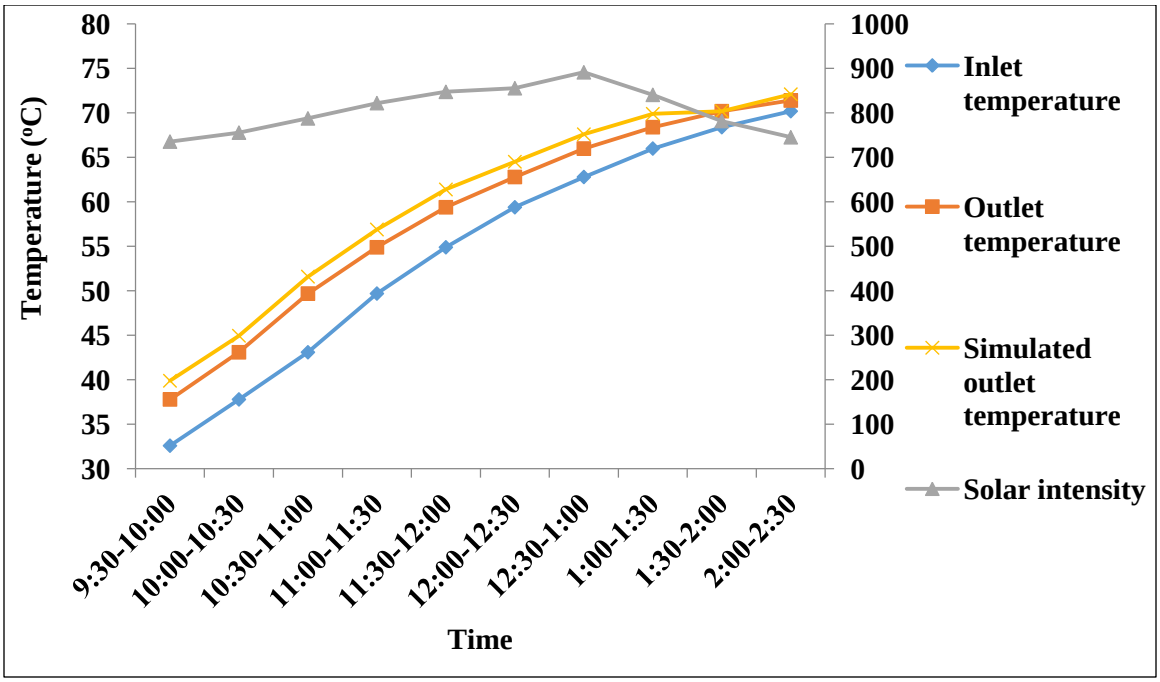

Figure 5.5: Variation in solar intensity and temperature with time for CuO-H_2O based nanofluid (0.05% conc.) at vol. flow rate of 130 l/hr

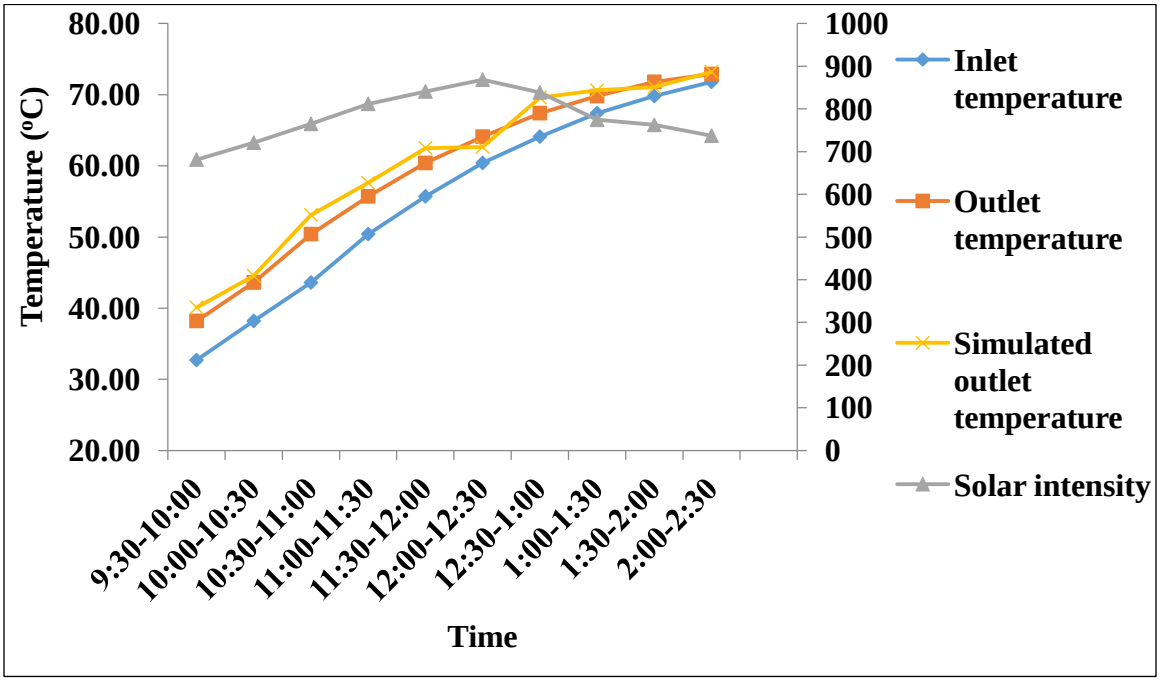

Figure 5.6: Variation in solar intensity and temperature with time for CuO-H_2O based nanofluid (0.05% conc.) at vol. flow rate of 160 l/hr

III. For CuO- H_2O based nanofluid (0.1% conc.)

The figures 5.7, 5.8 and 5.9 show the variation in solar intensity and temperature with time at 0.1% concentration of nanoparticles for 100, 130 and 160 l/hr, respectively. Readings has been taken from 9:30 am to 2:30 pm in the month of May. As the concentration increases, the maximum rise in temperature also increases because thermal conductivity is directly dependent on the concentration. The maximum temperature rise at 100,130 and 160 l/hr was found to be 72.3, 73.5 and 74.5˚C, respectively. Variation in solar intensity shows the same trend as in the previous figures.These results are also validated with the CFD simulations.

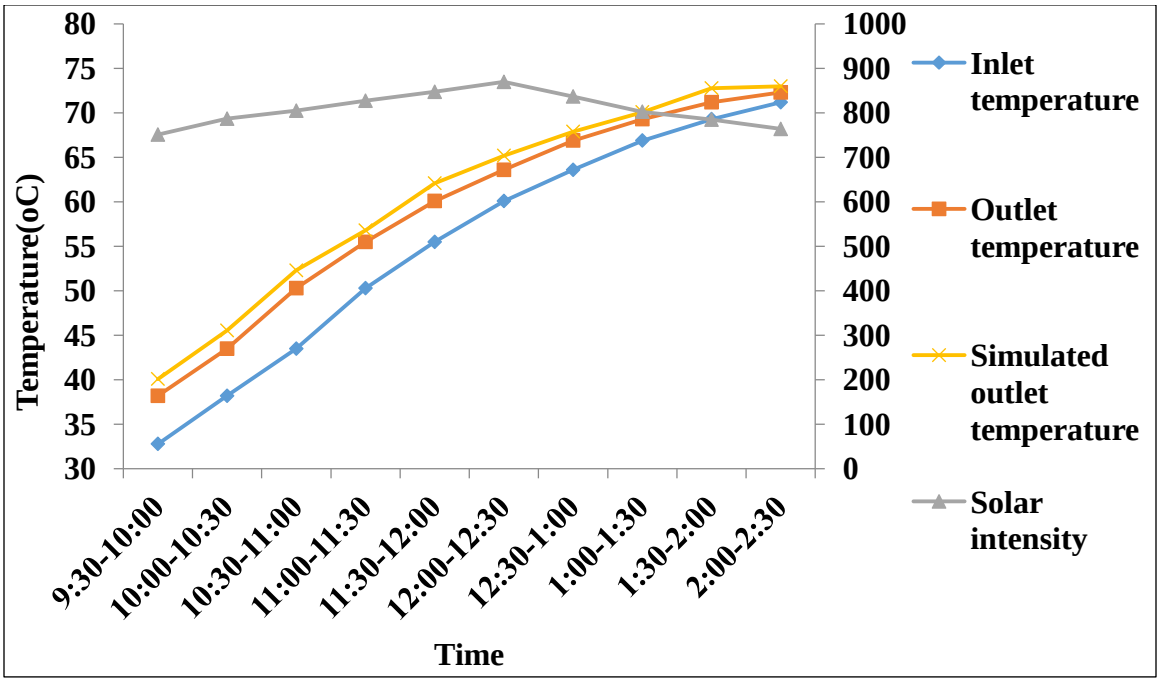

Figure 5.7: Variation in solar intensity and temperature with time for CuO-H_2O based nanofluid (0.1% conc.) at vol. flow rate of 100 l/hr

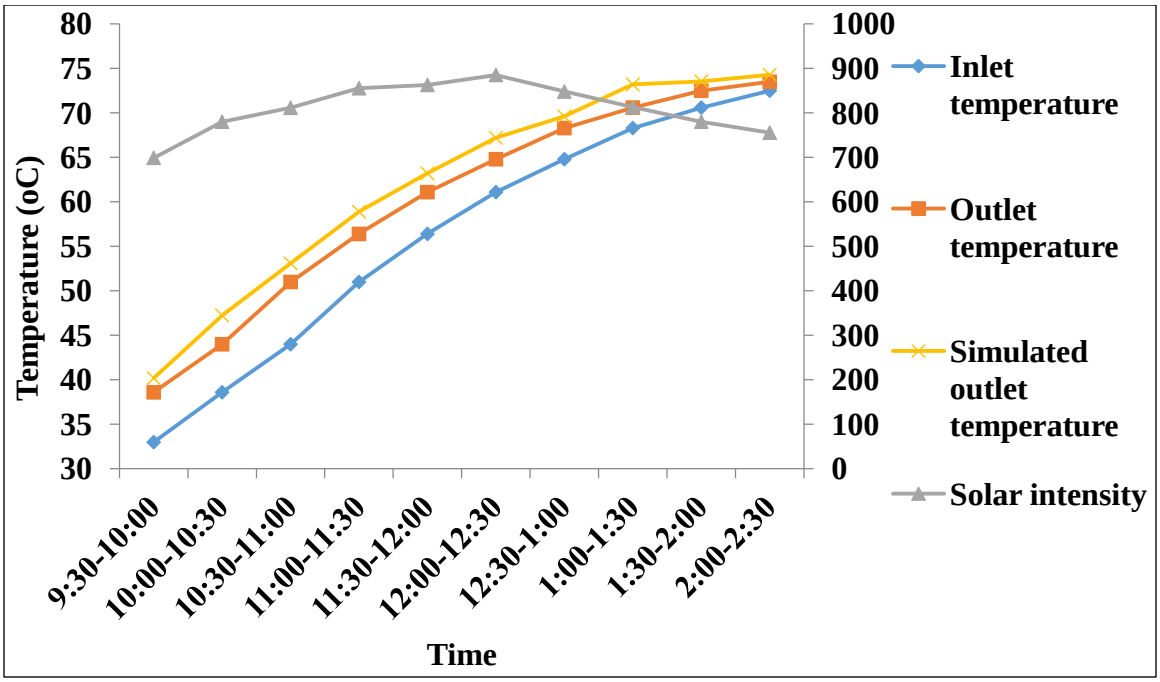

Figure 5.8: Variation in solar intensity and temperature with time for CuO-H_2O based nanofluid (0.1% conc.) at vol. flow rate of 130 l/hr

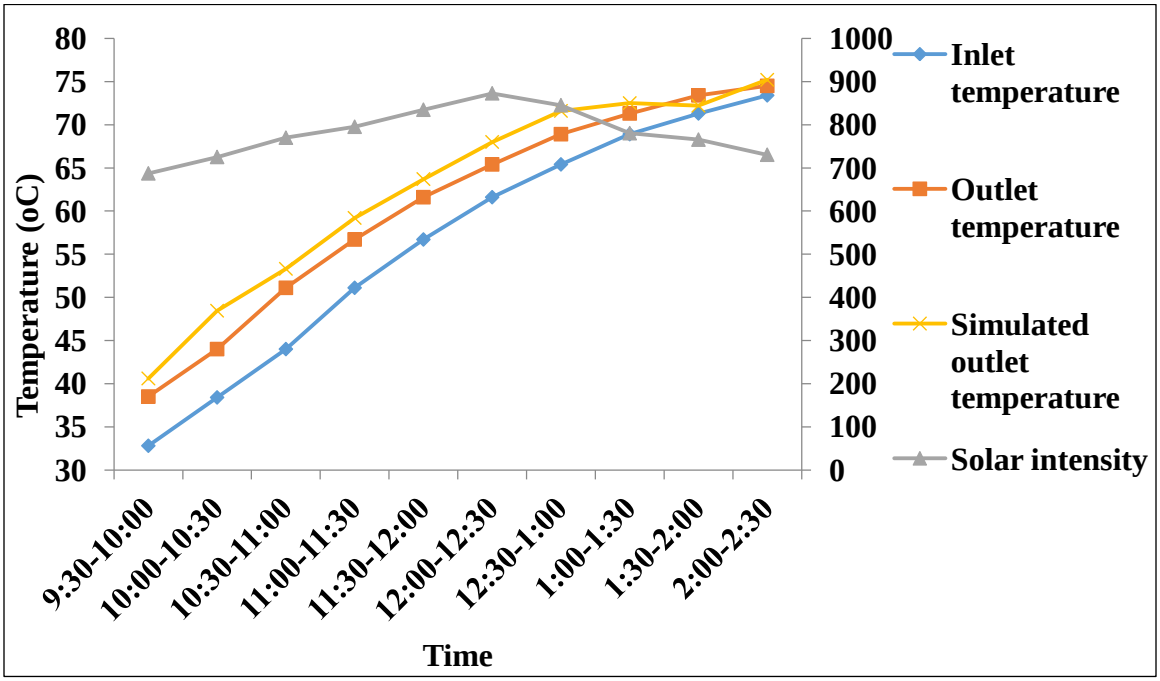

Figure 5.9: Variation in solar intensity and temperature with time for CuO-H_2O based nanofluid (0.1% conc.) at vol. flow rate of 160 l/hr

5.1.2 Variation in temperature difference with time for CuO- H_2O based nanofluid

These figure 5.10, 5.11 and 5.12 shows the variation in temperature difference of nanofluids with time at different flow rates (100 l/hr, 130 l/hr and 160 l/hr) for a particular concentration. Temperature difference is directly proportional to the heat intensity and is dependent on several factors such as, wind speed, power supply etc. Maximum temperature difference is reported on the 160 l/hr flow rate. At the lowest mass flow rate i.e. 100 l/hr, the residence time of working fluid is high inside the collector but heat losses are predominant. Therefore, temperature difference is minimum in this flow rate. The graphs also show that with increase in concentration of nanoparticle, the temperature difference increases.

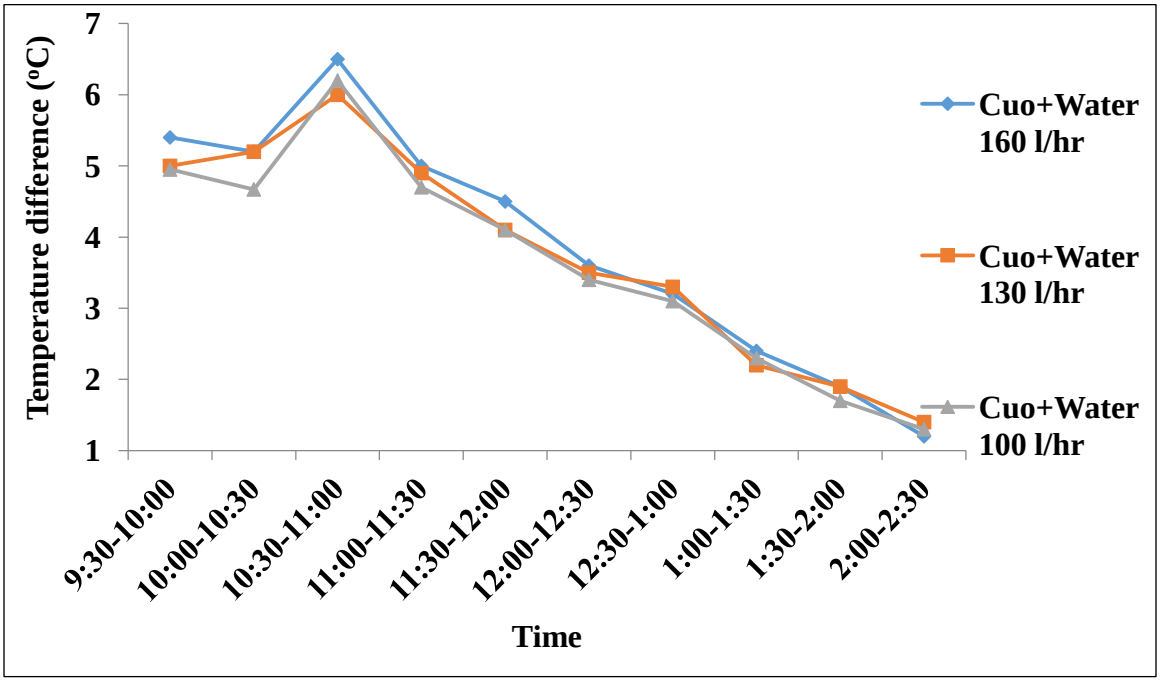

Figure 5.10: Variation in temperature difference with time for CuO-H_2O based nanofluid (0.01% conc.) at different vol. flow rate

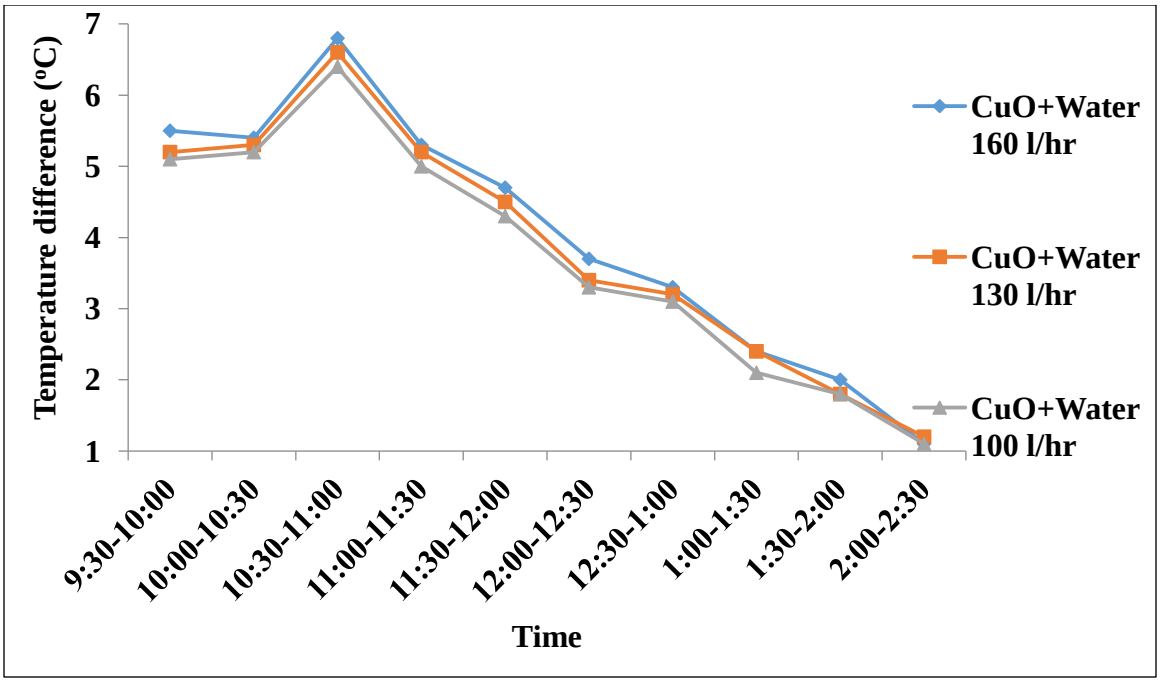

Figure 5.11: Variation in temperature difference with time for CuO-H_2O based nanofluid (0.05% conc.) at different vol. flow rate

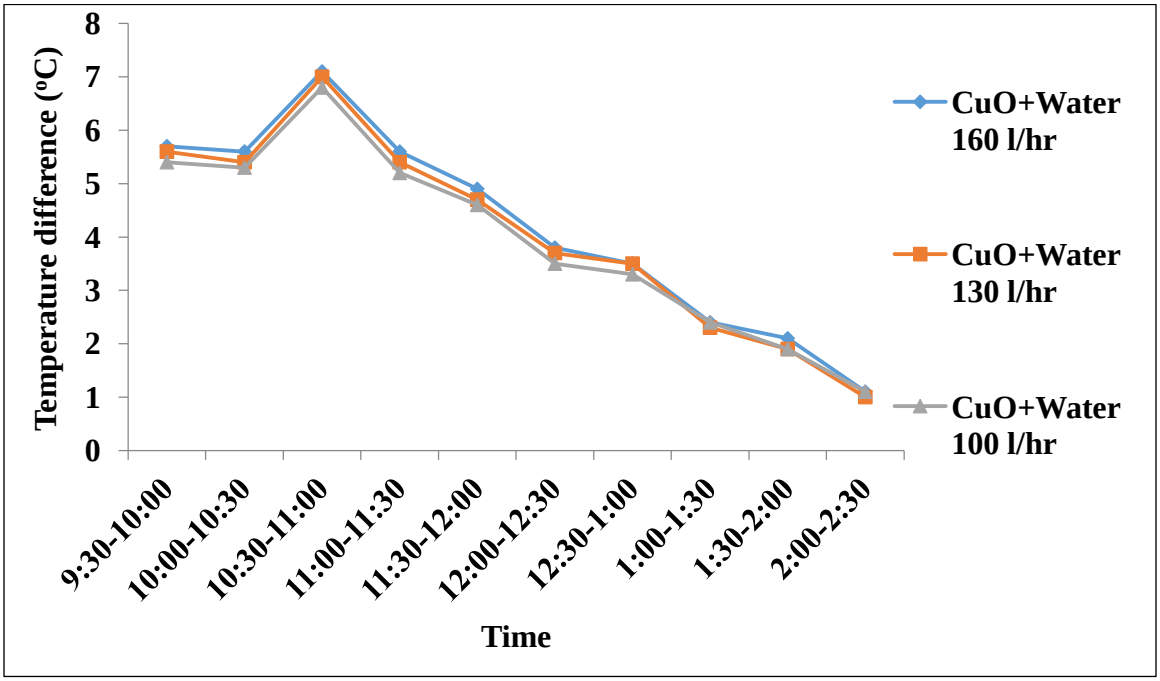

Figure 5.12: Variation in temperature difference with time for CuO-H_2O based nanofluid (0.1% conc.) at different vol. flow rate

5.1.3Variation in useful heat gain with time for CuO-water based nanofluid

The Figures5.13, 5.14 and 5.15 show the variation in the useful heat gain with time at different flow rates. Useful heat gain depends on various parameters such as, solar intensity, temperature, mass flow rate and specific heat of the fluid. At 0.0

1% concentration, specific heat of the nanofluid is less and higher temperature difference is reported, when compared to the base fluid. Useful heat gain increases with the increase in the mass flow rate. The maximum useful heat gain is found to be 1144.31 Watt between 10:30 am and 11:00 am.

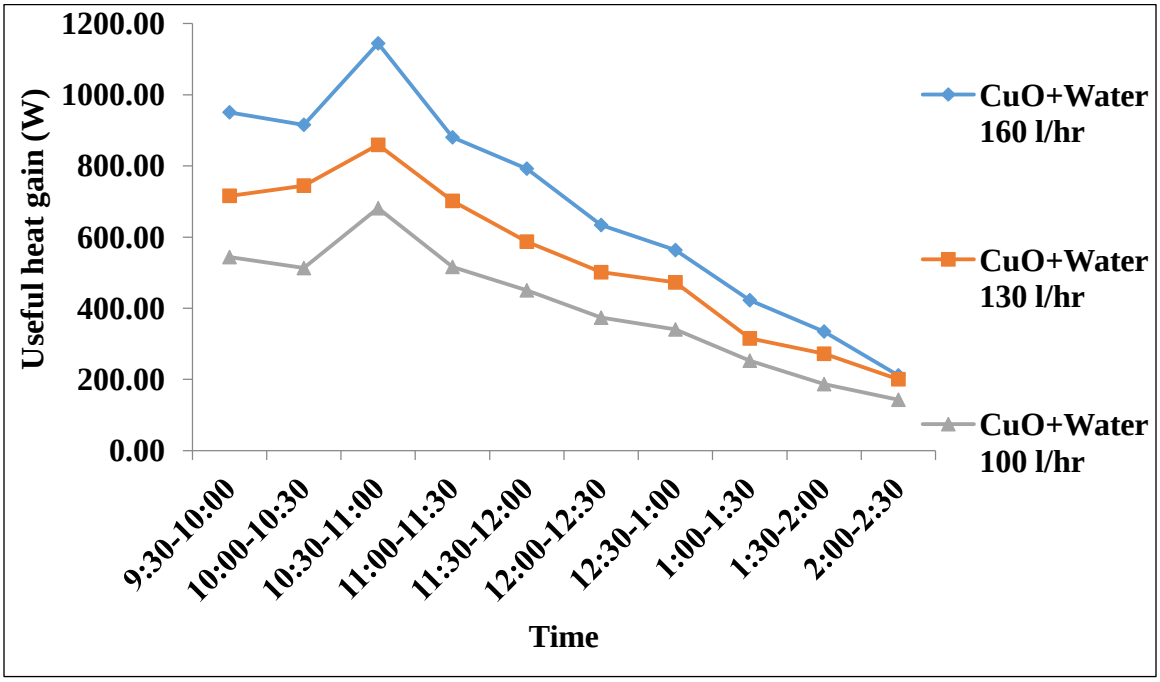

Figure 5.13: Variation in useful heat gain with time for CuO-H_2O based nanofluid (0.01% conc.) at different vol. flow rate

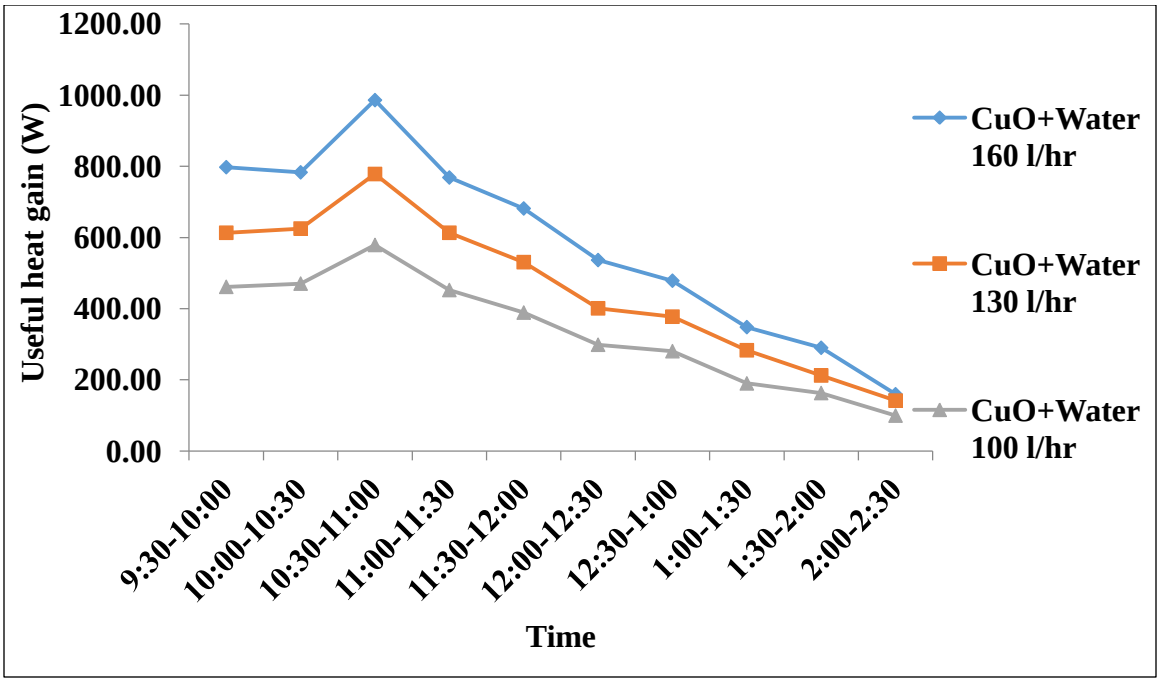

Figure 5.14: Variation in useful heat gain with time for CuO-H_2O based nanofluid (0.05% conc.) at different vol. flow rate

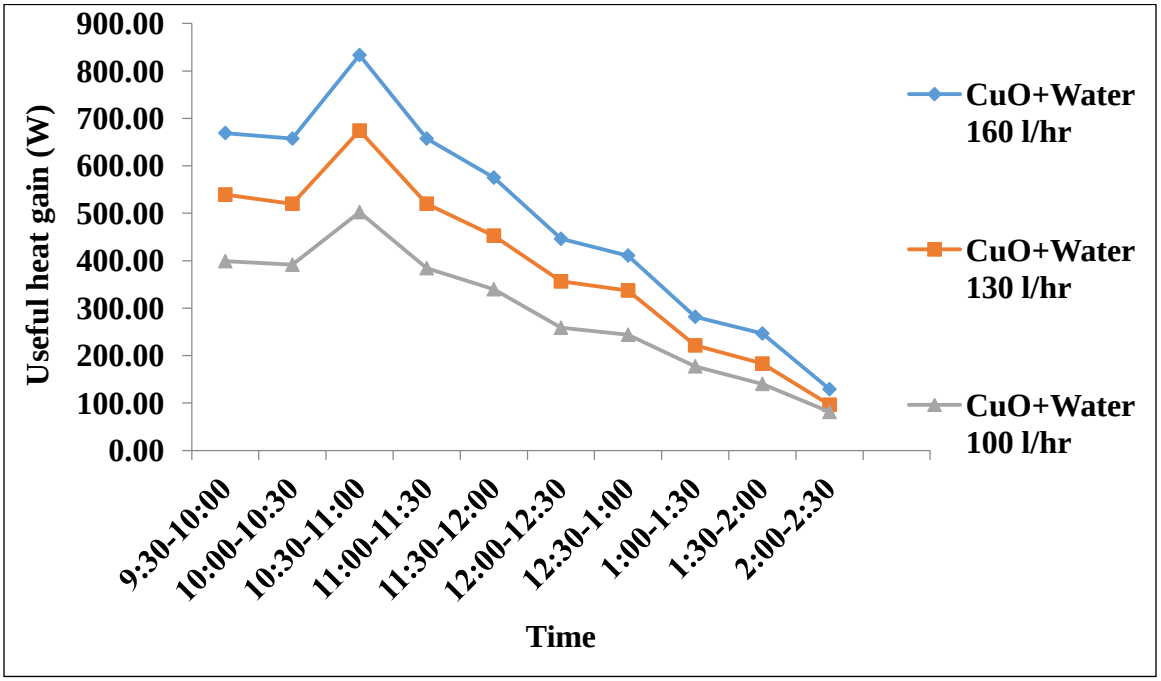

Figure 5.15: Variation in useful heat gain with time for CuO-H_2O based nanofluid (0.1% conc.) at different vol. flow rate

5.1.4 Variation in instantaneous efficiency with time for CuO-water based nanofluid

The Figures 5.16, 5.17 and 5.18 shows the variation in the instantaneous efficiency with time at different flow rates (100, 130 and 160 l/hr) for 0.01, 0.05 and 0.1% conc., respectively.All the graph shows that the maximum instantaneous efficiency was obtained between 10:30 and 11:00 am. The graph also shows that maximum instantaneous efficiency was obtained at 160 l/hr, followed by the nanofluids at 130 l/hr and 100 l/hr. The reason behind this is the high useful heat gain and the highest temperature difference, in the beginning.

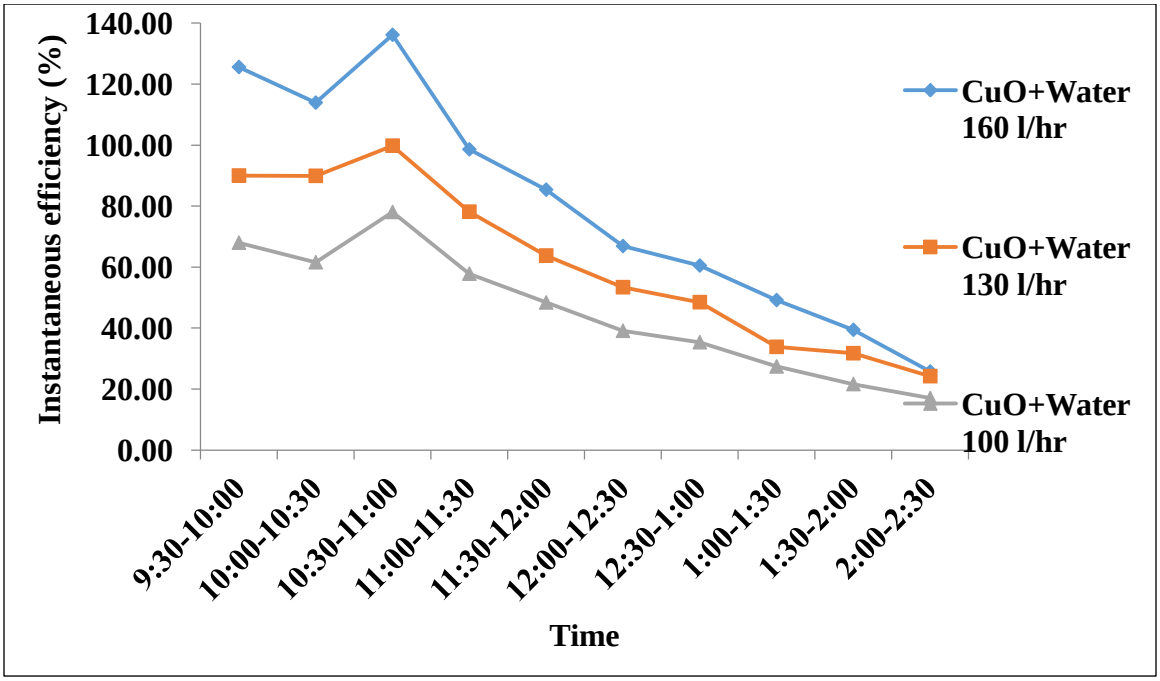

Figure 5.16: Variation in instantaneous efficiency with time for CuO-H_2O based nanofluid (0.01% conc.) at different vol. flow rate

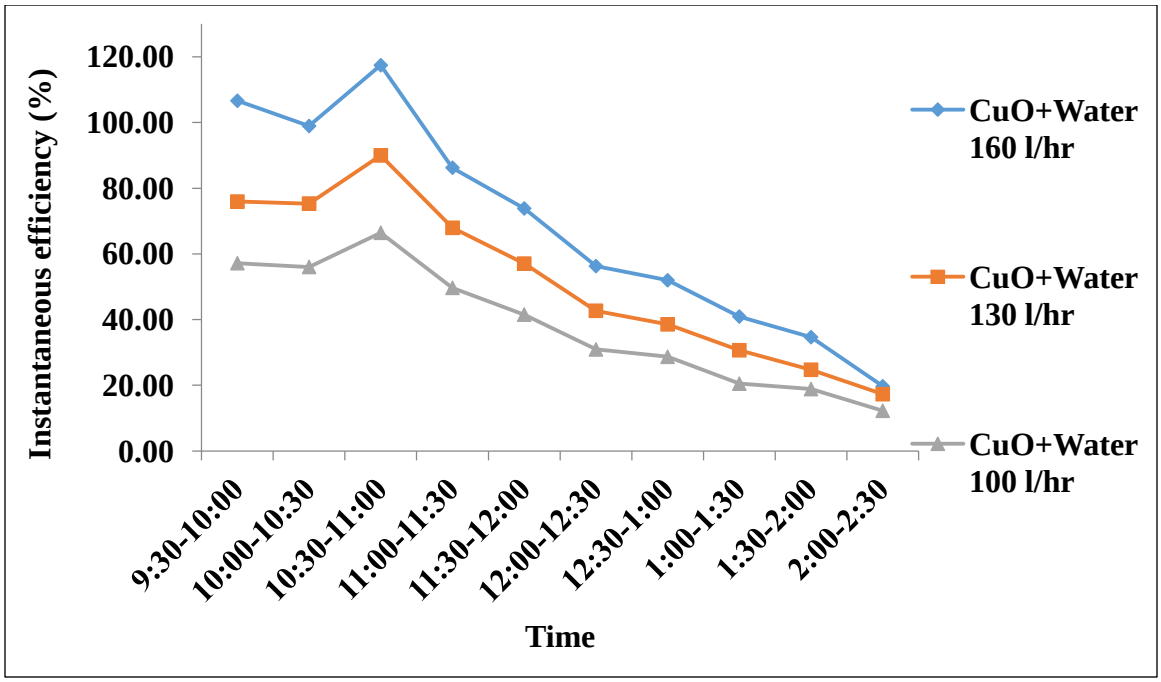

Figure 5.17: Variation in instantaneous efficiency with time for CuO-H_2O based nanofluid (0.05% conc.) at different vol. flow rate

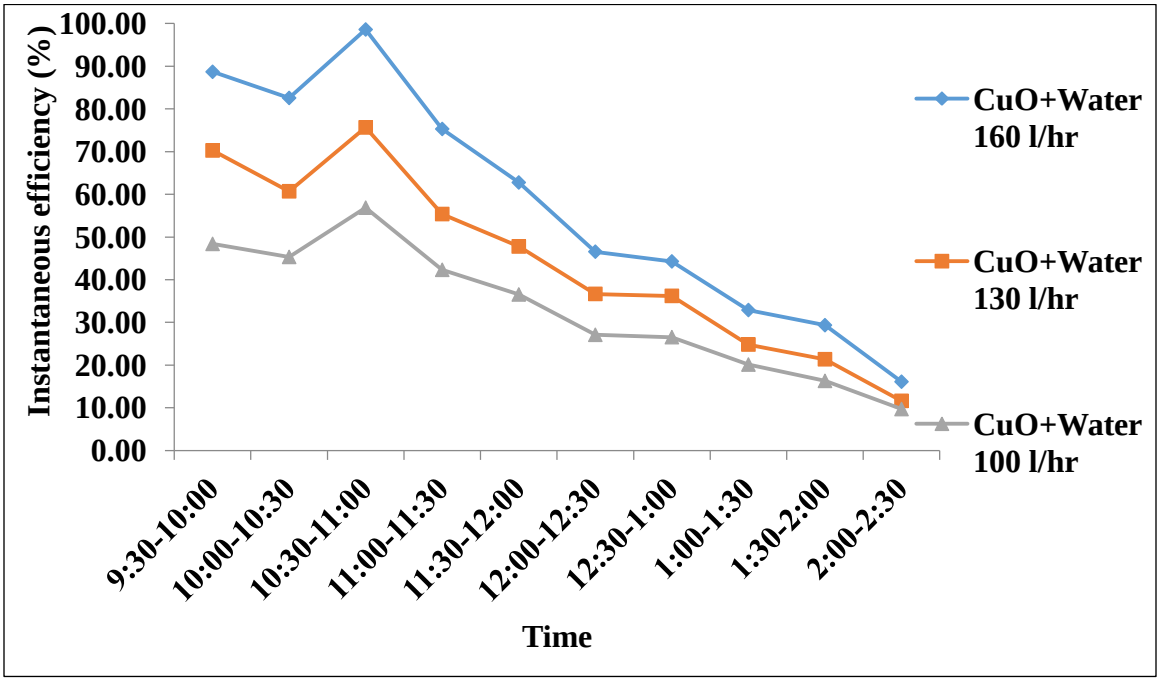

Figure 5.18: Variation in instantaneous efficiency with time for CuO-H_2O based nanofluid (0.1% conc.) at different vol. flow rate

5.1.5 Variation in thermal efficiency with time for CuO-water based nanofluid

The Figures 5.19, 5.20 and 5.21 show the variation of the thermal efficiency with time at different flow rates (100, 130 and 160 l/hr). The maximum thermal efficiency was observed at the highest flow rate (160 l/hr) due to the highest useful gain, highest temperature difference and minimum convection losses. The maximum thermal efficiency at 0.05% concentration was 8.6151, 8.9521 and 9.502% observed at 100, 130 and 160l/hr.

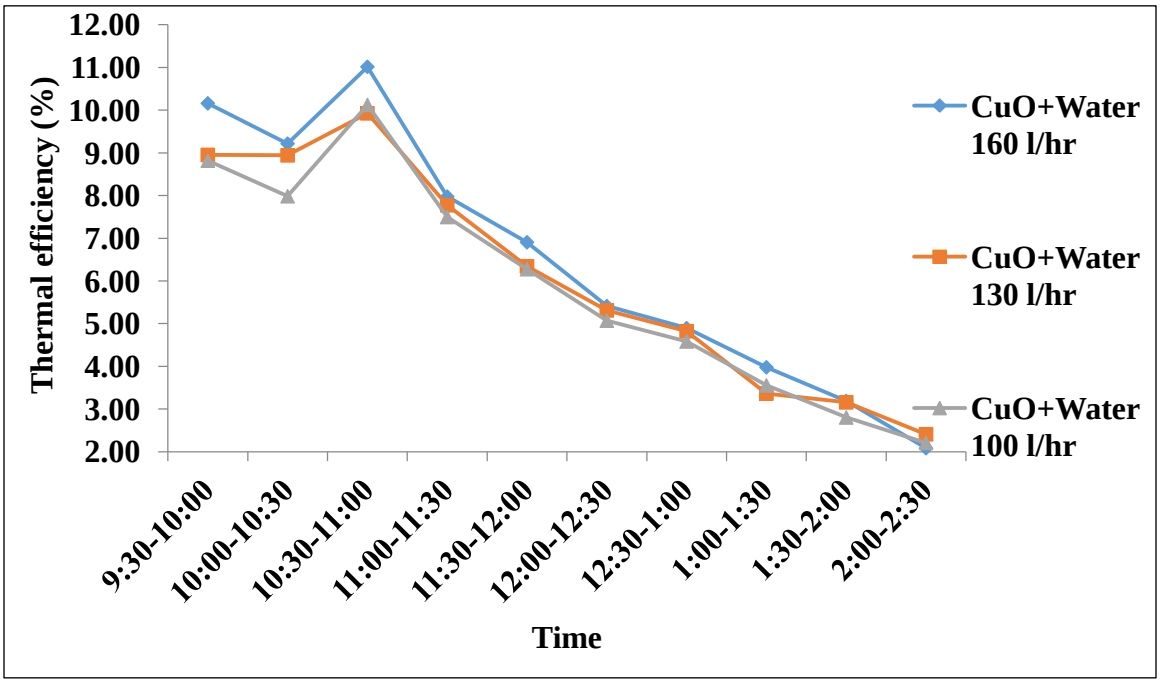

Figure 5.19: Variation in thermal efficiency with time for CuO-H_2O based nanofluid (0.01% conc.) at different vol. flow rate

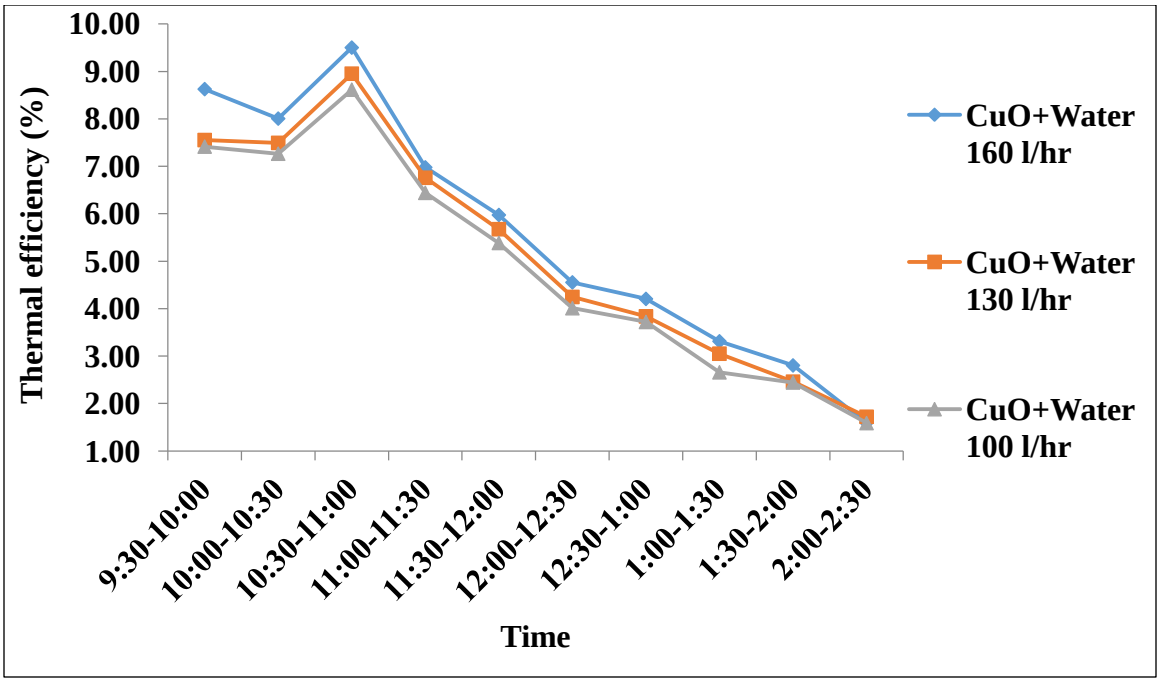

Figure 5.20: Variation in thermal efficiency with time for CuO-H_2O based nanofluid (0.05% conc.) at different vol. flow rate

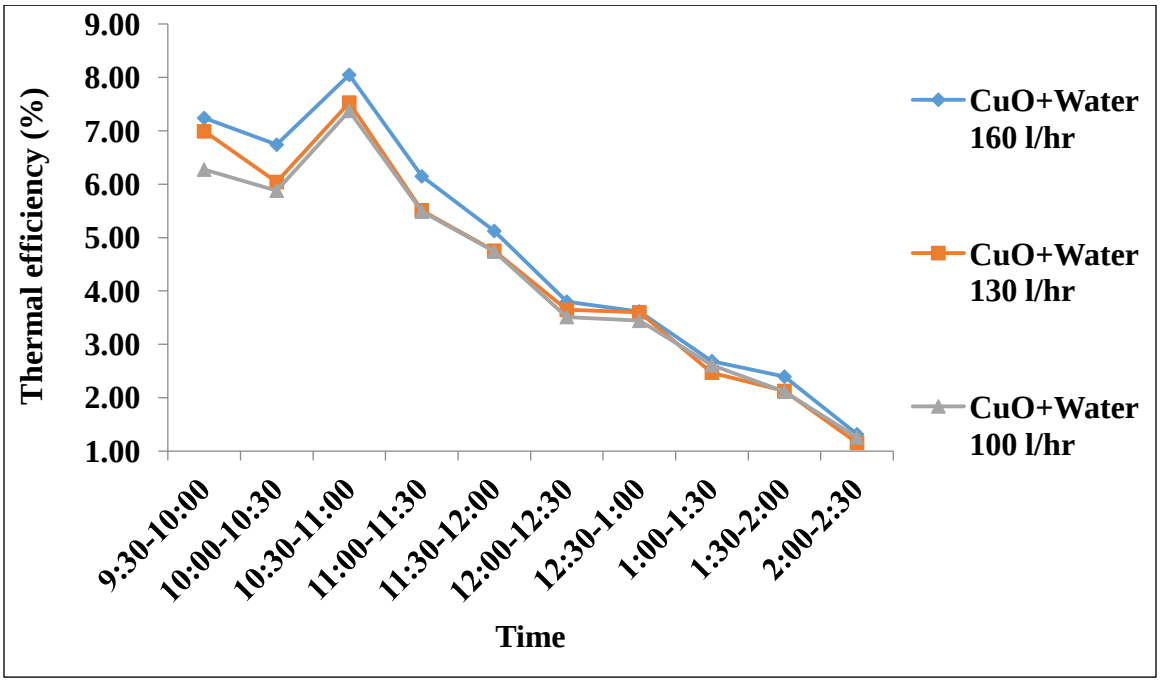

Figure 5.21: Variation in thermal efficiency with time for CuO-H_2O based nanofluid (0.1% conc.) at different vol. flow rate

5.2 Performance Of Parabolic Solar Collector Using Cuo-Ethylene Glycol Based Nanofluids

5.2.1 Variation in solar intensity and temperature with time

I. For CuO-EG (40:60) based nanofluid (0.01% conc.)

Figures 5.22, 5.23 and 5.24 show the variation in solar intensity and temperature with time at 0.01% concentration of nanoparticles for 100, 130 and 160 l/hr, respectively. Readings has been taken from 9:30 am to 2:30 pm in the month of May. In this case, initially, solar intensity rises from 9:30 am to 12:30 pm and after that, it goes on decreasing. Due to the recirculating system, inlet and outlet temperature continuously increases with time from 9:30 am to 2:30 pm. But in the beginning, rises in temperature was found to be higher and with the increase in time, it gets lessened. These results are also validated with the CFD simulations. Maximum value of solar intensity observed was 878.704, 876.469 and 858.589 for 100, 130 and 160 l/hr, respectively.

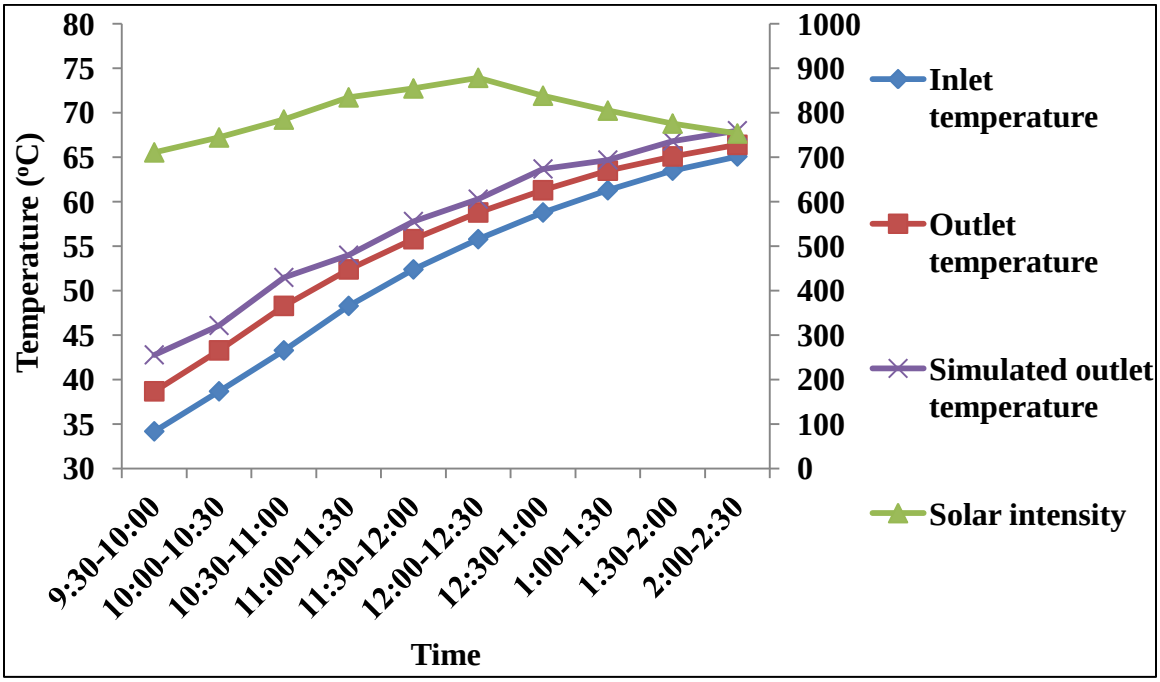

Figure 5.22: Variation in solar intensity and temperature with time for CuO-EG based nanofluid (0.01% conc.) at vol. flow rate of 100 l/hr

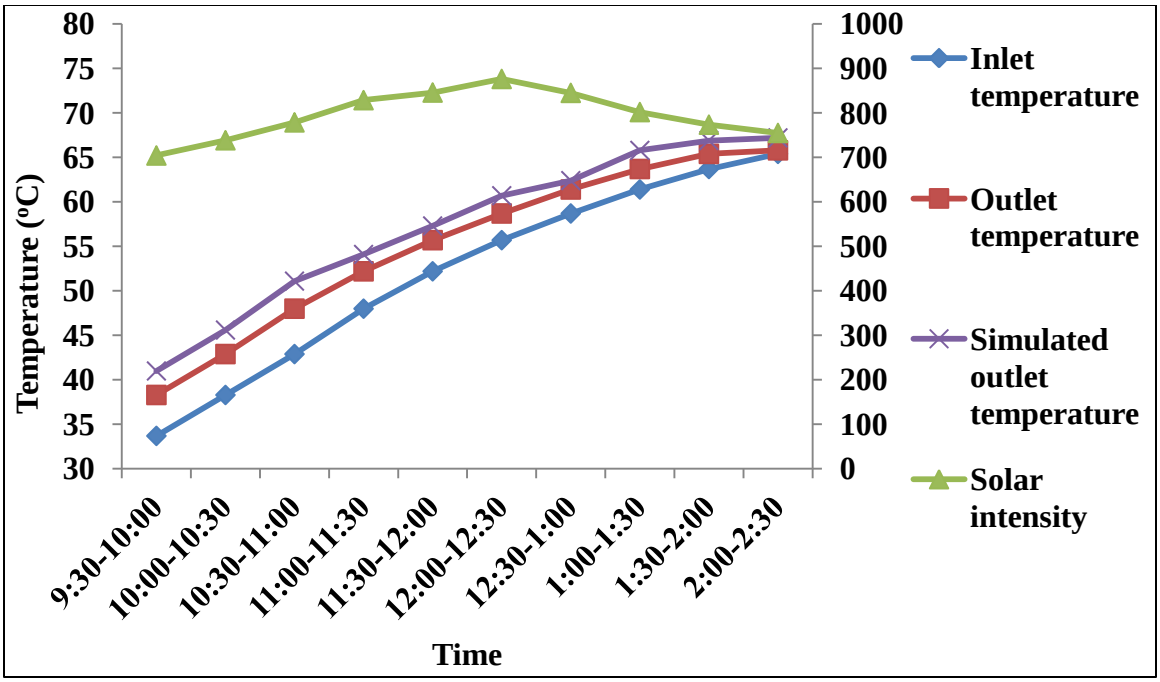

Figure 5.23: Variation in solar intensity and temperature with time for CuO-EG based nanofluid (0.05% conc.) at vol. flow rate of 130 l/hr

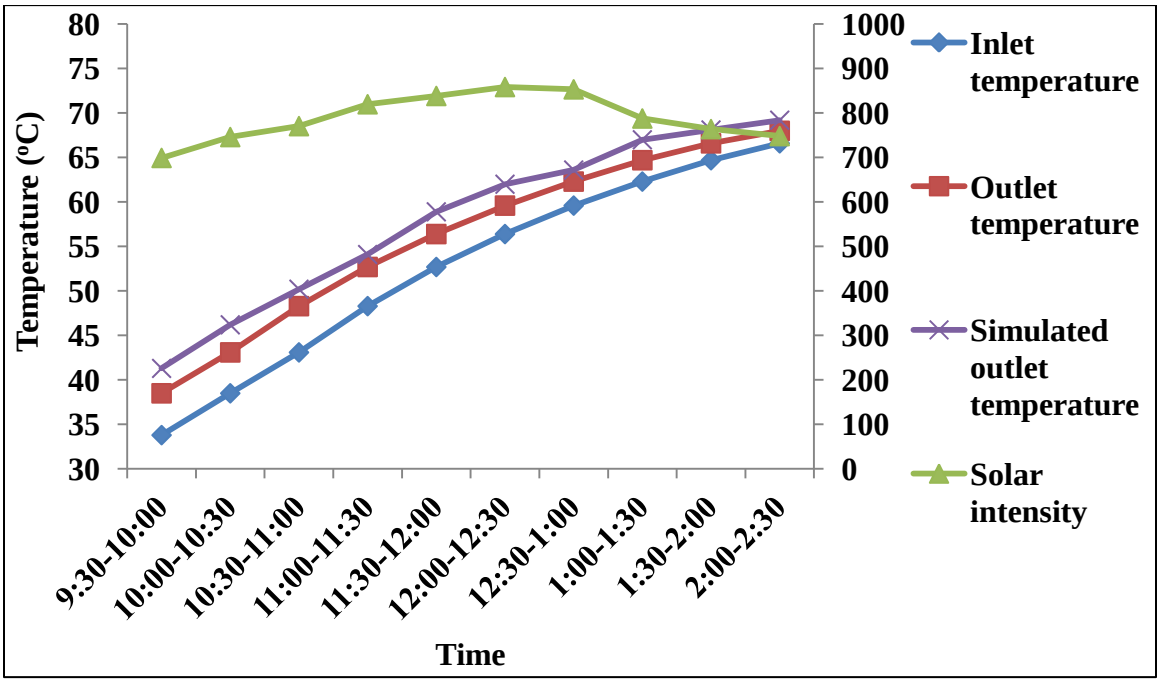

Figure 5.24: Variation in solar intensity and temperature with time for CuO-EG based nanofluid (0.01% conc.) at vol. flow rate of 160 l/hr

5.2.2 Variation in temperature difference with time for CuO-ethylene glycol based nanofluid

These figures 5.25 and 5.26 show the variation in temperature difference of nanofluids with time at different flow rates (100 l/hr, 130 l/hr and 160 l/hr) for a particular concentration. Temperature difference is directly proportional to the heat intensity and is dependent on several factors such as, wind speed, power supply etc. Maximum temperature difference is reported on the 160 l/hr flow rate. At the lowest mass flow rate i.e. 100 l/hr, the residence time of working fluid is high inside the collector but heat losses are predominant. Therefore, temperature difference is minimum in this flow rate. The graphs also show that with increase in concentration of nanoparticle, the temperature difference increases.

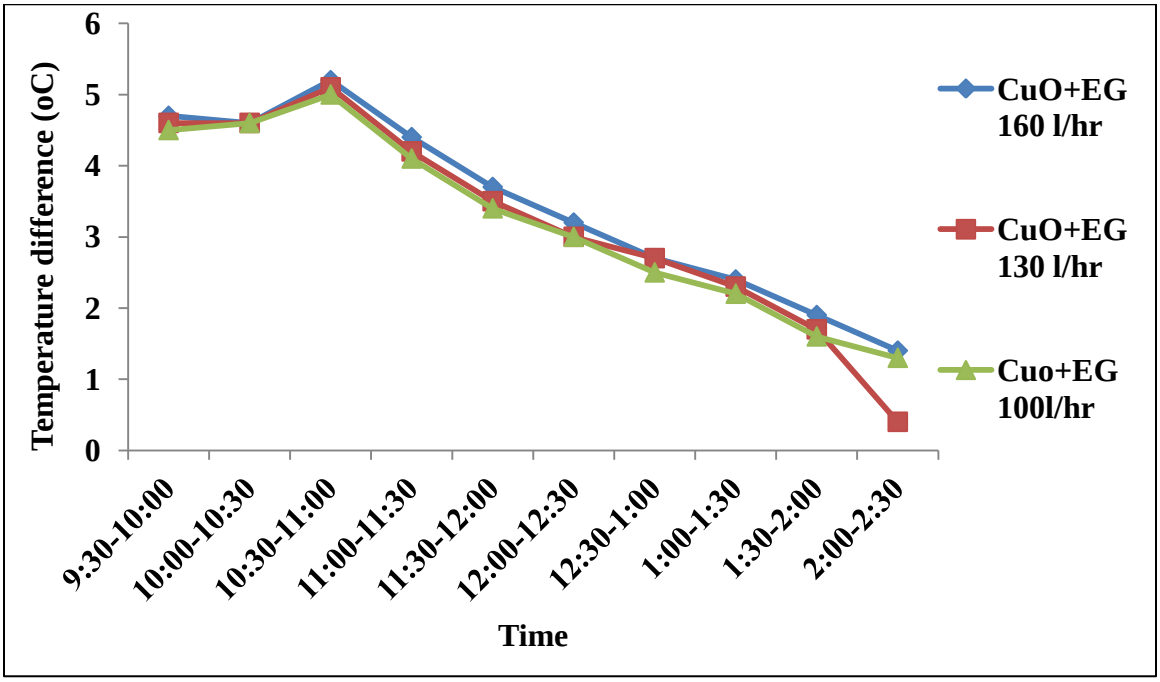

Figure 5.25: Variation in temperature difference with time for CuO-EG based nanofluid (0.01% conc.) at different vol. flow rate

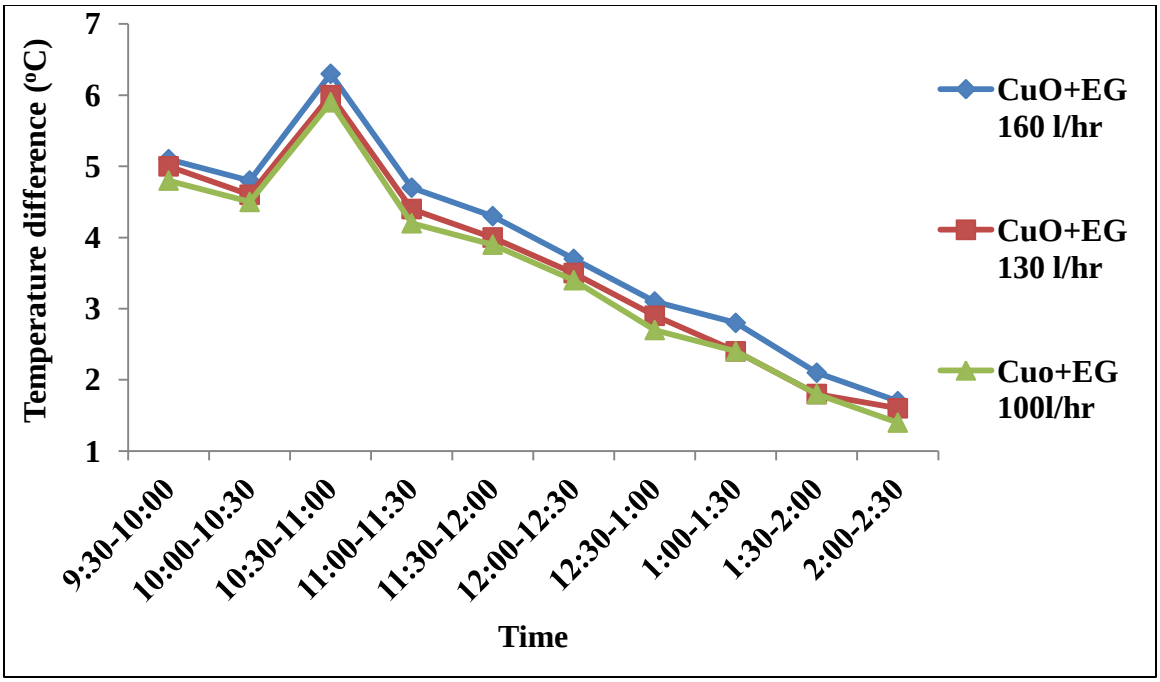

Figure 5.26: Variation in temperature difference with time for CuO-EG based nanofluid (0.1% conc.) at different vol. flow rate

5.2.3 Variation in useful heat gain with time for CuO-ethylene glycol based nanofluid

The Figures 5.27 and 5.28 show the variation in the useful heat gain with time at different flow rates. Useful heat gain depends on various parameters such as, solar intensity, temperature, mass flow rate and specific heat of the fluid. At 0.01% concentration, specific heat of the nanofluid is less and higher temperature difference is reported, when compared to the base fluid. Useful heat gain increases with the increase in the mass flow rate. The maximum useful heat gain is found to be 832.88 Watt between 10:30 am and 11:00 am.

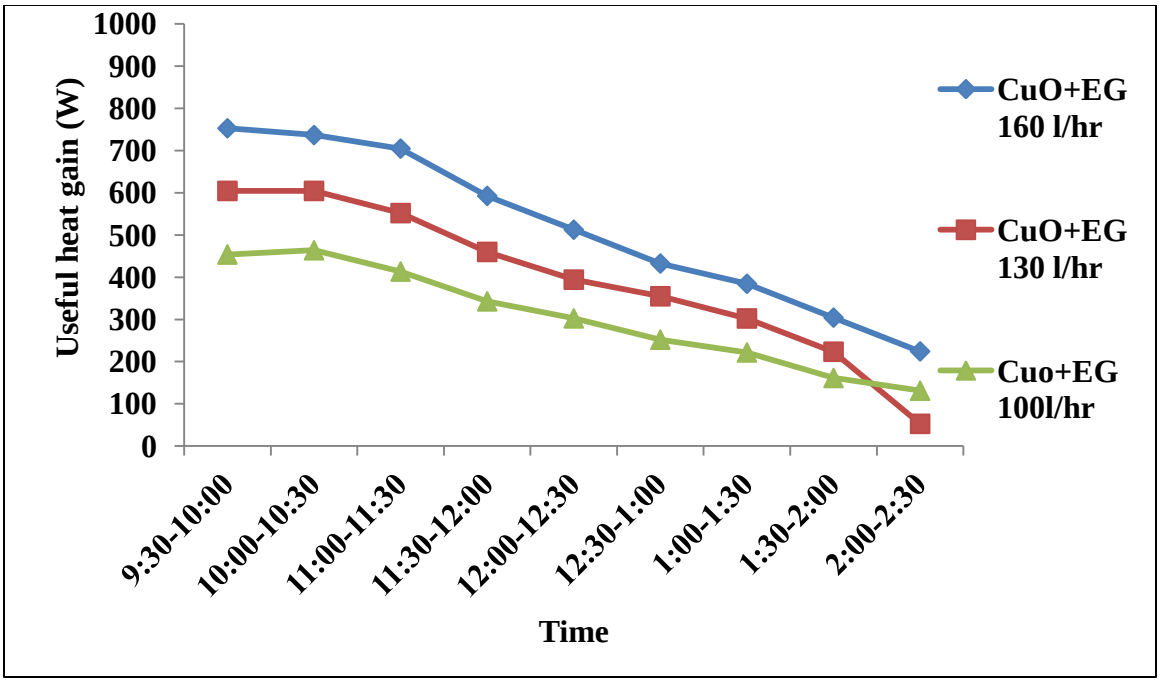

Figure 5.27: Variation in useful heat gain with time for CuO-EG based nanofluid (0.01% conc.) at different vol. flow rate

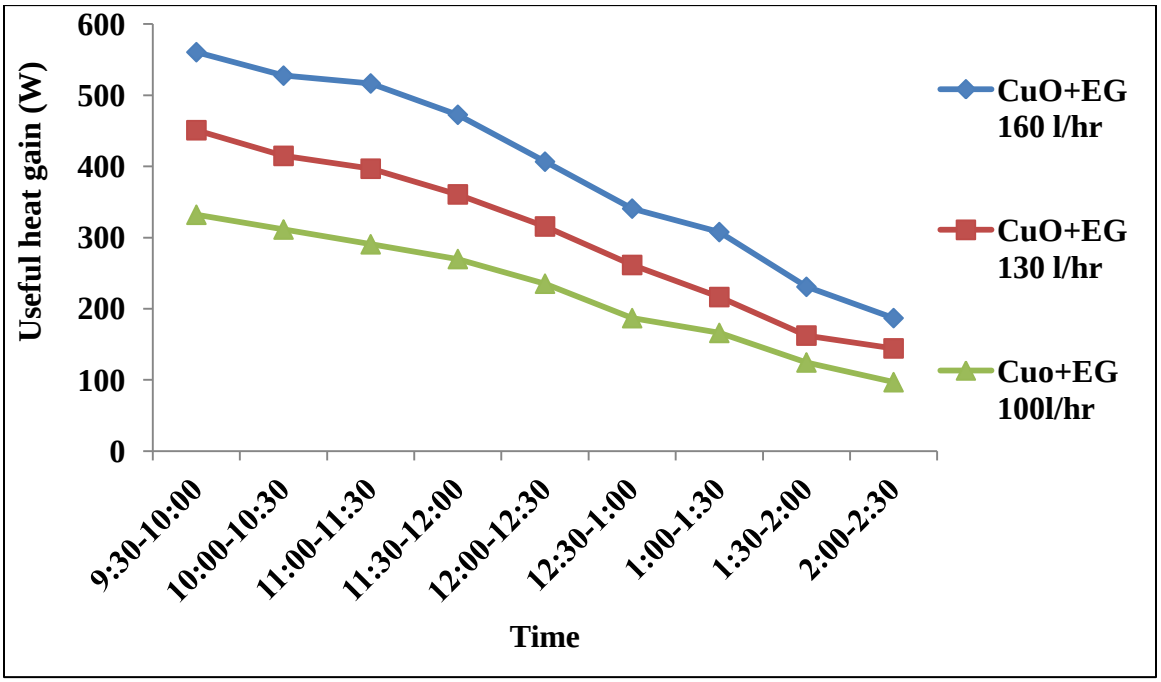

Figure 5.28: Variation in useful heat gain with time for CuO-EG based nanofluid (0.1% conc.) at different vol. flow rate

5.2.4 Variation in instantaneous efficiency with time for CuO-ethylene glycol based nanofluid

The Figures 5.29 and 5.30 show the variation in the instantaneous efficiency with time at different flow rates (100, 130 and 160 l/hr) for 0.01, 0.05 and 0.1% conc., respectively. All the graph shows that the maximum instantaneous efficiency was obtained between 10:30 and 11:00 am and with the increase in time, instantaneous efficiency decreases for all the flow rates. The graph also shows that maximum instantaneous efficiency was obtained at 160 l/hr, followed by the nanofluids at 130 l/hr and 100 l/hr. The reason behind this is the high useful heat gain and the highest temperature difference, in the beginning.

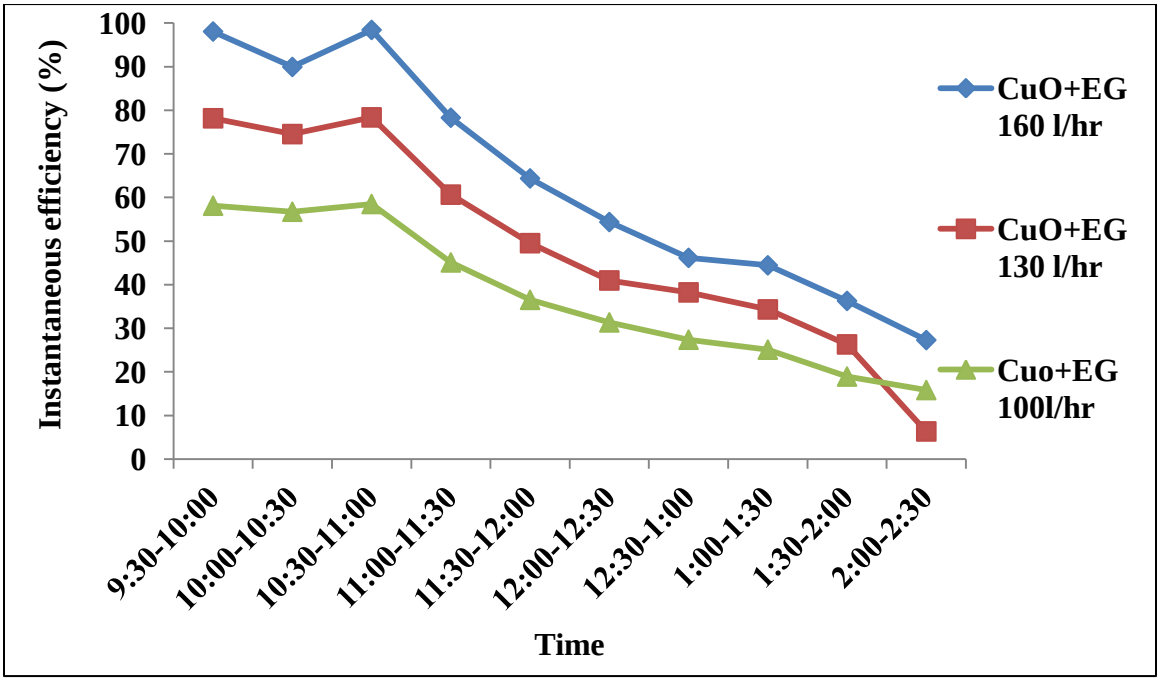

Figure 5.29: Variation in instantaneous efficiency with time for CuO-EG based nanofluid (0.01% conc.) at different vol. flow rate

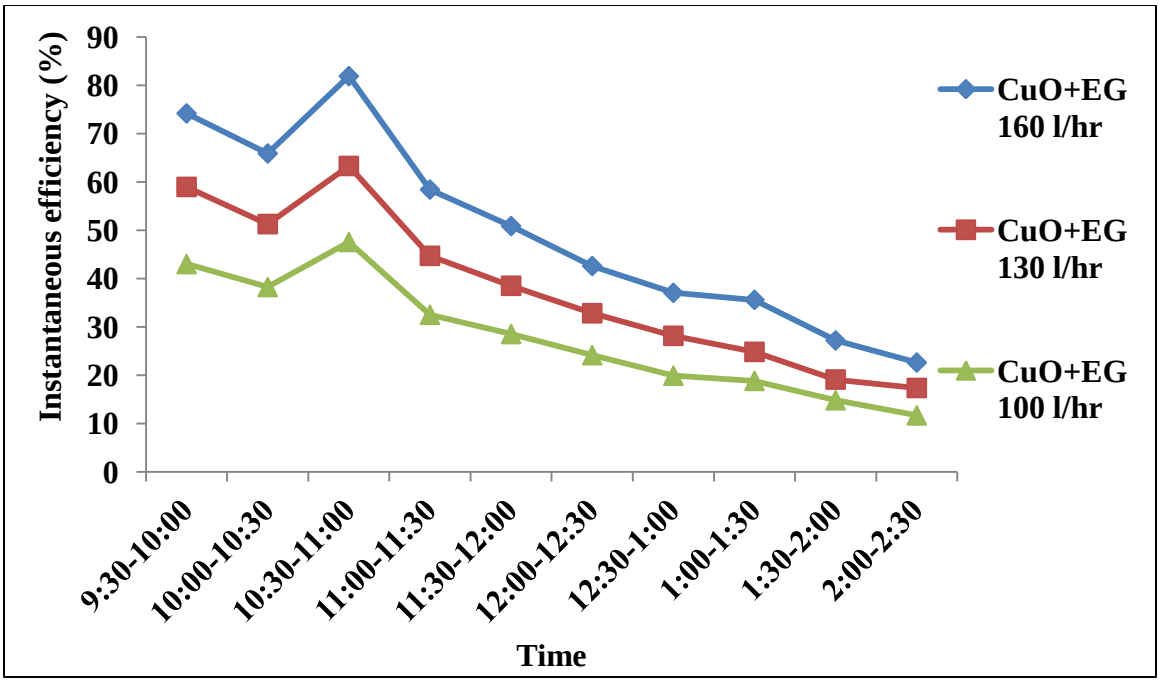

Figure 5.30: Variation in instantaneous efficiency with time for CuO-EG based nanofluid (0.1% conc.) at different vol. flow rate

5.2.5 Variation in thermal efficiency with time for CuO-ethylene glycol based nanofluid

This Figure 5.31 shows the variation of the thermal efficiency with time at different flow rates (100, 130 and 160 l/hr). The maximum thermal efficiency was observed at the highest flow rate (160 l/hr) due to the highest useful gain, highest temperature difference and minimum convection losses. The maximum thermal efficiency at 0.1% concentration was 6.17, 6.30 and 6.68% observed at 100, 130 and 160 l/hr.

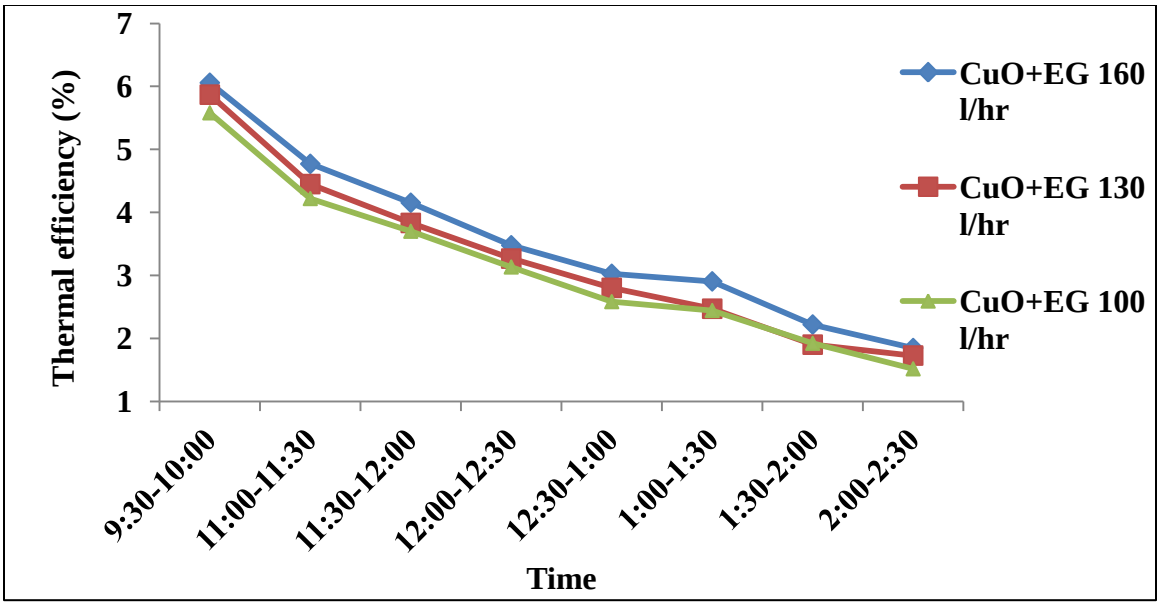

Figure 5.31: Variation in thermal efficiency with time for CuO-EG based nanofluid (0.1% conc.) at different vol. flow rate

5.3 Comparison of thermal efficiency of nanofluids (CuO-water and CuO-ethylene glycol based nanofluids) and base fluids (water and ethylene glycol)

I. For 0.01% concentration

The Figures 5.32 and 5.33 show the comparison of thermal efficiency between nanofluids (CuO-water and CuO-ethylene glycol based nanofluids)and base fluids (water and ethylene glycol) at 0.01% concentration for 100 and 160 l/hr. CuO-water based nanofluids show maximum thermal efficiency. At the starting, efficiency is high and as the time progresses, efficiency starts declining due to the decrease in temperature rise. CuO-water based nanofluid has highest efficiency as compared to CuO-ethylene glycol nanofluids, water and ethylene glycol because of the highest conductivity. Water has the maximum specific heat as compared to other fluids but due to less temperature rise, its efficiency is less than the CuO-water based nanofluid. With the addition of CuO nanoparticle in water, maximum temperature rise occurs and also, it has higher specific heat as compared to ethylene glycol and CuO-ethylene glycol based nanofluid. Therefore, CuO-water based nanofluid has the highest efficiency.

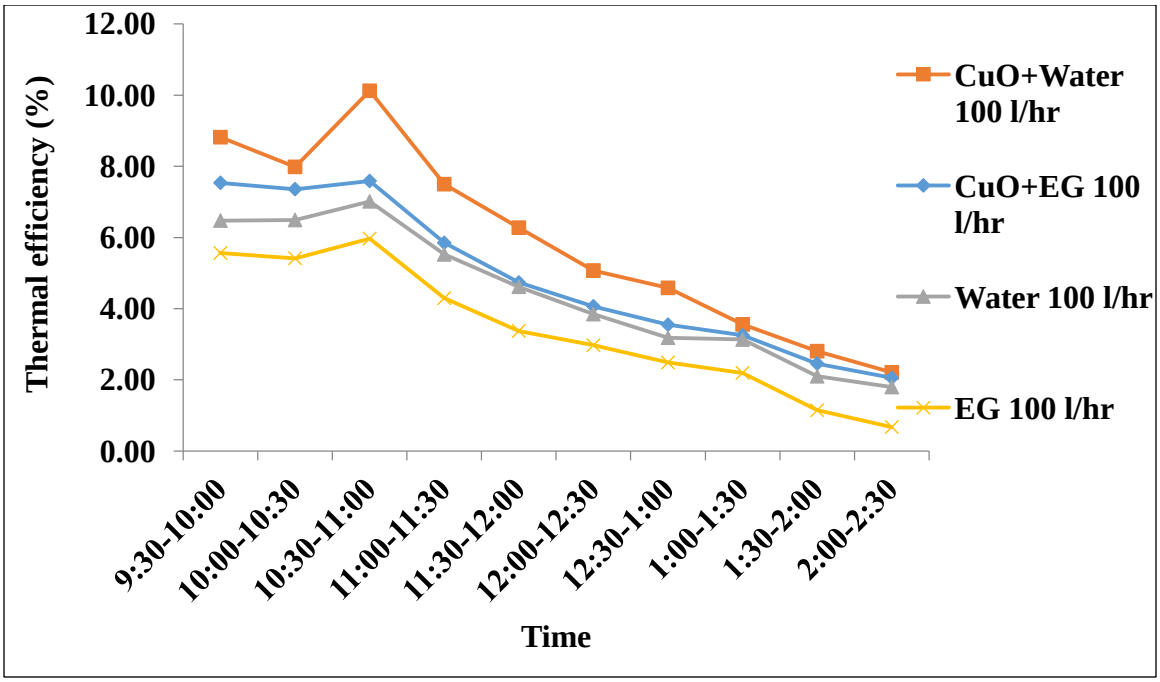

Figure 5.32: Variation in thermal efficiency with time for nanofluids (0.01%) and base fluids at 100 l/hr vol. flow rate

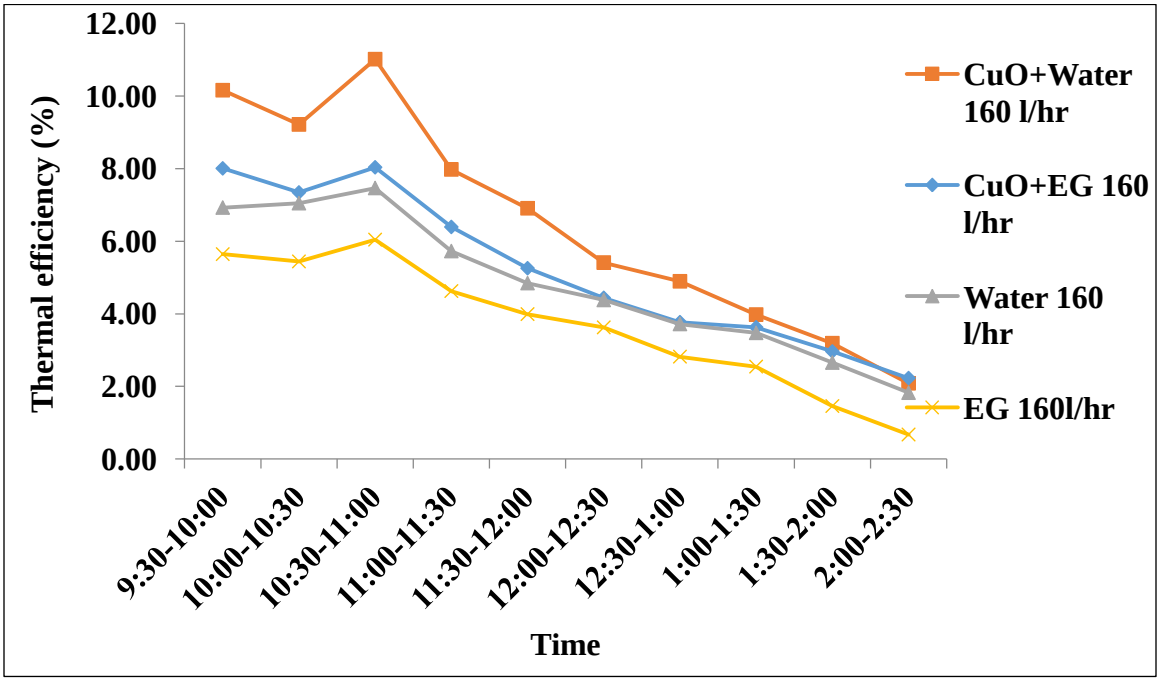

Figure 5.33: Variation in thermal efficiency with time for nanofluids (0.01%) and base fluids at 160 l/hr vol. flow rate

II. For 0.05% concentration

The Figure 5.34 shows the comparison of thermal efficiency between nanofluids (CuO-water and CuO-ethylene glycol based nanofluids)and base fluids (water and ethylene glycol) at 0.05% concentration for 100 l/hr. The graph shows the similar trend same as that of the 0.01% conc.

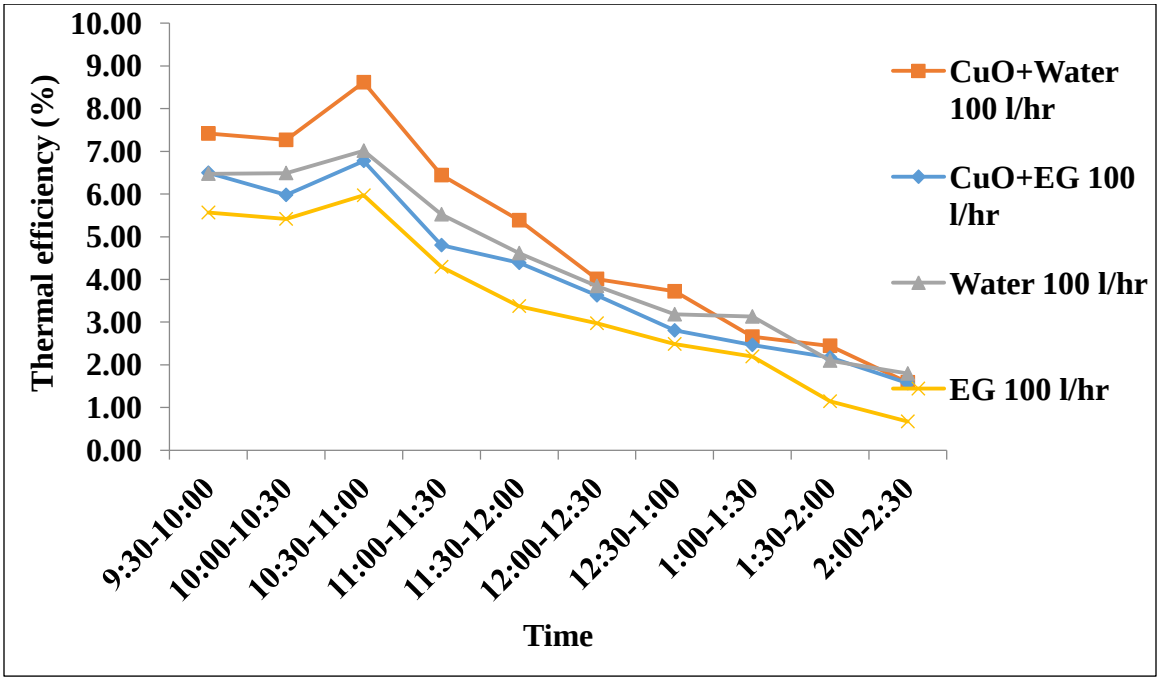

Figure 5.34: Variation in thermal efficiency with time for nanofluids (0.05%) and base fluids at 100 l/hr vol. flow rate

III. For 0.1% concentration

In the figure 5.35, water and CuO-water based nanofluid have almost similar thermal efficiencies. Because at a higher concentration of nanoparticle, the temperature rise in nanofluid is more as compared to the base fluid but, the specific heat of base fluid is much more than the nanofluid. So, considering both these effects, thermal efficiencies of both the fluids are almost similar. And the same case goes with ethylene glycol and CuO-ethylene glycol based nanofluids.

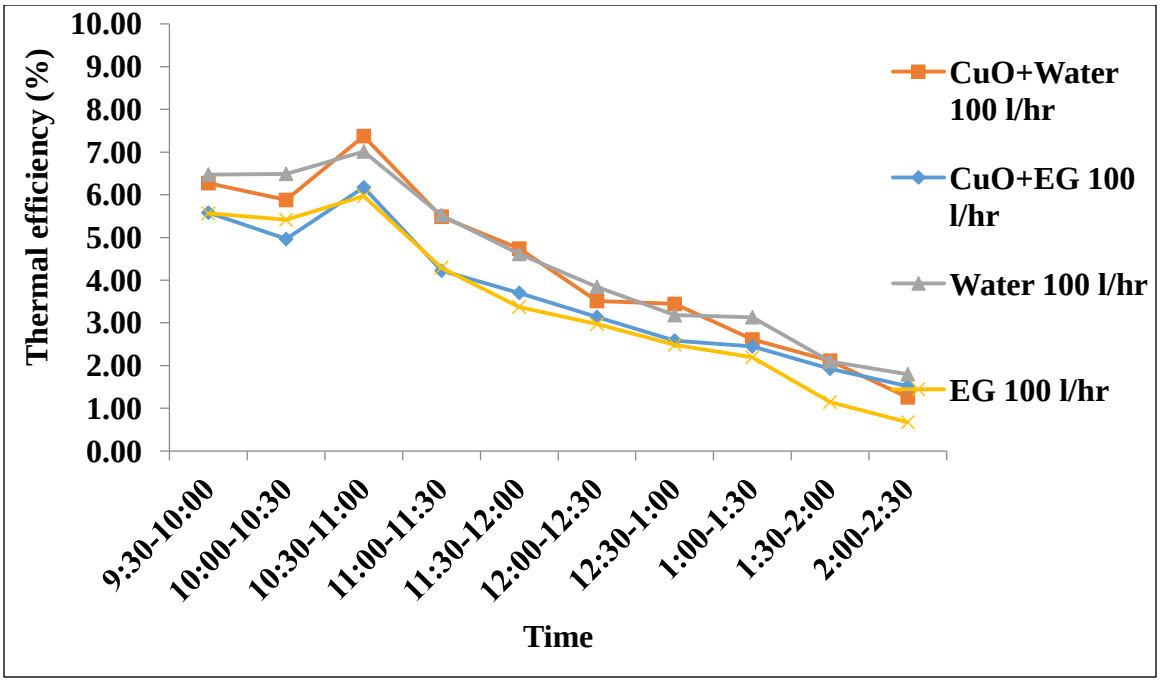

Figure 5.35: Variation in thermal efficiency with time for nanofluids (0.1%) and base fluids at 100 l/hr vol. flow rate

5.4 Comparison of instantaneous efficiency of nanofluids (CuO-water and CuO-ethylene glycol based nanofluids) and base fluids (water and ethylene glycol)

I. For 0.01% concentration

In this case, CuO-water has the maximum instantaneous efficiency as compared to the other fluids. At the starting point, instantaneous efficiency is found to be maximum and heat losses to the atmosphere becomes minimum because of the less temperature difference between the working fluid and surroundings and due to this reason, it enables the maximum utilization of the heat input. As the time progresses, instantaneous efficiency starts reducing since, the temp rise of fluid becomes less and the losses to the surroundings increase due to the high temperature difference between the fluid and surrounding.

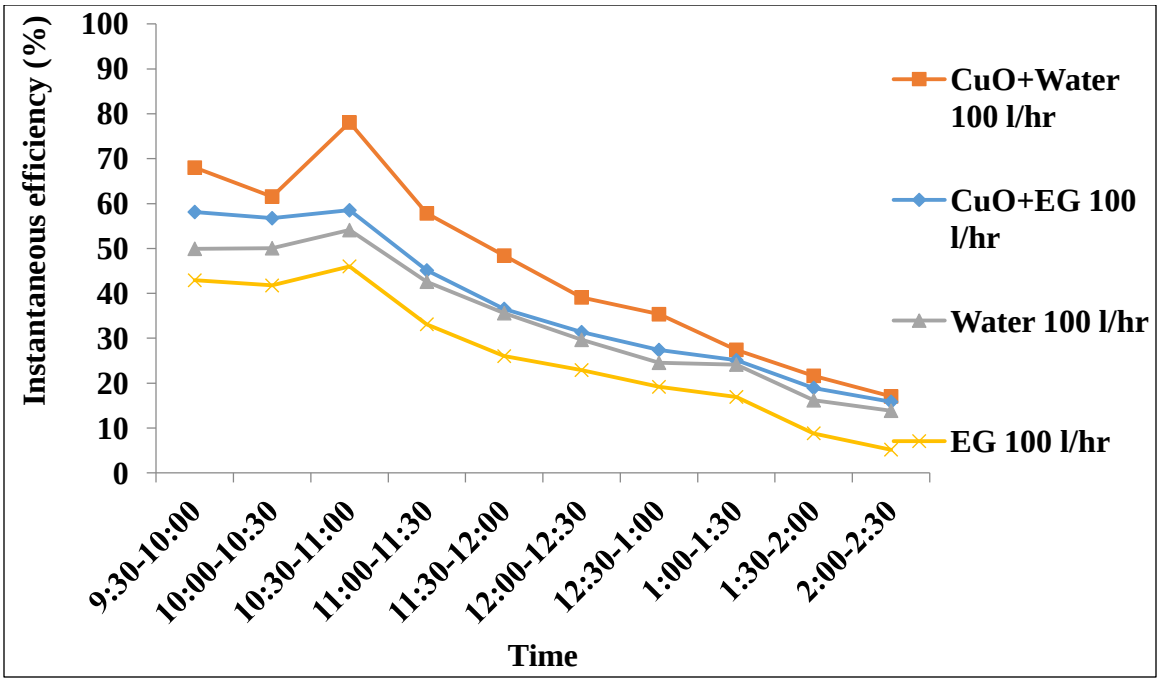

Figure 5.36: Variation in instantaneous efficiency with time for nanofluids (0.01%) and base fluids at 100 l/hr vol. flow rate

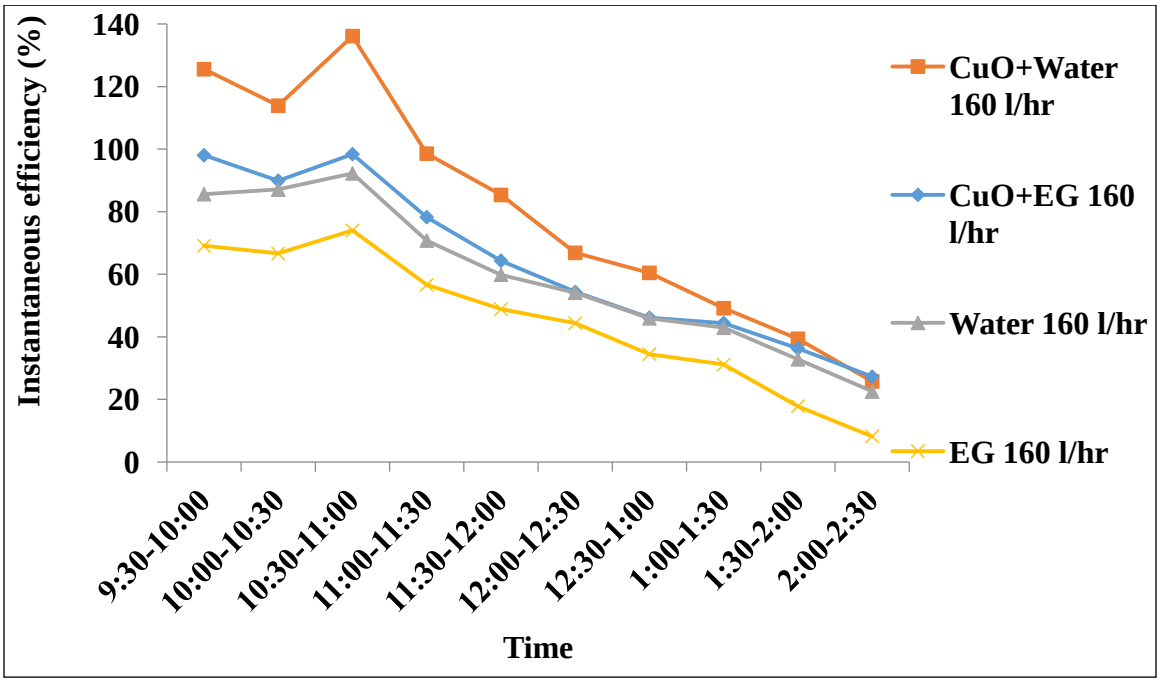

Figure 5.37: Variation in instantaneous efficiency with time for nanofluids (0.01%) and base fluids at 160 l/hr vol. flow rate

II. For 0.05% concentration

This figure shows the variation in instantaneous efficiency with time at 0.05% concentration for 100 l/hr volume flow rate. It shows similar trend as of 0.01% concentration i.e. CuO-H_2O based nanofluid has the highest instantaneous efficiency followed by water, CuO-EG based nanofluid and EG.

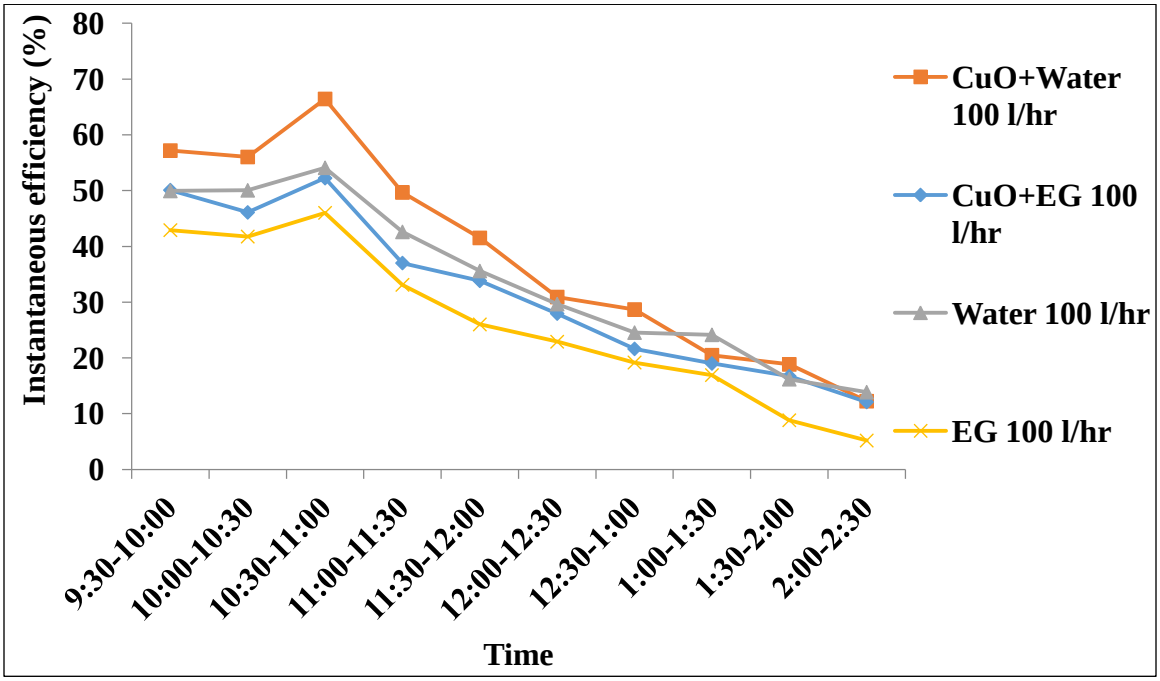

Figure 5.38: Variation in instantaneous efficiency with time for nanofluids (0.01%) and base fluids at 160 l/hr vol. flow rate

III. For 0.1% concentration

This figure 5.39 shows the variation in instantaneous efficiency with time for nanofluids (0.1%) and base fluids at 100 l/hr vol. flow rate.

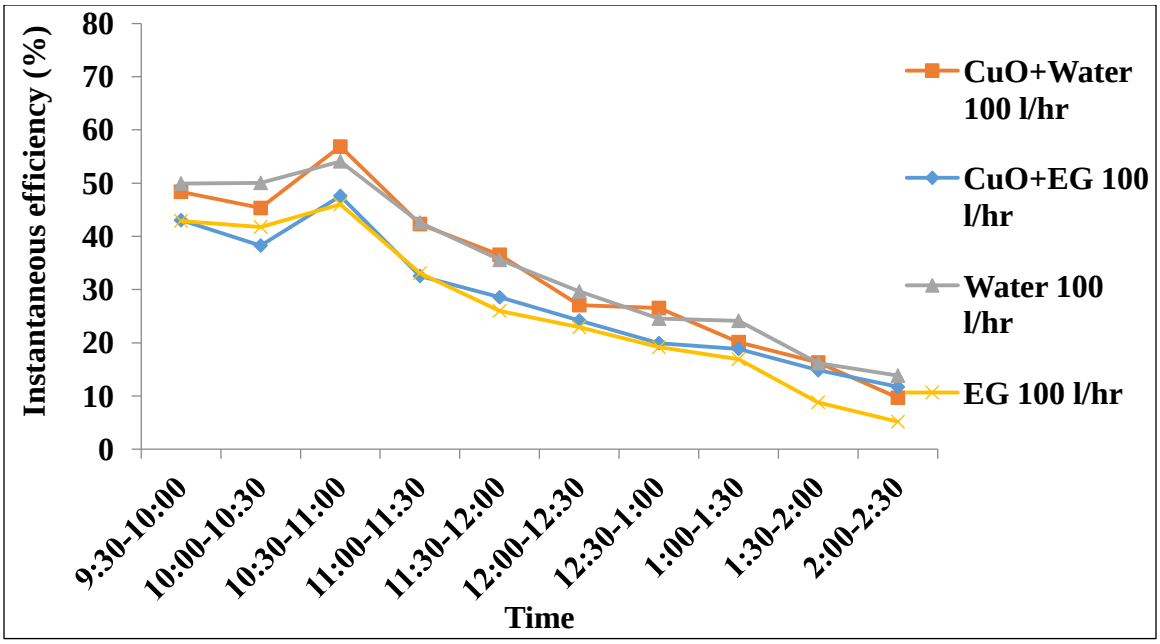

Figure 5.39: Variation in instantaneous efficiency with time for nanofluids (0.1%) and base fluids at 100 l/hr vol. flow rate

5.5 Pressure and temperature contours

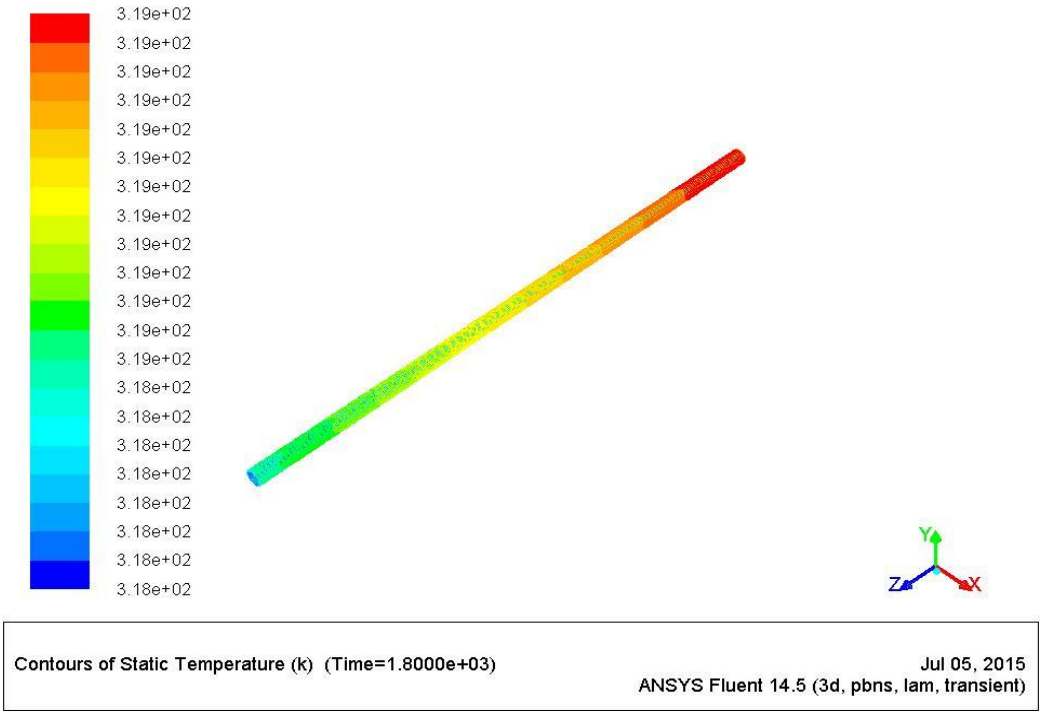

Figure 5.40: Temperature contour for CuO-H_2Onanofluid at 0.01% conc. and 100 l/hr

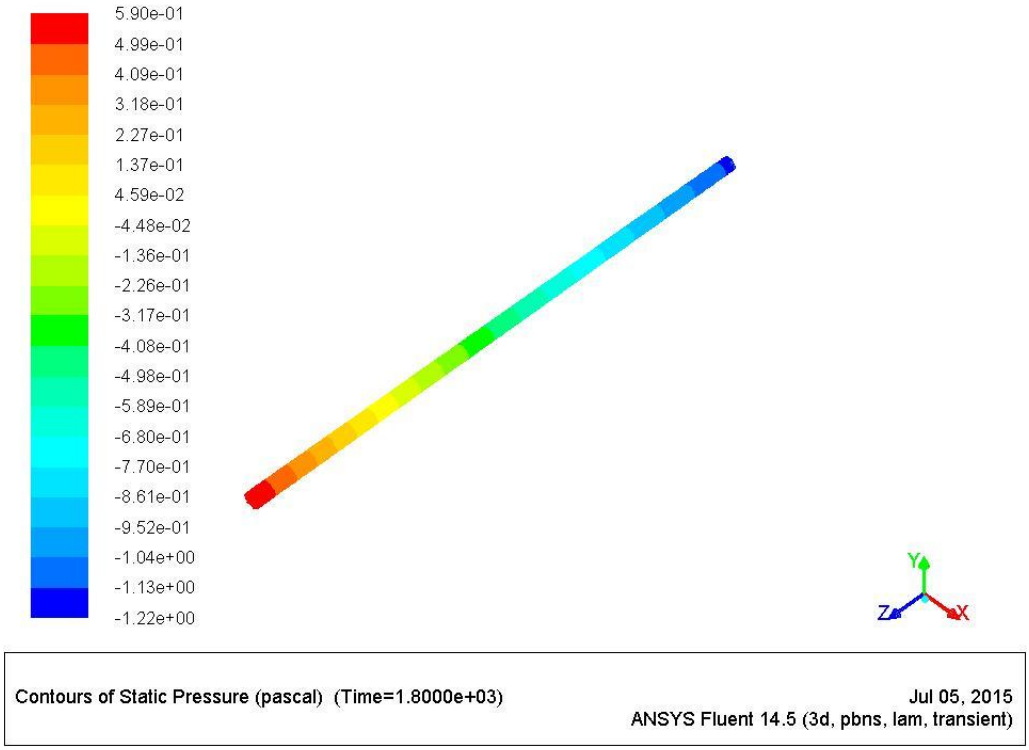

Figure 5.41 Pressurecontour for CuO-H_2Onanofluid at 0.01% conc. and 100 l/hr

Figures 5.40 and 5.41 show the temperature and pressure distribution along the length of the tube for CuO-H_2O nanofluid at 0.01% vol. conc. and at 100 l/hr, respectively. As the nanofluid has travelled along the length of the tube, its temperature has increased due to the solar heat flux across the surface area of the tube. The temperature increase at any instant is very small due to the very small length of the tube (i.e. 1 m). The fluid near the immediate vicinity of the tube surface is having higher temperature as compared to temperature of the fluid which is passing through center of tube. Pressure has dropped along the length of the tube. Very small pressure drop is observed due to the very small length of tube and volumetric flow rate of the nanofluid. Pressure drop was observed to be 7.12 pa.

CHAPTER 6

CONCLUSION AND FUTURE SCOPE

6.1 Conclusion

In order to meet the objectives specified in this study, experimentation has been carried out to check the performance of parabolic solar collector using CuO-H_2O based nanofluids and CuO-ethylene glycol nanofluids and then, comparing it with traditional fluids i.e. water and ethylene glycol. Experiments are performed at different volume fractions and different mass flow rates. The results are also validated with the help of CFD software.

Based on the results of experimental work, following conclusions can be made:

1) The maximum temperature attained from CuO-H_2O based nanofluid, CuO-ethylene glycol based nanofluid, water and ethylene glycol are 74.5°C, 72.6°C, 62.8°C and 60.3°C respectively at 2:30 pm.

2) Temperature difference is maximum at the 160 l/hr volume flow rate and minimum at 100 l/hr. Initially, temperature difference increases because heat flux is maximum from 9:30 am to 12:30 pm and afterwards, temperature difference goes on decreasing.

3) Useful heat gain is found to be maximum at 160 l/hr and minimum at 100 l/hr. In the beginning, useful heat gain is more and with time, it starts to fall, for all three mass flow rates.

4) The maximum thermal efficiency is found to be 11.01%, 8.03%, 7.46% and 6.04% for CuO-H_2O based nanofluid, CuO-ethylene glycol based nanofluid, water and ethylene glycol respectively. At the highest flow rate (160 l/h), maximum thermal efficiency is observed due to the highest useful gain, highest temperature difference and minimum convection losses.

5) The maximum overall thermal efficiency was found to be 4.4%, 3.82%, 3.1% and 2.8% for CuO-H_2O based nanofluid, CuO-ethylene glycol based nanofluid, water and ethylene glycol respectively.

6) Instantaneous efficiency increases with the increase in volume flow rates.

7) CuO-water based nanofluid has the highest thermal efficiency as compared to CuO-ethylene glycol nanofluids, water and ethylene glycol because of the highest conductivity. At the starting, efficiency is high and as the time progresses, efficiency starts declining due to the decrease in temperature rise.

8) The maximum convective heat transfer coefficient and heat removal factor is 730.59 W/m^2K and 0.978 respectively in CuO-water based nanofluid.

6.2 Future scope of work

Based on the points discussed in conclusion, it has been observed that, there are still many areas left in the experimentation to enhance the performance of parabolic solar collector:

1) Manual tracking mechanism has been employed in the present work. Automatic tracking mechanism could be used to enhance the performance of the solar collector, so that maximum solar radiation can be absorbed.

2) To calculate the volume flow rate, stopwatch system is used. Rotameter can be utilized for the accurate measurement of the flow rate.

3) In the present work, reflector consists of the mirror glass strips. Instead, a proper reflector can be used to reflect the maximum amount of solar radiations onto the receiver.

4) The support structure is made up of cast iron to withstand the effect of wind, load etc. Other suitable materials can also be used in place of it.

5) The absorber tube is made up of copper. Stainless steel, pyrex glass, quartz etc. can also be used.

6) The diameter and material of the cover tube can be varied to prevent the heat losses.

7) In this work, 0.01%, 0.05% and 0.1% concentrations have been used. In the future, higher concentrations and various sizes can be used to increase the efficiency of the collector.

REFERENCES

Barlev, D.,Vidu, R. and Stroeve, P.(2011).Innovation in concentrated solar power.*Solar energy materials and solar cells*.95:2703-2725.

Bayon, R., Rojas, E., Valenzuela, L., Zarza, E. and Leon, J. (2010). Analysis of the experimental behaviour of a 100 KW latent heat storage system for direct steam generation in solar thermal power plants. *Applied thermal engineering*.30:2643-2651.

Chaudhari, S.K. and Walke, P.V. (2014). Applications of nanofluid in solar energy-A review. *International Journal of Engineering Research & Technology*.3(3).

Das, S.K., Choi, S.U.S., Yu, W. andPradee, T. (2008).Nanofluids science and technology.*Wiley Publication.*

Hachicha, A.A., Rodriguez, I., Capdevila, R. andOliva, A. (2013). Heat transfer analysis and numerical simulation of a parabolic trough solar collector. *Applied Energy*. 111:581-592.

Hua, Y.L.,Wie, Q.U. andChao,F.J. (2007). Temperature dependence of thermal conductivity of nanofluids. *Chinese Phys. Lett*. 25:3319

Ingle, P. W.,Pawar, A. A., Deshmukh, B. D. and Bhosale, K. C. (2013). CFD analysis of solar flat plate collector.International journal of emerging technology and advanced engineering.3(4).

John,T. and Krishnakumar, T. S. (2013). Experimental studies of thermal conductivity, viscosity and stability of ethylene glycol nanofluids. *International Journal of Innovative Research in Science, Engineering and Technology:* 2319-8753

Kaygusuz, K.(1999).The viability of thermal storage.*Energy sources*.21:745-755.

Khullar, V. and Tyagi, H. (2010). Application of nanofluids as the working fluid in concentrating parabolic solar collectors.*International conference on fluid mechanics and fluid power.*

Khullar, V. and Tyagi, H.(2011).Enhancing optical efficiency of a linear parabolic solar collector through nanofluids.

Kumar, D.S.(2009).Heat and mass transfer.*S.K.Kataria& Sons Publications*:819

Kuravi, S., Trahan, J.,Goswami, D.Y.,Rahman,M.M. andStefanakos, E.K.(2013).Thermal energy storage technologies and systems for concentrating solar power plants.*Progress in energy and combustion science*:1-35.

Lee, S., Choi, S.U.S.,Li, S. and Eastman, J.A.(1999).Measuring thermal conductivity of fluids containing oxide nanoparticles.*Journal of heat transfer*.121:280-289.

Mahian, O., Kianifar, A.,Kalogirou, S.A., Pop, I. and Wongwises, S.(2013).A review of the applications of nanofluids in solar energy.*International journal of heat and mass transfer*.57:582-594.

Manikandan, K. S., Kumaresan, G.,Velraj, R. and Iniyan,S.(2012).Parametric study of parabolic trough collector system.*Asian journal of applied sciences*.

Nerella, S., Sudheer, N.V.V.S and Bhramara. (2014).Enhancement of heat transfer by nanofluids in solar collectors. *International Journal of Innovations in Engineering and Technology*.3(4).

Roman, A.(2011).Simulation analysis of thermal storage for concentrating solar power.*Applied thermal engineering.*31:3588-3594

Romano, J.M., Parker, J.C. and Ford,Q.B.(1997).Application opportunities for nanoparticles made from condensation of physical vapors.*Adv. Powder Metallurgy particulate materials*.2:12-13.

Saidur, R., Leong, K.Y. and Mohmmad,H.A.(2011).A review on applications and challenges of nanofluids.*Renewable and sustainable energy reviews.*15:1646-1668.

Selmi,M., Khawaja, M.J.A. and Marafia, A. (2008). Validation of CFD simulation for flat plate solar energy collector.*Renewable energy*.33:373-387.

Basavanna, S. and Shashishekar, K.S. (2013). CFD analysis of triangular absorber tube of a solar flat plate collector.*International Journal of Mechanical Engineering and Robotics research.*2:19-24.

Sukhatme, S.P. (1984).Solar energy principles of thermal collection and storage.*TataMcgraw-Hill Publications*:158-180.

Taylor, R.A., Phelan, P.E., Otanicar, T.P., Walker, C.A., Nguyen, M., Trimble, S. and Prasher, R. (2011). Applicability of nanofluids in high flux solar collectors. *Journal of renewable and sustainable energy*. 46: 2665-2672.

Tian, Y. and Zhao, C.Y. (2013). A review of solar collectors and thermal energy storage in solar thermal applications. *Applied energy*. 104:538-553.

Waghole Warkhedkar, R.M. and Kulkarni, V.S. (2013).Experimental analysis on heat transfer of absorber/receiver of parabolic trough collector.*International journal of research in advent technology*.1(5).

Wu, Z., Li, S., Yuan, G., Lei, D. and Wang, Z. (2014).Three-dimensional numerical study of heat transfer characteristics of parabolic trough receiver.*Applied energy*.113:902-911.

Xie, H., Wang, J., Xi, T.,Liu, Y., Ai, F. and Wu, Q. (2002).Thermal conductivity enhancement of suspensions containing nanosized alumina particles. *Journal of applied physics*.91:4568-72.

Yaseen, T.A. (2012).Experimental and theoretical study of a parabolic trough solar collector.*Anbar journal for engineering sciences*.34: 219-246.

APPENDIX A1

Table A1.1: Values of Re, Pr, Nu, h_f, F', F_R for CuO nanofluid (0.01% conc.) at different vol. flow rates

	100 l/hr	130 l/hr	160 l/hr
Re	3131.20	4081.86	4973.744
Pr	2.409	2.41	2.409
Nu	20.47	25.30	29.635
h_f (W/m^2K)	520.74	643.79	754.05
F'	0.974	0.979	0.982
F_R	0.968	0.974	0.978

Table A1.2: Values of Re, Pr, Nu, h_f, F', F_R for CuO nanofluid (0.05% conc.) at different vol. flow rates

	100 l/hr	130 l/hr	160 l/hr
Re	2827.10	4440.707	4490.701
Pr	1.902	1.902	1.902
Nu	17.16	24.62	24.844
h_f (W/m^2K)	504.54	724.08	730.59
F'	0.973	0.981	0.981
F_R	0.9661	0.976	0.977

Table A1.3: Values of Re, Pr, Nu, h_f, F', F_R for CuO nanofluid (0.01% conc.) at different vol. flow rates

	100 l/hr	130 l/hr	160 l/hr
Re	1571.563	2048.706	2496.346
Pr	2.331	2.331	2.331
Nu	11.637	14.386	16.851
h_f (W/m^2K)	384.017	474.753	556.068
F'	0.965	0.972	0.976
F_R	0.956	0.965	0.970

APPENDIX A2

Table A2.1: Values of temperature, solar intensity and wind speed with time

Date 23/05/2015_for CuO-H_2O nanofluid (0.01% conc.) at vol. flow rate of 100 l/hr					
Time	Inlet temperature (˚C)	Outlet temperature (˚C)	Temperature difference (˚C)	Solar intensity (W/m^2)	Wind speed (m/sec)
9:30-10:00 AM	33	37.95	4.95	728.214	0.5
10:00-10:30 AM	37.98	42.65	4.67	758.759	1.6
10:30-11:00 AM	42.65	48.85	6.2	794.519	0.6
11:00-11:30 AM	48.85	53.55	4.7	813.144	2.7
11:30-12:00 AM	53.55	57.65	4.1	847.414	3.3
12:00-12:30 PM	57.65	61.05	3.4	869.764	1.9
12:30-1:00 PM	61.05	64.15	3.1	877.214	0.6
1:00-1:30 PM	64.15	66.45	2.3	839.219	0.8
1:30-2:00 PM	66.45	68.15	1.7	786.324	1.6
2:00-2:30 PM	68.15	69.45	1.3	763.229	1

Table A2.2: Values of temperature, solar intensity and wind speed with time

Date 24/05/2015_for CuO-H_2O nanofluid (0.01% conc.) at vol. flow rate of 130 l/hr					
Time	Inlet temperature (˚C)	Outlet temperature (˚C)	Temperature difference (˚C)	Solar intensity (W/m^2)	Wind speed (m/sec)
9:30-10:00 AM	32.7	37.7	5	724.489	0.8
10:00-10:30 AM	37.7	42.9	5.2	754.289	1.3
10:30-11:00 AM	42.9	48.9	6	784.089	0.1
11:00-11:30 AM	48.9	53.8	4.9	817.614	3.2
11:30-12:00 AM	53.8	57.9	4.1	838.474	2.4

12:00-12:30 PM	57.9	61.4	3.5	854.864	1.7
12:30-1:00 PM	61.4	64.7	3.3	887.644	1.9
1:00-1:30 PM	64.7	66.9	2.2	848.159	0.5
1:30-2:00 PM	66.9	68.8	1.9	780.364	2.2
2:00-2:30 PM	68.8	70.2	1.4	753.544	2.1

Table A2.3: Values of temperature, solar intensity and wind speed with time

Date 25/05/2015_for CuO-H_2O nanofluid (0.01% conc.) at vol. flow rate of 160 l/hr					
Time	Inlet temperature (˚C)	Outlet temperature (˚C)	Temperature difference (˚C)	Solar intensity (W/m^2)	Wind speed (m/sec)
9:30-10:00 AM	32.5	37.9	5.4	689.47	0.1
10:00-10:30 AM	37.9	43.1	5.2	731.94	1.5
10:30-11:00 AM	43.1	49.6	6.5	765.46	0.7
11:00-11:30 AM	49.6	54.6	5	813.14	0.3
11:30-12:00 AM	54.6	59.1	4.5	845.18	3.2
12:00-12:30 PM	59.1	62.7	3.6	863.06	2
12:30-1:00 PM	62.7	65.9	3.2	848.16	3.5
1:00-1:30 PM	65.9	68.3	2.4	782.60	0.1
1:30-2:00 PM	68.3	70.2	1.9	772.91	3
2:00-2:30 PM	70.2	71.4	1.2	746.84	2

Table A2.4: Values of temperature, solar intensity and wind speed with time

Date 26/05/2015_for CuO-H_2O nanofluid (0.05% conc.) at vol. flow rate of 100 l/hr					
Time	Inlet temperature (˚C)	Outlet temperature (˚C)	Temperature difference (˚C)	Solar intensity (W/m^2)	Wind speed (m/sec)

9:30-10:00 AM	32.7	37.8	5.1	734.92	2.10
10:00-10:30 AM	37.8	43	5.2	764.72	4.20
10:30-11:00 AM	43	49.4	6.4	793.77	3.30
11:00-11:30 AM	49.4	54.4	5	829.53	2.40
11:30-12:00 AM	54.4	58.7	4.3	853.37	3.30
12:00-12:30 PM	58.7	62	3.3	879.45	1.70
12:30-1:00 PM	62	65.1	3.1	890.62	2.70
1:00-1:30 PM	65.1	67.2	2.1	844.43	6.00
1:30-2:00 PM	67.2	69	1.8	787.07	4.80
2:00-2:30 PM	69	70.1	1.1	740.13	2.30

Table A2.5: Values of temperature, solar intensity and wind speed with time

Date 27/05/2015_for CuO-H_2O nanofluid (0.05% conc.) at vol. flow rate of 130 l/hr					
Time	Inlet temperature (˚C)	Outlet temperature (˚C)	Temperature difference (˚C)	Solar intensity (W/m^2)	Wind speed (m/sec)
9:30-10:00 AM	32.6	37.8	5.2	735.664	2.1
10:00-10:30 AM	37.8	43.1	5.3	755.779	4.2
10:30-11:00 AM	43.1	49.7	6.6	787.814	3.3
11:00-11:30 AM	49.7	54.9	5.2	822.084	2.4
11:30-12:00 AM	54.9	59.4	4.5	847.414	3.3
12:00-12:30 PM	59.4	62.8	3.4	855.609	1.7
12:30-1:00 PM	62.8	66	3.2	891.369	2.7
1:00-1:30 PM	66	68.4	2.4	840.709	6
1:30-2:00 PM	68.4	70.2	1.8	781.854	4.8

2:00-2:30 PM	70.2	71.4	1.2	745.349	2.3

Table A2.6: Values of temperature, solar intensity and wind speed with time

Date 28/05/2015_for CuO-H_2O nanofluid (0.05% conc.) at vol. flow rate of 160 l/hr					
Time	Inlet temperature (˚C)	Outlet temperature (˚C)	Temperature difference (˚C)	Solar intensity (W/m^2)	Wind speed (m/sec)
9:30-10:00 AM	32.7	38.2	5.5	681.279	0.2
10:00-10:30 AM	38.2	43.6	5.4	720.764	0.6
10:30-11:00 AM	43.6	50.4	6.8	764.719	0.8
11:00-11:30 AM	50.4	55.7	5.3	811.654	0.1
11:30-12:00 AM	55.7	60.4	4.7	840.709	1.2
12:00-12:30 PM	60.4	64.1	3.7	868.274	1.6
12:30-1:00 PM	64.1	67.4	3.3	838.474	2.1
1:00-1:30 PM	67.4	69.8	2.4	774.404	1.1
1:30-2:00 PM	69.8	71.8	2	762.484	2.6
2:00-2:30 PM	71.8	72.9	1.1	737.154	1.6

Table A2.7: Values of temperature, solar intensity and wind speed with time

Date 29/05/2015_for CuO-H_2O nanofluid (0.1% conc.) at vol. flow rate of 100 l/hr					
Time	Inlet temperature (˚C)	Outlet temperature (˚C)	Temperature difference (˚C)	Solar intensity (W/m^2)	Wind speed (m/sec)
9:30-10:00 AM	32.8	38.2	5.4	751.309	0.4
10:00-10:30 AM	38.2	43.5	5.3	787.069	0.7
10:30-11:00 AM	43.5	50.3	6.8	804.949	0.5
11:00-11:30 AM	50.3	55.5	5.2	827.299	2.1

11:30-12:00 AM	55.5	60.1	4.6	847.414	0.7
12:00-12:30 PM	60.1	63.6	3.5	869.764	0.1
12:30-1:00 PM	63.6	66.9	3.3	836.984	0.5
1:00-1:30 PM	66.9	69.3	2.4	802.714	0.2
1:30-2:00 PM	69.3	71.2	1.9	784.834	0.32
2:00-2:30 PM	71.2	72.3	1.1	763.974	0.23

Table A2.8: Values of temperature, solar intensity and wind speed with time

Date 30/05/2015_for CuO-H_2O nanofluid (0.1% conc.) at vol. flow rate of 130 l/hr					
Time	Inlet temperature (˚C)	Outlet temperature (˚C)	Temperature difference (˚C)	Solar intensity (W/m^2)	Wind speed (m/sec)
9:30-10:00 AM	33	38.6	5.6	699.159	0.4
10:00-10:30 AM	38.6	44	5.4	780.364	0.7
10:30-11:00 AM	44	51	7	811.654	0.5
11:00-11:30 AM	51	56.4	5.4	855.609	2.1
11:30-12:00 AM	56.4	61.1	4.7	863.059	0.7
12:00-12:30 PM	61.1	64.8	3.7	885.409	0.1
12:30-1:00 PM	64.8	68.3	3.5	848.159	0.5
1:00-1:30 PM	68.3	70.6	2.3	813.144	0.2
1:30-2:00 PM	70.6	72.5	1.9	780.364	0.32
2:00-2:30 PM	72.5	73.5	1	755.779	0.23

Table A2.9: Values of temperature, solar intensity and wind speed with time

Date 31/05/2015_for CuO-H_2O nanofluid (0.1% conc.) at vol. flow rate of 160 l/hr					
Time	Inlet temperature (˚C)	Outlet temperature (˚C)	Temperature difference (˚C)	Solar intensity (W/m^2)	Wind speed (m/sec)
9:30-10:00 AM	32.8	38.5	5.7	687.239	0.4
10:00-10:30 AM	38.4	44	5.6	725.234	0.1
10:30-11:00 AM	44	51.1	7.1	769.934	0.7
11:00-11:30 AM	51.1	56.7	5.6	795.264	1.1
11:30-12:00 AM	56.7	61.6	4.9	834.749	0.3
12:00-12:30 PM	61.6	65.4	3.8	872.744	0.7
12:30-1:00 PM	65.4	68.9	3.5	845.179	0.1
1:00-1:30 PM	68.9	71.3	2.4	780.364	1
1:30-2:00 PM	71.3	73.4	2.1	765.464	0.8
2:00-2:30 PM	73.4	74.5	1.1	730.449	0.6

Table A2.10: Values of temperature, solar intensity and wind speed with time

Date 02/06/2015_for CuO-EG nanofluid (0.01% conc.) at vol. flow rate of 100 l/hr					
Time	Inlet temperature (˚C)	Outlet temperature (˚C)	Temperature difference (˚C)	Solar intensity (W/m^2)	Wind speed (m/sec)
9:30-10:00 AM	34.2	38.7	4.5	711.079	2
10:00-10:30 AM	38.7	43.3	4.6	744.604	1.2
10:30-11:00 AM	43.3	48.3	5	784.834	5
11:00-11:30 AM	48.3	52.4	4.1	834.749	0.2
11:30-12:00 AM	52.4	55.8	3.4	854.864	2.1
12:00-12:30 PM	55.8	58.8	3	878.704	2.6

12:30-1:00 PM	58.8	61.3	2.5	838.474	1
1:00-1:30 PM	61.3	63.5	2.2	804.949	1
1:30-2:00 PM	63.5	65.1	1.6	775.894	2.3
2:00-2:30 PM	65.1	66.4	1.3	753.544	1.1

Table A2.11: Values of temperature, solar intensity and wind speed with time

Date 04/06/2015_for CuO-EG nanofluid (0.01% conc.) at vol. flow rate of 160 l/hr					
Time	Inlet temperature (˚C)	Outlet temperature (˚C)	Temperature difference (˚C)	Solar intensity (W/m^2)	Wind speed (m/sec)
9:30-10:00 AM	33.8	38.5	4.7	699.159	0.1
10:00-10:30 AM	38.5	43.1	4.6	746.094	1.5
10:30-11:00 AM	43.1	48.3	5.2	770.679	0.7
11:00-11:30 AM	48.3	52.7	4.4	819.849	0.3
11:30-12:00 AM	52.7	56.4	3.7	838.474	3.2
12:00-12:30 PM	56.4	59.6	3.2	858.589	2
12:30-1:00 PM	59.6	62.3	2.7	853.374	3.5
1:00-1:30 PM	62.3	64.7	2.4	787.814	0.1
1:30-2:00 PM	64.7	66.6	1.9	763.974	3
2:00-2:30 PM	66.6	68	1.4	748.329	2

Table A2.12: Values of temperature, solar intensity and wind speed with time

Date 05/06/2015_for CuO-EG nanofluid (0.05% conc.) at vol. flow rate of 100 l/hr					
Time	Inlet temperature (˚C)	Outlet temperature (˚C)	Temperature difference (˚C)	Solar intensity (W/m^2)	Wind speed (m/sec)
9:30-10:00 AM	33.9	38.6	4.7	717.039	2

10:00-10:30 AM	38.6	43.1	4.5	746.094	1.2
10:30-11:00 AM	43.1	48.5	5.4	790.049	5
11:00-11:30 AM	48.5	52.5	4	825.809	0.2
11:30-12:00 AM	52.5	56.3	3.8	858.589	2.1
12:00-12:30 PM	56.3	59.5	3.2	874.979	2.6
12:30-1:00 PM	59.5	61.9	2.4	848.159	1
1:00-1:30 PM	61.9	64.1	2.2	884.664	1
1:30-2:00 PM	64.1	65.8	1.7	776.639	2.3
2:00-2:30 PM	65.8	67	1.2	758.014	1.1

Table A2.13: Values of temperature, solar intensity and wind speed with time

Date 08/06/2015_for CuO-EG nanofluid (0.1% conc.) at vol. flow rate of 100 l/hr					
Time	Inlet temperature (˚C)	Outlet temperature (˚C)	Temperature difference (˚C)	Solar intensity (W/m^2)	Wind speed (m/sec)
9:30-10:00 AM	33.9	38.7	4.8	702.884	2
10:00-10:30 AM	38.7	43.2	4.5	740.879	1.2
10:30-11:00 AM	43.2	49.1	5.9	781.109	5
11:00-11:30 AM	49.1	53.3	4.2	813.144	0.2
11:30-12:00 AM	53.3	57.2	3.9	860.824	2.1
12:00-12:30 PM	57.2	60.6	3.4	886.154	2.6
12:30-1:00 PM	60.6	63.3	2.7	853.374	1
1:00-1:30 PM	63.3	65.7	2.4	801.969	1
1:30-2:00 PM	65.7	67.5	1.8	763.974	2.3
2:00-2:30 PM	67.5	68.9	1.4	752.799	1.1

Table A2.14: Values of absorbed heat flux, useful heat gain and efficiencies with time

$CuO-H_2O$ nanofluid (0.01% conc.) at vol. flow rate of 100 l/hr					
Time	Absorbed heat flux (W/m^2)	Useful heat gain (W)	Instantaneous efficiency (%)	Thermal efficiency (%)	Overall efficiency (%)
9:30-10:00 AM	509.55	543.67	67.99	8.82	5.85
10:00-10:30 AM	530.93	512.91	61.57	7.98	
10:30-11:00 AM	555.95	680.96	78.06	10.12	
11:00-11:30 AM	568.98	516.21	57.82	7.50	
11:30-12:00 AM	592.96	450.31	48.40	6.28	
12:00-12:30 PM	608.60	373.43	39.10	5.07	
12:30-1:00 PM	613.81	340.48	35.35	4.58	
1:00-1:30 PM	587.23	252.61	27.41	3.56	
1:30-2:00 PM	550.22	186.71	21.63	2.80	
2:00-2:30 PM	534.06	142.78	17.04	2.21	

Table A2.15: Values of absorbed heat flux, useful heat gain and efficiencies with time

$CuO-H_2O$ nanofluid (0.01% conc.) at vol. flow rate of 130 l/hr					
Time	Absorbed heat flux (W/m^2)	Useful heat gain (W)	Instantaneous efficiency (%)	Thermal efficiency (%)	Overall efficiency (%)
9:30-10:00 AM	506.95	715.89	89.99	8.95	6.08
10:00-10:30 AM	527.80	744.53	89.90	8.94	
10:30-11:00 AM	548.65	859.07	99.78	9.93	
11:00-11:30 AM	572.11	701.57	78.15	7.77	
11:30-12:00 AM	586.71	587.03	63.76	6.34	
12:00-12:30 PM	598.18	501.12	53.39	5.31	

12:30-1:00 PM	621.11	472.49	48.48	4.82	
1:00-1:30 PM	593.48	314.99	33.82	3.36	
1:30-2:00 PM	546.05	272.04	31.75	3.16	
2:00-2:30 PM	527.28	200.45	24.23	2.41	

Table A2.16: Values of absorbed heat flux, useful heat gain and efficiencies with time

$CuO-H_2O$ nanofluid (0.01% conc.) at vol. flow rate of 160 l/hr					
Time	Absorbed heat flux (W/m^2)	Useful heat gain (W)	Instantaneous efficiency (%)	Thermal efficiency (%)	Overall efficiency (%)
9:30-10:00 AM	482.45	950.66	125.58	10.16	6.42
10:00-10:30 AM	512.16	915.45	113.91	9.22	
10:30-11:00 AM	535.62	1144.31	136.15	11.02	
11:00-11:30 AM	568.98	880.24	98.59	7.98	
11:30-12:00 AM	591.40	792.22	85.37	6.91	
12:00-12:30 PM	603.91	633.77	66.88	5.41	
12:30-1:00 PM	593.48	563.35	60.49	4.89	
1:00-1:30 PM	547.61	422.52	49.17	3.98	
1:30-2:00 PM	540.83	334.49	39.41	3.19	
2:00-2:30 PM	522.59	211.26	25.76	2.08	

Table A2.17: Values of absorbed heat flux, useful heat gain and efficiencies with time

$CuO-H_2O$ nanofluid (0.05% conc.) at vol. flow rate of 100 l/hr					
Time	Absorbed heat flux (W/m^2)	Useful heat gain (W)	Instantaneous efficiency (%)	Thermal efficiency (%)	Overall efficiency (%)
9:30-10:00 AM	514.25	461.39	57.18	7.42	4.92

10:00-10:30 AM	535.10	470.43	56.03	7.27	
10:30-11:00 AM	555.43	579.00	66.43	8.62	
11:00-11:30 AM	580.45	452.34	49.66	6.44	
11:30-12:00 AM	597.13	389.01	41.52	5.38	
12:00-12:30 PM	615.38	298.55	30.92	4.01	
12:30-1:00 PM	623.20	280.45	28.68	3.72	
1:00-1:30 PM	590.88	189.98	20.49	2.66	
1:30-2:00 PM	550.74	162.84	18.84	2.44	
2:00-2:30 PM	517.90	99.52	12.25	1.59	

Table A2.18: Values of absorbed heat flux, useful heat gain and efficiencies with time

$CuO-H_2O$ nanofluid (0.05% conc.) at vol. flow rate of 130 l/hr					
Time	Absorbed heat flux (W/m^2)	Useful heat gain (W)	Instantaneous efficiency (%)	Thermal efficiency (%)	Overall efficiency (%)
9:30-10:00 AM	514.77	613.26	75.92	7.55	5.14
10:00-10:30 AM	528.84	625.06	75.32	7.49	
10:30-11:00 AM	551.26	778.37	89.98	8.95	
11:00-11:30 AM	575.24	613.26	67.94	6.76	
11:30-12:00 AM	592.96	530.71	57.04	5.67	
12:00-12:30 PM	598.70	400.98	42.68	4.25	
12:30-1:00 PM	623.72	377.39	38.56	3.84	
1:00-1:30 PM	588.27	283.04	30.66	3.05	
1:30-2:00 PM	547.09	212.28	24.73	2.46	
2:00-2:30 PM	521.54	141.52	17.29	1.72	

Table A2.19: Values of absorbed heat flux, useful heat gain and efficiencies with time

$CuO-H_2O$ nanofluid (0.05% conc.) at vol. flow rate of 160 l/hr					
Time	Absorbed heat flux (W/m^2)	Useful heat gain (W)	Instantaneous efficiency (%)	Thermal efficiency (%)	Overall efficiency (%)
9:30-10:00 AM	476.71	797.56	106.62	8.63	5.51
10:00-10:30 AM	504.34	783.06	98.95	8.01	
10:30-11:00 AM	535.10	986.07	117.44	9.50	
11:00-11:30 AM	567.94	768.56	86.24	6.98	
11:30-12:00 AM	588.27	681.55	73.83	5.97	
12:00-12:30 PM	607.56	536.54	56.28	4.55	
12:30-1:00 PM	586.71	478.53	51.98	4.21	
1:00-1:30 PM	541.88	348.02	40.93	3.31	
1:30-2:00 PM	533.53	290.02	34.64	2.80	
2:00-2:30 PM	515.81	159.51	19.71	1.59	

Table A2.20: Values of absorbed heat flux, useful heat gain and efficiencies with time

$CuO-H_2O$ nanofluid (0.1% conc.) at vol. flow rate of 100 l/hr					
Time	Absorbed heat flux (W/m^2)	Useful heat gain (W)	Instantaneous efficiency (%)	Thermal efficiency (%)	Overall efficiency (%)
9:30-10:00 AM	525.71	399.07	48.38	6.27	4.26
10:00-10:30 AM	550.74	391.68	45.32	5.88	
10:30-11:00 AM	563.25	502.53	56.86	7.37	
11:00-11:30 AM	578.89	384.29	42.30	5.49	
11:30-12:00 AM	592.96	339.95	36.54	4.74	
12:00-12:30 PM	608.60	258.65	27.08	3.51	

12:30-1:00 PM	585.66	243.87	26.54	3.44	
1:00-1:30 PM	561.68	177.36	20.12	2.61	
1:30-2:00 PM	549.17	140.41	16.29	2.11	
2:00-2:30 PM	534.58	81.29	9.69	1.26	

Table A2.21: Values of absorbed heat flux, useful heat gain and efficiencies with time

$CuO-H_2O$ nanofluid (0.1% conc.) at vol. flow rate of 130 l/hr					
Time	Absorbed heat flux (W/m^2)	Useful heat gain (W)	Instantaneous efficiency (%)	Thermal efficiency (%)	Overall efficiency (%)
9:30-10:00 AM	489.22	539.34	70.26	6.99	4.36
10:00-10:30 AM	546.05	520.08	60.70	6.04	
10:30-11:00 AM	567.94	674.18	75.65	7.53	
11:00-11:30 AM	598.70	520.08	55.36	5.51	
11:30-12:00 AM	603.91	452.66	47.77	4.75	
12:00-12:30 PM	619.55	356.35	36.66	3.65	
12:30-1:00 PM	593.48	337.09	36.20	3.60	
1:00-1:30 PM	568.98	221.52	24.81	2.47	
1:30-2:00 PM	546.05	182.99	21.36	2.13	
2:00-2:30 PM	528.84	96.31	11.61	1.15	

Table A2.22: Values of absorbed heat flux, useful heat gain and efficiencies with time

$CuO-H_2O$ nanofluid (0.1% conc.) at vol. flow rate of 160 l/hr					
Time	Absorbed heat flux (W/m^2)	Useful heat gain (W)	Instantaneous efficiency (%)	Thermal efficiency (%)	Overall efficiency (%)
9:30-10:00 AM	669.11	480.88	88.67	7.24	

10:00-10:30 AM	657.37	507.47	82.55	6.74	4.66
10:30-11:00 AM	833.46	538.75	98.59	8.05	
11:00-11:30 AM	657.37	556.47	75.28	6.15	
11:30-12:00 AM	575.20	584.10	62.76	5.12	
12:00-12:30 PM	446.07	610.69	46.55	3.80	
12:30-1:00 PM	410.86	591.40	44.27	3.61	
1:00-1:30 PM	281.73	546.05	32.88	2.68	
1:30-2:00 PM	246.51	535.62	29.33	2.39	
2:00-2:30 PM	129.13	511.12	16.10	1.31	

Table A2.23: Values of absorbed heat flux, useful heat gain and efficiencies with time

CuO-EG nanofluid (0.01% conc.) at vol. flow rate of 100 l/hr					
Time	Absorbed heat flux (W/m^2)	Useful heat gain (W)	Instantaneous efficiency (%)	Thermal efficiency (%)	Overall efficiency (%)
9:30-10:00 AM	497.56	453.76	58.12	7.24	4.80
10:00-10:30 AM	521.02	463.84	56.73	6.74	
10:30-11:00 AM	549.17	504.17	58.51	8.05	
11:00-11:30 AM	584.10	413.42	45.11	6.15	
11:30-12:00 AM	598.18	342.84	36.52	5.12	
12:00-12:30 PM	614.86	302.50	31.35	3.80	
12:30-1:00 PM	586.71	252.09	27.38	3.61	
1:00-1:30 PM	563.25	221.84	25.10	2.68	
1:30-2:00 PM	542.92	161.34	18.94	2.39	
2:00-2:30 PM	527.28	131.09	15.84	1.31	

Table A2.24: Values of absorbed heat flux, useful heat gain and efficiencies with time

CuO-EG nanofluid (0.01% conc.) at vol. flow rate of 160 l/hr					
Time	Absorbed heat flux (W/m^2)	Useful heat gain (W)	Instantaneous efficiency (%)	Thermal efficiency (%)	Overall efficiency (%)
9:30-10:00 AM	489.22	752.80	98.06	8.01	5.17
10:00-10:30 AM	522.07	736.78	89.94	7.34	
10:30-11:00 AM	539.27	832.89	98.43	8.04	
11:00-11:30 AM	573.67	704.75	78.29	6.39	
11:30-12:00 AM	586.71	592.63	64.37	5.26	
12:00-12:30 PM	600.78	512.55	54.37	4.44	
12:30-1:00 PM	597.13	432.46	46.15	3.77	
1:00-1:30 PM	551.26	384.41	44.44	3.63	
1:30-2:00 PM	534.58	304.32	36.28	2.96	
2:00-2:30 PM	523.63	224.24	27.29	2.23	

Table A2.25: Values of absorbed heat flux, useful heat gain and efficiencies with time

CuO-EG nanofluid (0.05% conc.) at vol. flow rate of 100 l/hr					
Time	Absorbed heat flux (W/m^2)	Useful heat gain (W)	Instantaneous efficiency (%)	Thermal efficiency (%)	Overall efficiency (%)
9:30-10:00 AM	501.74	394.38	50.09	6.50	4.06
10:00-10:30 AM	522.07	377.60	46.09	5.98	
10:30-11:00 AM	552.82	453.12	52.23	6.77	
11:00-11:30 AM	577.84	335.64	37.02	4.80	
11:30-12:00 AM	600.78	318.86	33.82	4.39	
12:00-12:30 PM	612.25	268.51	27.95	3.62	

12:30-1:00 PM	593.48	201.38	21.62	2.80	
1:00-1:30 PM	619.03	184.60	19.00	2.46	
1:30-2:00 PM	543.44	142.65	16.73	2.17	
2:00-2:30 PM	530.41	100.69	12.10	1.57	

Table A2.26: Values of absorbed heat flux, useful heat gain and efficiencies with time

CuO-EG nanofluid (0.1% conc.) at vol. flow rate of 100 l/hr					
Time	Absorbed heat flux (W/m^2)	Useful heat gain (W)	Instantaneous efficiency (%)	Thermal efficiency (%)	Overall efficiency (%)
9:30-10:00 AM	491.83	332.12	43.03	5.58	3.59
10:00-10:30 AM	518.42	311.36	38.27	4.96	
10:30-11:00 AM	546.57	408.23	47.60	6.17	
11:00-11:30 AM	568.98	290.60	32.55	4.22	
11:30-12:00 AM	602.35	269.84	28.55	3.70	
12:00-12:30 PM	620.07	235.25	24.18	3.14	
12:30-1:00 PM	597.13	186.82	19.94	2.59	
1:00-1:30 PM	561.16	166.06	18.86	2.45	
1:30-2:00 PM	534.58	124.54	14.85	1.93	
2:00-2:30 PM	526.76	96.87	11.72	1.52	

APPENDIX A3

Table A3.1: Thermophysical properties of working fluids

Thermophysical properties	Water	EG (40:60)	CuO-H_2O based nanofluid (0.01% conc.)	CuO-H_2O based nanofluid (0.05% conc.)	CuO-H_2O based nanofluid (0.1% conc.)	CuO- EG based nanofluid (0.01% conc.)	CuO- EG based nanofluid (0.05% conc.)	CuO- EG based nanofluid (0.1% conc.)
Density (kg/m^3)	1000	1048	1054	1270	1540	1101.52	1315.6	1583.2
Specific heat (J/kgK)	4187	3832	3965.05	3266	2497.87	3640.24	3029.25	2497.87
Thermal conductivity (W/mK)	0.667	0.434	0.68701	0.794	0.891	0.52	0.59	0.69
Viscosity (m^2/s)	0.415×10^{-6}	0.022	0.396×10^{-6}	0.364×10^{-6}	0.54×10^{-6}	2.153×10^{-6}	2.387×10^{-6}	2.731×10^{-6}